Resonant zones, inner and outer splittings in generic and low order resonances of APM

C. Simó, A. Vieiro
Departament de Matemàtica Aplicada i Anàlisi
Universitat de Barcelona
Gran Via, 585, 08007, Barcelona, Spain
e-mail: carles@maia.ub.es, vieiro@maia.ub.es

February 26, 2009

Abstract

We consider a one-parameter family of APM in a neighbourhood of an elliptic fixed point. As the parameter evolves hyperbolic and elliptic periodic orbits of different periods are created. The exceptional resonances of order less than 5 have to be considered separately. The invariant manifolds of the hyperbolic periodic points bound islands containing the elliptic periodic points. Generically, these manifolds split. It turns out that the inner and outer splittings are different under suitable conditions. We provide accurate formulae describing the splittings of these manifolds as a function of the parameter and the relative values of these magnitudes as a function of geometric properties. The numerical agreement is illustrated using mainly the Hénon map as an example.

1 Introduction

Let F_δ, $\delta \in \mathbb{R}$ be a one-parameter family of area preserving maps (APM) having an elliptic fixed point $p_\delta \in \mathbb{R}^2$ (that is $F_\delta(p_\delta) = p_\delta$). Without loss of generality it can be assumed that, in local Cartesian coordinates, the fixed point is the origin and it will be denoted by $E_0 = (0,0) \in \mathbb{R}^2$. This can be achieved by a δ-depending change of coordinates. Moreover, we also assume $\mathrm{Spec}(DF_\delta(E_0)) = \{\lambda, \bar{\lambda}\}$, with $\lambda = e^{2\pi i q/m + \delta}$, $q, m \in \mathbb{Z}$, $0 < q < m$, $\delta \in \mathbb{R}$. From now on through the paper, it will be assumed $(q,m) = 1$. We shall consider $|\delta|$ to be sufficiently small.

The dynamics of F_δ in a neighbourhood of the elliptic point is quite rich. As δ evolves the rotation number at the elliptic point (see below for definition) changes giving rise to creation or destruction of different resonant islands. These islands are bounded by the separatrices associated to hyperbolic periodic points. Generically these manifolds split.

There are mainly two splittings to consider: the inner splitting and the outer one (see 5.2 for definitions). Non-rigorously let us say that the inner splitting is the one associated to the point q in the sketch given in figure 2 (section 3.3) while the outer one is associated to the point p.

Our interest in this work is to describe the behaviour of these splittings as δ varies and their dynamical implications. In this sense, one of the main results shows that the inner splitting is different from the outer one under suitable (reasonable) assumptions. Moreover, the difference

between both splittings, at least in a relatively large neighbourhood of the elliptic point E_0, can be explained in terms of the twist properties of F_δ. Before facing the splitting problem the different resonances are described, including the low order ones and some degenerate cases.

The difference between both splittings can be observed in many examples. For instance, consider the conservative Hénon map ([23])

$$H_\alpha : \begin{pmatrix} x \\ y \end{pmatrix} \longmapsto R_{2\pi\alpha} \begin{pmatrix} x \\ y - x^2 \end{pmatrix}, \qquad \alpha \in (0, 1/2), \tag{1}$$

where $R_{2\pi\alpha}$ denotes a rotation of angle $2\pi\alpha$.

Choosing $\alpha = 0.212$ we observe 5-periodic islands. The splitting between the separatrices can be seen in an easy way close to a hyperbolic point. Hence, we focus on the 5-periodic hyperbolic point $(x, y) \approx (0.5846661277925608, 0.1709172404939729)$. In figure 1 one can guess the invariant manifolds that bound the 5-periodic island having the elliptic point located on the symmetry axis $y = \tan(\pi\alpha)x$. Clearly there is a big difference between the size of the folds of the manifold, as can be checked from the scales used in plots.

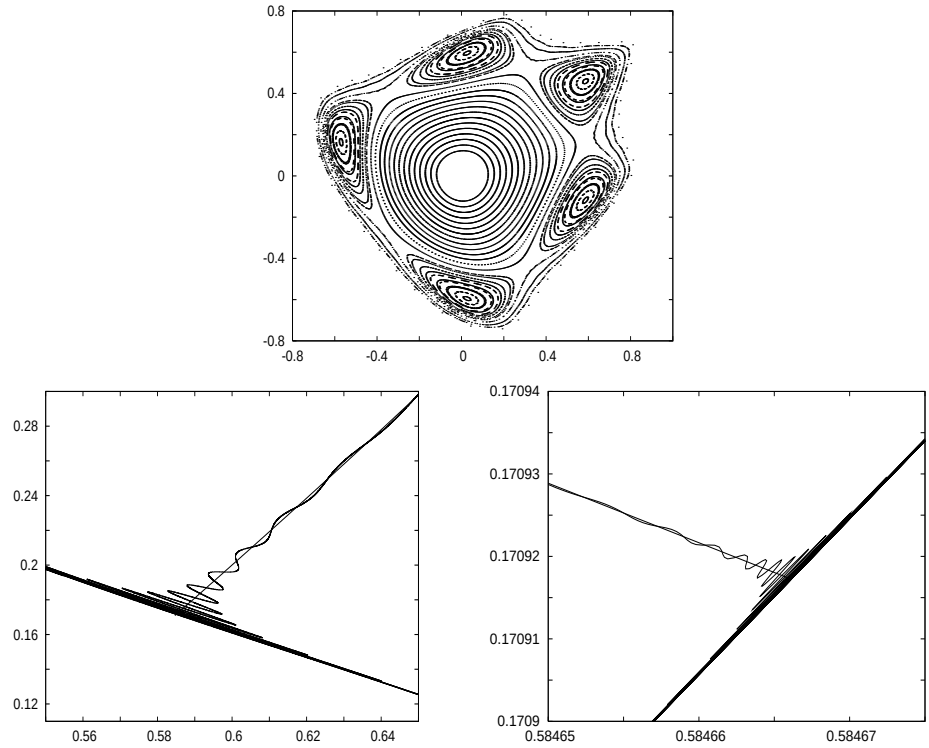

Figure 1: Comparison of inner and outer splittings for map (1) with $\alpha = 0.212$. Top: phase space of the Hénon map. Bottom: outer splitting (left) and inner splitting (right). Observe that the size of the bottom left (right) window is approximately 0.1×0.19 ($2.4 \cdot 10^{-5} \times 4 \cdot 10^{-5}$). The factor between the scales is of the order of 10^4.

We note that, as often happens in the analytic category, the splitting is exponentially small with respect to a suitable parameter. On the other hand, for the Hénon map all the separatrices of the hyperbolic periodic orbits split. This follows from Ushiki's theorem [41] as observed in [16].

In this work we will illustrate most of the results numerically using (1) as a paradigmatic example. The reader is referred to [23] for information about some properties of the Hénon map

and to [38] for local/global properties of that and similar maps.

As noticed before, our goal is to analyse a generic family F_δ. Obviously, when moving the parameter δ both splittings evolve. In particular, when δ goes to zero they tend to zero too. To determine the evolution of these splittings of separatrices an appropriate model describing the dynamics in a chain of resonant islands is required (section 3).

To get this model we consider a Birkhoff Normal Form (BNF for short) of F_δ around the elliptic point. In particular, an accurate description of the dynamics in a ball containing the m-order resonance is obtained. Generically, there exists a Cantor set of invariant curves surrounding the elliptic point for the BNF. However in the strong resonance cases $m < 5$ this can be no longer true. A detailed description of the dynamics in the strong resonance cases is given in section 4. Special interest in this section is devoted to the Hénon map. In particular, it is shown the non-generic behaviour of this map when unfolding the fourth order resonance, while the third order one is generic. To clarify the behaviour of the resonant zones far away from the fixed elliptic point, a generic model, obtained as a perturbation of a twist map, is also introduced.

It turns out that it becomes necessary to keep the first and second twist terms in BNF to describe the behaviour of the splittings as is noted in section 5 and in the computations related to the splitting (see Appendix). The first order twist analysis is enough to conclude that for δ sufficiently small the outer splitting is larger than the inner one. Furthermore, a suitable scaling and the good approximation provided by the BNF allow to control quite accurately the behaviour of the splittings in resonant zones close to the elliptic fixed point.

The reader familiarised with APM theory will recognise some parts of the topics presented, mainly the classical BNF theory used to get the models. However, we briefly include these parts to stress some relevant properties to be used in later discussions.

2 Preliminaries

It is assumed that all the maps involved are analytical diffeomorphisms. However many things, excluding the exponentially small splitting of separatrices, can be generalised to the $\mathcal{C}^\infty$ case and even to the $\mathcal{C}^r$ one for sufficiently large r.

2.1 Area preserving maps

We start by briefly recalling some well-known facts of area preserving maps. From now on we consider orientation preserving maps. Most results are still valid in the orientation reversing case by taking F^2 instead of F, despite the square of an orientation reversing map has some special properties.

Integrability condition. An area preserving map (APM), $F : U \to \mathbb{R}^2$, $U \subset \mathbb{R}^2$ an open domain, is said to be (analytically) *integrable* if there exists an (analytic) function $G : U \to \mathbb{R}$ such that $G(x) = G(F(x))$ for all $x \in U$. In particular, if for a suitable $m \geq 1$ there exists an autonomous Hamiltonian flow, defined on $V \subset U$, $\phi_t^{\mathcal{H}}$, such that for some τ the time-τ map coincides with the diffeomorphism F^m, that is, $\phi_\tau^{\mathcal{H}}(x) = F^m(x)$ for all $x \in V$, then the map F is obviously integrable in V (this is a sufficient condition for integrability).

The phase space of an integrable APM in a neighbourhood of an elliptic fixed point can be a

foliation of invariant rotational curves but generically some resonances show up. In the last case, the resonances are characterised by the sequence of islands (say, m islands, $m \geq 2$) that form the resonance strip. For $m > 4$, the phase portrait of the power m map F^m around an island is like the one of a classical pendulum. Inside each island there is an elliptic fixed point of F^m while at the edge of the boundary of the island a hyperbolic fixed point of F^m is located. Each island is bounded by the separatrices of the hyperbolic periodic points. These separatrices are barriers between the librational motion around the elliptic point and the rotational motion.

Loosing the integrability condition. When the integrability is lost the phase portrait suffers some topological changes. In the resonance zones the splitting of the separatrices provides a set of homoclinic points, transversal or at least topologically transversal. That is, points where the stable manifold crosses the unstable one creating a collection of lobes that are mapped one to each other respecting the area preserving and the orientation preserving properties of the map. In particular, a homoclinic tangle is created and, as it is well-known, this geometrical structure gives rise to sensitivity with respect to initial conditions and to the existence of invariant hyperbolic Cantor sets [39]. The splitting of the invariant manifolds is bounded by a quantity of the form $N \exp(-C/\log(\lambda))$, where $N > 0$ is a constant, $C > 0$ is a constant that depends on the width of the strip of analyticity of the separatrix of the limit Hamiltonian, and λ is the dominant eigenvalue of the near-the-identity family considered (see [11]).

In [9] a perturbed pendulum model around an island of a resonance of a Hamiltonian flow was constructed. Of course, a similar approach is obtained from the BNF of a symplectic map.

Twist map. It is well-known that in the case of non-strong resonances the BNF of an APM is a twist map, provided not all the lower order Birkhoff coefficients are zero.

Let F be an APM of the annulus $\mathbb{S}^1 \times (0,1)$. F is called *twist map* if the following holds:

1. F preserves orientation,
2. F preserves barrier components: there exists $\epsilon > 0$ such that if $(x,y) \in \mathbb{S}^1 \times (0,\epsilon)$ then $F(x,y) \in \mathbb{S}^1 \times (0,1/2)$, that is, the image of a curve $\{x\} \times (0,1)$ connecting barrier components of the annulus should connect the barrier components,
3. if $\hat{F} = (\hat{F}_1, \hat{F}_2)$ is a lift of F (i.e. $\hat{F} : \mathbb{R} \times (0,1) \to \mathbb{R} \times (0,1)$, $\pi \circ \hat{F} = F \circ \pi$, where π denotes the projection $\mathbb{R} \to \mathbb{S}^1$) then $\frac{\partial}{\partial y}\hat{F}_1(x,y) \neq 0$, $\forall y \in (0,1)$, $\forall x \in \mathbb{R}$.

The most important consequence of the twist condition is Moser's twist theorem, which provides a condition for the existence of a family of invariant rotational curves under a sufficiently small APM perturbation of an integrable map (see [29]). It is important to remark that a sufficient condition on a curve to be preserved is to have a Diophantine rotation number.

Rotation number. Let $g : \mathbb{S}^1 \to \mathbb{S}^1$ be a homeomorphism of the circle. The *rotation number* is defined to be the limit

$$\rho(\hat{g}) = \lim_{n\to\infty} \frac{\hat{g}^n(x) - x}{n}, \tag{2}$$

where $\hat{g}$ is a lift of the map g, that is, a map $\hat{g} : \mathbb{R} \to \mathbb{R}$ such that $\pi \circ \hat{g} = g \circ \pi$ where π denotes the projection $x \mapsto x \pmod 1$, from $\mathbb{R}$ to $\mathbb{S}^1$.

Limit (2) exists for all $x \in \mathbb{R}$ and it is independent of the initial point chosen. On the other hand, the limit does not depend on the lift which means that $\rho(g) = \rho(\hat{g}) \pmod 1$ is well-defined.

When we study the rotation number for an APM it is clear that the definition applies on the rotational invariant curves. For an elliptic fixed point, if the eigenvalues are $\exp(\pm 2\pi i\rho)$, we take ρ as rotation number. For periodic points of period m closing after performing q revolutions

around the fixed point, we take $\rho = q/m$, and we can denote them as q/m-periodic points. The same value is taken for the eventual islands around these periodic points and for the eventual stable manifolds of them. The rotation number for other points may be not defined. This is often used as an indicator of chaoticity.

2.2 The Hénon map

As noticed in [23] the Hénon map (1) is the simplest planar map with non-trivial behaviour which makes it a good model for numerical exploration (it is a quadratic map and so is the inverse map). Furthermore, any planar conservative quadratic map having an elliptic fixed point can be reduced to the conservative Hénon map.

It is easy to check that the map (1) has two fixed points. The origin is an elliptic fixed point while the point of coordinates $P_h = \big(2\tan(\pi\alpha), 2\tan^2(\pi\alpha)\big)$ is a hyperbolic fixed point. It is important also to take into account that the map (1) is reversible with respect to the axis $y = \tan(\pi\alpha)x$ and with respect to the parabola $y = x^2/2$ by means of the involutions $(x, y) \mapsto (\cos(2\pi\alpha)x + \sin(2\pi\alpha)y,\ \sin(2\pi\alpha)x - \cos(2\pi\alpha)y)$ and $(x, y) \mapsto (x, x^2 - y)$, respectively.

When studying the Hénon map we will use different versions depending on the phenomena we are looking for. In the complex variable $z = x + iy$ the map (1) is expressed as

$$z \longmapsto \lambda z - \frac{\lambda}{4} i z^2 - \frac{\lambda}{4} i \bar{z}^2 - \frac{\lambda}{2} i z \bar{z}. \tag{3}$$

The change of variables $x = \gamma u + k_1$, $y = \beta u + \nu v + k_2$, where $k_1 = -\cot(2\pi\alpha)$, $k_2 = -\cos(2\pi\alpha)\sec^2(\pi\alpha)/2$, $\beta = k_2\cos(2\pi\alpha) - \cot^2(2\pi\alpha)$, $\nu = \beta/\cos(2\pi\alpha)$, $\gamma = -\beta\tan(2\pi\alpha)$, allows to write Hénon map (1) as

$$H_a : \begin{pmatrix} u \\ v \end{pmatrix} \to \begin{pmatrix} 1 - au^2 + v \\ bu \end{pmatrix}, \tag{4}$$

where $b = -1$ and $a = \cos^2(2\pi\alpha) - 2\cos(2\pi\alpha)$, $a \neq 0$. The case $\alpha = 1/4$, and hence $a = 0$, requires a different formulation like (1) or (5). The map (4) with $|b| < 1$ is the well-known Hénon dissipative map.

In fact, map (4) is slightly more general than the original version (1). The fixed point of (1) located at the origin has new coordinates

$$(u_0, v_0) = \big((-1 + \sqrt{1+a})/a, (1 - \sqrt{1+a})/a\big)$$

and it is elliptic if $-1 \leq a \leq 3$ (if $a < -1$ the fixed point does not exist while for $a > 3$ it becomes hyperbolic with reflection). The hyperbolic fixed point of the Hénon map has coordinates

$$(u_h, v_h) = \big((-1 - \sqrt{1+a})/a, (1 + \sqrt{1+a})/a\big)\,.$$

The change of variables $x = (au + 1)/\sqrt{a+1}$, $y = (av - 1)/\sqrt{a+1}$, allows to write (4) as

$$H_c : \begin{pmatrix} x \\ y \end{pmatrix} \mapsto \begin{pmatrix} c(1 - x^2) + 2x + y \\ -x \end{pmatrix}, \tag{5}$$

where $c = \sqrt{1+a}$. For $0 < c < 2$ the variables x, y have the nice property of having the elliptic (resp. hyperbolic) fixed point located at $(1, -1)$ (resp. at $(-1, 1)$) independently of the value of c. When $c > 2$ the elliptic point located at $(-1, 1)$ becomes hyperbolic with reflexion. On the

other hand, for $c = 0$ the line $y = -x$ is made of fixed points while for $c < 0$ the elliptic and the hyperbolic points interchange their role via the symmetry $(x, y, c) \longmapsto (-x, -y, -c)$.

For small c the map can be approximated by a flow. Indeed, the symplectic change

$$\begin{pmatrix} x \\ y \end{pmatrix} = \frac{1}{\sqrt{2}} \begin{pmatrix} r+s \\ r-s \end{pmatrix}$$

and the introduction of $s = q$, $r = dp$, where $d = \sqrt{c/\sqrt{2}}$, gives the close to the identity map

$$\begin{pmatrix} q \\ p \end{pmatrix} \longmapsto \begin{pmatrix} q + 2dp + O(d^2) \\ p + d(1 - \frac{1}{2}q^2) + O(d^2) \end{pmatrix}.$$

A map of the form $(q, p)^t \mapsto (q + df(q, p) + O(d^2), p + dg(q, p) + O(d^2))^t$ can be approximated by the time-d flow of $(\dot{q}, \dot{p})^t = (f, g)^t$, giving now

$$\dot{q} = 2p, \qquad \dot{p} = 1 - \frac{1}{2}q^2, \tag{6}$$

which comes from the Hamiltonian $K(q, p) = p^2 - q + \frac{1}{6}q^3$. The level $K = \frac{2}{3}\sqrt{2}$ containing the hyperbolic point $q = -\sqrt{2}, p = 0$ corresponds to a separatrix, enclosing the elliptic point $q = \sqrt{2}, p = 0$. The splitting for the manifolds of the map is exponentially small in d. Also invariant curves of the map exist at an exponentially small distance of the manifolds. These claims will be proved later for general cases.

3 A suitable Hamiltonian model around a generic resonance

The local study of the dynamics of an APM F in a neighbourhood of an elliptic fixed point can be elucidated by its BNF (see [29]) and the so-called interpolating Hamiltonian. This section is devoted to obtain a Hamiltonian model describing an approximation of the dynamics in a generic resonance. The particular case of strong resonances will be analysed in the next section.

3.1 Birkhoff resonant normal form.

A map F is said to be in Birkhoff normal form around a fixed point $p \in \mathbb{R}^n$ if it commutes with the linear part $DF(p)$. Given a general APM F there exists a formal canonical change of variables such that F is in BNF around E_0 in the new coordinates. If we only require commutation up to terms of order $n - 1$ we shall talk about BNF to order n or simply BNF_n.

Let $\alpha \in (0, 1)$ be the rotation number at the fixed point E_0 and let $\lambda = e^{2\pi i\alpha}$ be the associated multiplier when the map is written in complex variables. In order to compute a coordinate change to remove a term of the form $z^j \bar{z}^k$, $j, k \in \mathbb{N}$, from the Taylor series of F as a function of $z, \bar{z}$, the non-resonance condition $\lambda^{j-k-1} \neq 1$, $j + k \geq 2$, should be satisfied [2]. In particular, terms with $j = k + 1$ should be kept (the so-called *unavoidable resonances*). If λ is not a root of the unity, then the BNF contains only the linear part and the unavoidable resonances to any order. Otherwise some other terms have to be retained, giving rise to the so-called resonant Birkhoff normal form. Usually we shall denote it just as Birkhoff normal form.

To study the dynamics around a resonance of order m we assume that $\alpha = \frac{q}{m} + \delta$, $1 \leq q < m$, with δ around 0 sufficiently small to have $\lambda^{m-1} \simeq \bar{\lambda}$. Thus, when computing the BNF, the

corresponding term cannot be removed if we want to assure the existence of a relatively large domain, uniform for δ close to zero, where a good model could be obtained. In particular, the resonance of order m cannot be ignored because its effect is mainly located in a small neighbourhood of the elliptic point where the BNF approach will be used.

In terms of the $(z, \bar{z})$ variables F can be reduced to the BNF_m

$$\mathrm{BNF}_m(F) : z \longmapsto \lambda z + a_1 z^2 \bar{z} + \cdots + a_s z^{s+1} \bar{z}^s + \tilde{c} \bar{z}^{m-1} + \tilde{\mathcal{R}}_{m+1}(z, \bar{z}), \tag{7}$$

where $a_i \in \mathbb{C}$. By introducing the *Birkhoff coefficients*, b_i, it can be expressed as

$$\mathrm{BNF}_m(F) : z \longmapsto R_{2\pi \frac{q}{m}} \left(e^{2\pi i \gamma(r)} z + c \bar{z}^{m-1} \right) + \mathcal{R}_{m+1}(z, \bar{z}), \tag{8}$$

where $\gamma(r) = \delta + b_1 r^2 + b_2 r^4 + \cdots + b_s r^{2s}$, $r = |z|$.

The APM character of F implies that all the b_i coefficients are real. In (7) and (8) the terms of degree at least $m+1$ are denoted as $\tilde{\mathcal{R}}_{m+1}(z, \bar{z})$ and $\mathcal{R}_{m+1}(z, \bar{z})$, respectively, and $s = [(m-1)/2]$, where $[x]$ denotes the integer part of x. We note that if m is even there are no resonant terms of order m while if m is odd there is an m-order unavoidable resonant term which is included in $\gamma(r)$. The remainder is, hence, $\mathcal{O}_{m+1}$ in both cases.

Remarks.

1. In the expression (8) it is assumed that the coefficient of $\bar{z}^{m-1}$ is non zero. Otherwise, one should consider the first non-zero coefficient of a resonant monomial and the map is reduced to a similar normal form (see next subsection). Assume that the first non-zero coefficient is of the form $dz\bar{z}^m$ with $d \neq 0$. It can happen that when we unfold the degenerate case around $\delta = 0$ it gives a contribution of the form $c\delta\bar{z}^{m-1}$ with $c \neq 0$. On the resonant zone, located at $r^2 = \mathcal{O}(\delta)$, both terms are of the same order of magnitude $\mathcal{O}(\delta^{(m+1)/2})$ and can be studied together. Other cases can be analysed in a similar way.

2. In (8) one could extend the $\gamma(r)$ part as much as desired by cancellation of unavoidable resonances to high order. On the other hand, if q/m is the unique resonance up to order $2m-1$ (and this can be achieved if δ is small enough) then next resonant terms due to the q/m one of the form $z^j \bar{z}^{m-1+j}, 1 \leq j < m/2$ can be included, by replacing c by $c + c_1 r^2 + c_2 r^4 + \ldots$. In this way one can obtain a remainder $\mathcal{O}(r^{2m-1})$.

3. Note that the map in (7) or in (8) is equivalent to F possibly only in a domain which is smaller than the initial domain of analyticity of F in (x, y). This is due to the necessary inversion of functions in the canonical transformations (given, e.g., by polynomial generating functions). One would be tempted to truncate the BNF_m, that is, to skip the $\tilde{\mathcal{R}}_m(z, \bar{z})$ or $\mathcal{R}_m(z, \bar{z})$ terms, to have an approximation of F. However, in the presence of resonant terms, these truncated maps are not APM. In 3.3 the map $R_{-2\pi \frac{q}{m}} \circ F$ is approximated as the flow time-1 of a Hamiltonian. In that case the flow of truncated Hamiltonians provides APM approximations of $R_{-2\pi \frac{q}{m}} \circ F$.

Equivalently, the normal form can be expressed as

$$\mathrm{BNF}_m(F) : z \longmapsto R_{2\pi \frac{q}{m}} \circ K(z, \bar{z}, \delta),$$

where $K(z, \bar{z}, \delta) = e^{2\pi i \gamma(r)} z + c\bar{z}^{m-1} + \hat{\mathcal{R}}_{m+1}(z, \bar{z})$.

It is important to emphasise that the map K is a near-the-identity map such that the m-jet commutes with the rotation $R_{2\pi\frac{q}{m}}$. Scaling $z = \mu w$ with a suitable complex μ allows us to change the coefficient c of equation (8) to become the imaginary unit. Note, however, that the Birkhoff coefficients of the map have then been modified according to $\tilde{b}_j = |\mu|^{2j}\ b_j$. This has to be taken into account for quantitative estimates. Despite of this change on the coefficients we will again denote by b_j the "new" Birkhoff coefficients and also keep z as the independent variable. As a consequence, the analysis of the BNF_m can be reduced to study the map

$$K : z \mapsto e^{2\pi i\gamma(r)}z + i\bar{z}^{m-1} + R_{m+1}(z,\bar{z}). \tag{9}$$

3.2 Some comments on the influence of other resonances.

To get the expression (9) we have assumed that the m-order resonance cannot be removed when computing the normal form. Moreover, we have assumed that $\bar{z}^{m-1}$ is the first term corresponding to an avoidable resonance that cannot be removed. These generic assumptions are not a hard restriction in the sense that the results we will obtain can be applied also in the case that other resonances of similar order appear.

In order to give a justification of the last statement assume that there exist two different terms that cannot be removed when computing the normal form and that they correspond to resonances of orders m_1 and m_2, with $m_2 > m_1$. Assume also that we are interested in studying the m_2-order resonance. Hence, $\alpha = q_2/m_2 + \delta_2 = q_1/m_1 + \delta_1$ where $(q_1, m_1) = (q_2, m_2) = 1$ and δ_1 and δ_2 are assumed to be irrational and small. However they cannot be too small simultaneously because $|\delta_1| + |\delta_2| \geq \frac{1}{m_1 m_2}$.

The relation $\lambda \approx \bar{\lambda}^{m_1-1}$, since $\lambda\bar{\lambda} = 1$, implies the resonant terms $z^j\bar{z}^{m_1+j-1}$. In the same way, the relations $\lambda^{m_1+1} \approx \lambda$ and $\bar{\lambda}^{m_1-1} \approx \lambda$ provide terms $z^{km_1+j+1}\bar{z}^j$ and $\bar{z}^{sm_1+j-1}z^j$ that cannot be removed from the normal form. As a consequence, the map F can be reduced to

$$\begin{aligned}\mathrm{BNF}_{m_2}(F): \quad z \mapsto \quad R_{2\pi\frac{q_2}{m_2}}\Bigg(e^{2\pi i\gamma(r)}z + \sum_{s=1}^{[\frac{m_2}{m_1}]}\sum_{j=0}^{[\frac{m_2-sm_1+1}{2}]} c_{sj}z^j\bar{z}^{sm_1+j-1} + \\ + \sum_{k=1}^{[\frac{m_2-2}{m_1}]}\sum_{j=0}^{[\frac{m_2-km_1-1}{2}]} d_{kj}z^{km_1+j+1}\bar{z}^j + c_2\bar{z}^{m_2-1}\Bigg) + \mathcal{R}_{m_2+1}(z,\bar{z}),\end{aligned}$$

where $c_{1j}, c_2 \in \mathbb{C}$ for $j \geq 0$, and being $\gamma(r) = \delta_2 + \sum_{i>0} b_i r^{2i}$ (compare with (8)).

We try to determine which is the effect of a term $cz^j\bar{z}^{m_1+j-1}$ (corresponding to $s = 1$ above) when we are in a neighbourhood of the m_2-order resonance. More concretely, we are interested in an annulus surrounding the m_2 resonance, where the dynamics is almost a rotation of angle $\beta = 2\pi q_2/m_2$ (since $\gamma(r) \approx 0$). Let $\hat{F} : z \mapsto R_{2\pi q_2/m_2}\left(e^{2\pi i\gamma(r)}z + c_2\bar{z}^{m_2-1}\right) + \mathcal{R}_{m_2+1}(z,\bar{z})$, that is, the map we obtain if we ignore the m_1-resonance terms. Let z_0 be a point on the annulus surrounding the m_2 resonance and let $z_i = F^i(z_0)$. The contribution of the term $cz^j\bar{z}^{m_1+j-1}$ after m_2 iterates has a dominant part given by

$$\mathrm{BNF}_{m_2}^{m_2}(F)(z_0) - \hat{F}^{m_2}(z_0) \approx R_{2\pi\frac{q_2}{m_2}}^{m_2} cz_0^j\bar{z}_0{}^{m_1+j-1} + R_{2\pi\frac{q_2}{m_2}}^{m_2-1} cz_1^j\bar{z}_1{}^{m_1+j-1} + \cdots + R_{2\pi\frac{q_2}{m_2}} cz_{m_2-1}^j\bar{z}_{m_2-1}^{m_1+j-1}. \tag{10}$$

Expressing the point in polar coordinates, that is, $z_0 = r\exp(i\,\psi)$, $r = |z_0|$, $\psi \in [0, 2\pi)$, using the fact that $|z_k| = r + \mathcal{O}(r^{m_1-1})$ for $k = 1, \ldots, m_2 - 1$, and that the argument of a term in (10)

of the form $R^{m_2-k}_{2\pi\frac{q_2}{m_2}} c z_k^j \bar{z}_k^{m_1+j-1}$ is, approximately,

$$-(\psi+2\pi k\frac{q_2}{m_2})(m_1+j-1)+(m_2-k)2\pi\frac{q_2}{m_2}+j(\psi+2\pi k\frac{q_2}{m_2})+\beta \equiv -\psi(m_1-1)-2\pi k\frac{q_2}{m_2}m_1+\beta,$$

being β the argument of c, we observe that this dominant part adds to zero because $m_2 \nmid m_1$.

As a consequence, the contribution of the terms $c_{1j} z^j \bar{z}^{m_1+j-1}$ can be skipped to obtain an approximation to the dynamics. The contribution of the terms like $c_{sj} z^j \bar{z}^{sm_1+j-1}$ and $d_{kj} z^{km_1+j+1} \bar{z}^j$ is analysed in a similar way obtaining the same conclusion. In particular, this means that the study of the m_2 resonance is almost independent of the existence of the m_1 resonance.

Observe, however, that in the approximation (10) the second order terms are ignored (similarly for the approximations of the dominant parts of the contributions of the terms $c_{sj} z^j \bar{z}^{sm_1+j-1}$ and $d_{kj} z^{km_1+j+1} \bar{z}^j$). The terms we have ignored are of the order $\mathcal{O}(2sm_1+2j-3)$ in the case we are dealing with a term of the form $c_{sj} z^j \bar{z}^{sm_1+j-1}$, and of the order $\mathcal{O}(2km_1+2j+1)$ if the considered term is $d_{kj} z^{km_1+j+1} \bar{z}^j$. Hence it is necessary, beyond having r small (which requires δ_2 small enough) to have $2m_1-3 > m_2$, a condition which appears if $j=0$ above. That is, the reasoning above described applies to resonances of "similar" order.

Hence, we will try to describe the m-order resonance keeping in mind that the results we will obtain can be applied to any "important" resonance.

3.3 Flow approximation of the normal form.

A near-the-identity map, like map (9), can be approximated by a planar autonomous flow. In fact, by the interpolation lemma (see comments below) it can be expressed as a time-one map of a Hamiltonian flow plus higher order terms.

Let us introduce the Poincaré or action-angle variables (I,φ) defined by $z = \sqrt{2I}\exp(i\varphi)$. Furthermore, we denote δ as b_0 and define

$$\mathcal{H}_{nr}(I) = \pi \sum_{n=0}^{s} \frac{b_n}{n+1}(2I)^{n+1} \quad \text{and} \quad \mathcal{H}_r(I,\varphi) = \frac{1}{m}(2I)^{\frac{m}{2}}\cos(m\varphi),$$

as the non-resonant and resonant parts of the Hamiltonian, and let r_* be such that $\gamma(r_*)=0$, that is $r_* \approx (-\delta/b_1)^{1/2}$, where we assume $b_1 \neq 0$.

Theorem 3.1 *Let $\hat{K}$ denote the original diffeomorphism K expressed in Poincaré variables and assume $b_1 \neq 0$ and $m \geq 5$. Let $\nu > 0$ a fixed value (possibly small). Then the time-1 flow $\phi_{t=1}$ generated by the Hamiltonian*

$$\mathcal{H}(I,\varphi) = \mathcal{H}_{nr}(I) + \mathcal{H}_r(I,\varphi), \tag{11}$$

interpolates the map (9) with an error of order $m+1$ in the $(z,\bar{z})$-coordinates, that is,

$$\hat{K}(I,\varphi) = \phi_{t=1}(I,\varphi) + \mathcal{O}\left(I^{\frac{m+1}{2}}\right),$$

in an annulus centred in the resonance radius r_* of width $r_*^{1+\nu}$, for $|\delta|$ sufficiently small.

Remark. Later on we shall need approximations of $\hat{K}$ in a larger domain, in complex phase space, which excludes a small neighbourhood of the origin. The error bound will be slightly larger. But this is postponed until it will be required in Section 5.

Proof. As the map K is close to the identity, one can construct a non-autonomous vector field periodic with respect to the time, analytic with respect to z, such that the time-one map coincides with the diffeomorphism. Moreover, as the map is close to the identity and analytic, the vector field is a slow vector field and, after a suitable scaling and several averaging steps with respect to the time variable, the vector field can be written as an analytic autonomous vector field plus an exponentially small non-autonomous term (see [27, 7]). Moreover, the changes can be made symplectic in order to preserve the symplectic structure (see [35]).

Besides, the vector field $\dot{z} = (e^{2\pi i\gamma(r)} - 1)z + i\bar{z}^{m-1}$ provides an approximation of K up to order 2. Then, we can change successively the homogeneous terms of degrees 2 to m to obtain a new vector field that interpolates up to order m. This is a consequence of Takens theorem [40]. An important advantage of this process is that the terms of the vector field can be obtained explicitly. Note, however, that when carrying out Takens process, which can be applied to the $\mathcal{C}^\infty$ case, the interpolation error is flat but not exponentially small in general. If the process is applied to a $\mathcal{C}^\omega$ map it can be difficult to obtain sharp estimates on the terms of the expansion, so that the bounds would be the same than the ones corresponding to a Gevrey class. Instead of bounds like $\exp(-c/\epsilon)$, for some small parameter ϵ, one can perhaps obtain bounds like $\exp(-c/\epsilon^{1/k})$ for some $k > 1$ (see [32]).

Nevertheless, observe that the map (9) is $\mathcal{O}(r^{m+1})$-close to the map $T = T_2 \circ T_1(z)$ where $T_1(z) = e^{2\pi i\gamma(r)}z$ and $T_2(z) = z + i\bar{z}^{m-1}$. It is a consequence of the fact that T_1 is close to the identity.

The map T_1 is a rotation of angle $2\pi\gamma(r)$. In Poincaré variables it becomes $(I, \varphi) \to (I, \varphi + \omega(I))$ where $\omega(I) = \mathcal{H}'_{nr}(I) = 2\pi \sum_{k=0}^{s} b_k (2I)^k$. Then the flow $\dot{I} = 0$, $\dot{\varphi} = \omega(I)$ interpolates exactly the map T_1. Expressing this vector field in $(z, \bar{z})$-coordinates it is obtained that the vector field

$$\dot{z} = i\,\omega(I)z \tag{12}$$

interpolates exactly the map T_1.

On the other hand, the vector field

$$\dot{z} = i\bar{z}^{m-1} \tag{13}$$

provides an approximation up to order $\mathcal{O}(2m-3)$ of the map T_2.

We recall that the Lie bracket of two vector fields $\dot{x} = f(x)$, $\dot{y} = g(y)$ is the vector field $[f, g] = Df(x)g(x) - Dg(x)f(x)$. If the vector fields commute then the Lie bracket vanishes.

The Lie bracket of the vector fields (12) and (13) is a vector field of order higher than $m + 1 + \nu$ in an annulus of radius $r_*^{1+\nu}$, for $\nu > 0$, centred in the radius r_* where the resonance is located. Then, the effects of the rotation T_1 and the resonance T_2 can be considered independent and one can obtain the vector field as the sum of vector fields. After changing coordinates and computing the Hamiltonian we get the expression (11). □

Remark. In [3] was already stated that for a m-resonant fixed point the interpolating Hamiltonian is of the form $H(I, \varphi) = I^2\beta(I) + I^{m/2}\gamma(I)\cos(m\varphi) + \mathcal{O}(I^{1+m/2})$, being $\beta(I)$ and $\gamma(I)$ polynomials in I. Moreover, in [15] it is observed that this form can be extended up to any order by taking suitable advantage of the non-uniqueness of the normal form. In particular, high order resonant terms in BNF just modify the leading coefficients of the Hamiltonian (16) but not the format.

3.3.1 The periodic orbits of the m-order resonance.

The results contained in the sections 3.3.1 and 3.3.2, obtained from the flow approximation given above, describe the topology of the conservative map.

Lemma 3.1 *Let $F : \mathbb{R}^2 \to \mathbb{R}^2$ be a map having the origin as an elliptic fixed point such that $b_1 \neq 0$. Assume also that the rotation angle at the origin is of the form $\alpha = q/m + \delta$, $m \geq 5$, for δ sufficiently small and that the coefficient of the resonant term of order m is non-zero. If $b_1\delta < 0$ then the conservative dynamical system generated by F has a resonance of order m. Moreover, in the resonant zone there are two periodic orbits of period m located near two concentric circumferences (in the normal form coordinates). The closest orbit to the external one is elliptic while the nearest orbit to the internal circumference is hyperbolic.*

Proof. Consider the case b_1 positive. First we compute fixed points of the vector field generated by (11). Equation $\frac{\partial \mathcal{H}}{\partial \varphi} = 0$ admits as solutions, beyond the trivial one, the set

$$\varphi_j = \frac{j\pi}{m},\ j = 0, \ldots, 2m-1.$$

From equation $\frac{\partial \mathcal{H}}{\partial I} = 0$ we can obtain the following relation

$$\frac{\partial \mathcal{H}_{nr}(I)}{\partial I} + (2I)^{\frac{m}{2}-1}\cos(m\varphi_j) = 0. \tag{14}$$

Ignoring the resonance term, equation $\frac{\partial \mathcal{H}_{nr}(I)}{\partial I} = 0$ has

$$I_* = -\frac{\delta}{2b_1} + \mathcal{O}(\delta^2), \tag{15}$$

as a solution. Last expression defines a radius, if $\delta < 0$, which is an approximation to the radius where the m-order resonance is located. We look for a correction term ΔI such that $I_* + \Delta I$ is a solution to equation (14). The values

$$\Delta I_j = \frac{(-1)^{j+1}(2I_*)^{\frac{m}{2}-1}}{w'(I_*)} + \ldots = \frac{(-1)^{j+1}(2I_*)^{\frac{m}{2}-1}}{4\pi b_1}(1 + \mathcal{O}(I_*))$$

are obtained. Then the eigenvalues at the fixed points, if $m\varphi_j = j\pi, I = I_* + \Delta I_j$, are given by

$$\hat{\lambda}_j = \pm\left[(2I)^{\frac{m}{2}} m(-1)^j\left(\frac{\partial^2 \mathcal{H}_{nr}(I)}{\partial I^2} + \mathcal{O}((2I)^{\frac{m}{2}-2})\right)\right]^{1/2}, \qquad \frac{\partial^2 \mathcal{H}_{nr}(I)}{\partial I^2} = 4\pi b_1 + \mathcal{O}(\delta^\mu),$$

being $\mu = \min\{1, \frac{m}{2} - 2\}$. In particular, it allows us to ensure that the fixed points such that j is even are hyperbolic, while the ones with j odd are elliptic.

If $b_1 < 0$ the above computation can be carried out in a similar way ($\delta > 0$ in this case).

To justify that the map F has also the periodic points we observe that the fixed point condition $\hat{K}(I, \varphi) - (I, \varphi) = 0$ can be written, bounding $\mathcal{O}(I^{\frac{m+1+\nu}{2}})$ by $\mathcal{O}(I^{\frac{m+1}{2}})$, as

$$\phi_{t=1}(I, \varphi) - (I, \varphi) + \mathcal{O}(I^{\frac{m+1}{2}}) = 0.$$

Skipping last term, the determinant of the differential of the equation at the fixed points is $-4\pi b_1 m(2I)^{\frac{m}{2}}\cos(m\varphi_j)\,(1 + \mathcal{O}(\delta)) \neq 0$. The remainder terms add only to $\mathcal{O}(\delta^{\frac{m+1}{2}})$. Hence, the

implicit function theorem implies that the map $\hat{K}(I,\varphi)$ has the same number of periodic orbits located close to those of the flow $\phi_{t=1}$. □

Note that the eigenvalues $\hat{\lambda}_j$ for the flow are $\mathcal{O}(\delta^{m/4})$ and, hence, the ones for the map will be $\lambda_j = 1 \pm \mathcal{O}(\delta^{m/4})$.

For definiteness we shall denote as $H = (I_H, \varphi_H)$ and $E = (I_E, \varphi_E)$ the hyperbolic and elliptic points of $\hat{K}$. Note that, when taking into account the effect of the remainder, the corrections will depend on the concrete value of j. But they are small enough to be neglected.

3.3.2 The islands of the m-order resonance.

The invariant manifolds of the hyperbolic points of the same resonance bound a chain of islands. The following lemma determines the width of an island.

Lemma 3.2 *Let H and E, as before, be hyperbolic and elliptic periodic points, respectively, of the same island. Denote by p and q the points of the pendulum-like separatrices such that the distance from the circle of radius I_E reaches a maximum (see Fig. 2). Let δ_p and δ_q be these distances. Then the width of the resonance of order $m \geq 5$, $\delta_p + \delta_q$ is $\mathcal{O}\left(I_*^{\frac{m}{4}}\right)$.*

Figure 2 is a representation of the different variables we have introduced.

Proof. We assume $b_1 > 0$ (the other case is similar). As p, q are on the separatrices, one has $\mathcal{H}(H) = \mathcal{H}(p) = \mathcal{H}(q)$. From Hamiltonian (11), it is obtained

$$\begin{aligned}
\mathcal{H}(H) &= \mathcal{H}_{nr}(I_*) + \mathcal{H}_r(I_*, \varphi_H) + \left(\frac{\partial \mathcal{H}_{nr}}{\partial I}(I_*) + \frac{\partial \mathcal{H}_r}{\partial I}(I_*, \varphi_H)\right) \Delta I_H + \cdots, \\
\mathcal{H}(p) &= \mathcal{H}(E) + \frac{\partial \mathcal{H}}{\partial I}(E)\delta_p + \frac{1}{2}\frac{\partial^2 \mathcal{H}}{\partial I^2}(E)\delta_p^2 + \cdots, \\
\mathcal{H}(E) &= \mathcal{H}_{nr}(I_*) + \mathcal{H}_r(I_*, \varphi_E) + \left(\frac{\partial \mathcal{H}_{nr}}{\partial I}(I_*) + \frac{\partial \mathcal{H}_r}{\partial I}(I_*, \varphi_E)\right) \Delta I_E + \cdots.
\end{aligned}$$

Since $I = I_*$ is a curve of fixed points of the Hamiltonian $\mathcal{H}_{nr}$, then $(\partial \mathcal{H}_{nr}/\partial I)(I_*) = 0$. Moreover, as E is a fixed point of $\mathcal{H}$ then, $(\partial \mathcal{H}/\partial I)(E) = 0$. Finally, since $\mathcal{H}_r(I_*, \varphi_H) = -\mathcal{H}_r(I_*, \varphi_E) = (1/m)(2I_*)^{m/2}$, $(\partial \mathcal{H}_r/\partial I)(I_*, \varphi_H) = (-\partial \mathcal{H}_r/\partial I)(I_*, \varphi_E) = (2I_*)^{m/2-1}$, and $\Delta I_H = -\Delta I_E + \mathcal{O}(I_*^{m/2})$, $(\partial^2 \mathcal{H}/\partial I^2)(E) = 4\pi b_1 + \mathcal{O}(I_*^{\mu})$ (recall $\mu = \min\{1, \frac{m}{2} - 2\}$), the condition $\mathcal{H}(H) = \mathcal{H}(p)$, due to the fact that non-resonant Hamiltonian terms are canceled, is transcribed as $(2/m)(2I_*)^{m/2} = 2\pi b_1 \delta_p^2 + \mathcal{O}(I_*^{m-2}, I_*^{\mu}\delta_p^2, \delta_p^3)$, from which it is obtained

$$\delta_p = \left((2I_*)^{m/2}/m\pi b_1\right)^{1/2} (1 + \mathcal{O}(I_*^{\mu})).$$

The same conclusion can be achieved for δ_q by repeating the argument for the point q. □

To obtain realistic estimates of the width of the island we recall that, at the end of section 3.1 the coefficient of the resonant term has been scaled (by a finite constant) to obtain (9).

3.3.3 A numerical illustration

The general picture described along this section can be observed for a given example, for instance, the Hénon map. When computing the BNF for equation (3) it is found that the first Birkhoff

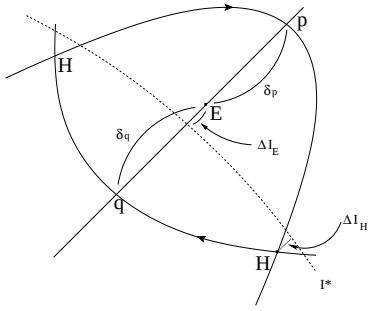

Figure 2: Sketch of the resonance of order m.

coefficient is equal to zero only for $\alpha \approx 0.29021531163$ (i.e. $\cos(2\pi\alpha) = -1/4$), while the second Birkhoff coefficient is zero for $\alpha_1 \approx 0.2308206101$, $\alpha_2 \approx 0.3137515644$ and $\alpha_3 \approx 0.3944381765$ (see [10]). Birkhoff coefficients can be computed numerically but we note that the changes of variables should be symplectic at each degree (see [24] for a general explanation about how to compute normal forms effectively and efficiently). Figure 3 shows the first and the second Birkhoff coefficients for the Hénon map.

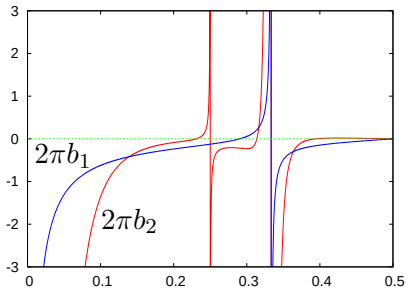

Figure 3: First (blue) and second (red) Birkhoff coefficients for equation (3). In the x-axis it is represented the value of α and in the y-axis the values of $2\pi b_1$ and $2\pi b_2$, respectively.

The analytical expression of the first Birkhoff coefficient as a function of α is given by

$$b_1 = \frac{1}{64\pi}\left(\frac{-3\sin(\hat{\alpha})}{\sin^2(\hat{\alpha}/2)} - \frac{\sin(3\hat{\alpha})}{\sin^2(3\hat{\alpha}/2)}\right),$$

being $\hat{\alpha} = 2\pi\alpha$. Note that b_1 has vertical asymptotes for $\alpha = 0$ and $\alpha = 1/3$. The same values of α correspond to asymptotes of b_2 which also has $\alpha = 1/4$ as an asymptote. The coefficient b_1 becomes zero for $\hat{\alpha} = 2\arcsin\sqrt{5/8}$. Around that value non-twist phenomena occur (see [31]).

Consider the 1:5 resonance and $\alpha = 0.21$. For this value $b_1 \approx -0.0341669659295153$, and the corresponding radius predicted by formula (15) is $r_* \approx 0.540999411522355$. We note that this value is affected by the near-the-identity change of variables to get the normal form from which expression (15) is obtained. Figure 4 shows the 1:5 resonance for $\alpha = 0.21$ of the map (1) and the average radius r_*. Note that in this illustration the value r_* is far from being small. Still a relatively good agreement with the theory is found.

To see how the width of a resonance zone evolves when changing the parameter we have chosen the 1:7 resonance for the Hénon map. Figure 5 shows the expected behaviour, that is, a growth rate of order $\delta^{7/4}$. The oscillations with respect to the predicted behaviour can be explained in terms of the higher order harmonics of the perturbations on the islands (see [28]). We note also that we have measured the width in the original coordinates of (1) and not in the BNF ones.

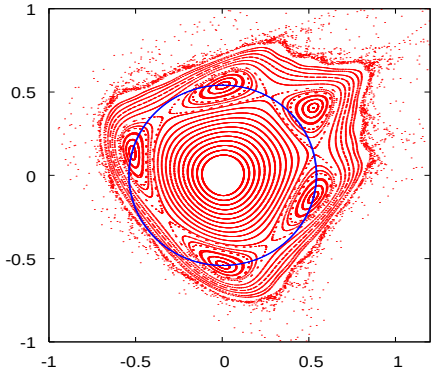

Figure 4: Resonance 1:5 of map (1) for $\alpha = 0.21$ and the approximated radius r_* (see text).

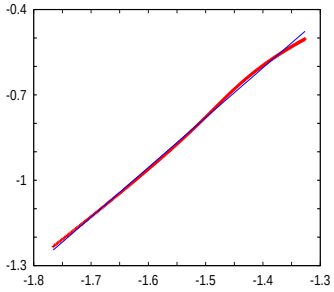

Figure 5: Hénon map (1), 1:7 resonance: in the x-axis it is represented $\log_{10}(\delta)$ and in the y-axis we plot the $\log_{10}$ of the width of the resonant island having the elliptic 7-periodic point located on the symmetry axis. The fitted straight line is $ax + b$ with $a = 7/4$ and $b \approx 1.84512$.

3.4 A Hamiltonian model around a generic resonance

Hamiltonian (11) describes, in particular, the dynamics in a narrow strip, of width $\mathcal{O}(I_*^{m/4})$ (for a suitable $\nu > 0$ depending on m, e.g. $\nu \leq m/2 - 2$, see theorem 3.1), containing the resonance of order m, $m > 4$. We can then localise the Hamiltonian around an island of the m-order resonance. Recall that the resonance is located at a distance $I_* \approx -\frac{\delta}{2b_1}$, such that the frequency $\omega(I_*)$ equals zero, value that corresponds to the approximated average between the hyperbolic and elliptic periodic point distances from the origin. Let λ be the dominant eigenvalue of the hyperbolic m-periodic point of F. Note that $\log(\lambda)$ is the dominant eigenvalue of the interpolating flow already computed in the proof of lemma 3.1.

Proposition 3.1 *For a generic APM F such that $\alpha = q/m + \delta$, $1 \leq q < m$, $m \geq 5$, $\delta < 0$, $b_1 > 0$, $b_2 \neq 0$, the dynamics around an island of the m-resonance strip can be modeled, after suitable scaling, by the time-γ map, with $\gamma = \log(\lambda)(1 + \mathcal{O}(\delta)) = \mathcal{O}(\delta^{m/4})$, of the flow generated by Hamiltonian*

$$\mathcal{H}(J, \psi) = \frac{1}{2}J^2 + \frac{c}{3}J^3 - (1 + dJ)\cos(\psi), \tag{16}$$

where

$$c \approx \frac{b_2}{\sqrt{m\pi}\ b_1^{\frac{6+m}{4}}}\ |\delta|^{\frac{m}{4}}, \quad d \approx \frac{\sqrt{m}}{2\sqrt{\pi}\ b_1^{\frac{m-2}{4}}}\ |\delta|^{\frac{m}{4}-1}.$$

In the (J, ψ) variables the resonant zone has a width $\mathcal{O}(1)$ and the above approximation gives an error $\mathcal{O}(\delta^{\frac{m+2}{4}})$ in that zone.

Remark. Later on we shall need flow approximations in a larger domain in $\mathbb{C}^2$ and (16) will be slightly modified. Details are postponed till Section 5, where this extension will be required.

Proof. By means of the translation $\tilde{I} = I - I_*$ Hamiltonian (11) is transformed to

$$\mathcal{H}(\tilde{I}, \varphi) = \pi \sum_{n=0}^{s} \frac{b_n}{n+1} \left(2\left(\tilde{I} + I_*\right)\right)^{n+1} + \frac{1}{m}\left(2\left(\tilde{I} + I_*\right)\right)^{\frac{m}{2}} \cos(m\varphi),$$

which, expanding the sum in the Hamiltonian, can be expressed as

$$\mathcal{H}(\tilde{I}, \varphi) = \sum_{k=0}^{s+1} \frac{1}{k!} \left.\frac{d^k \mathcal{H}_{nr}(I)}{dI^k}\right|_{I=I_*} \tilde{I}^{\,k} + \frac{1}{m}\left(2\left(\tilde{I} + I_*\right)\right)^{\frac{m}{2}} \cos(m\varphi). \tag{17}$$

From theorem (3.1), since $\tilde{I} << I_*$, the error of the time-one map determined by the flow defined by the above Hamiltonian with respect to the near-the-identity map $\hat{K}$ is $\mathcal{O}(I_*^{\frac{m+1}{2}})$.

In order to focus on a concrete island we introduce $J = \tilde{I}/m,\ \psi = m\varphi$. Assuming the studied resonance to be close to the origin (or in general, close to the invariant object around which we consider the normal form approach), Hamiltonian (17), truncated to third order, can be expressed in terms of Birkhoff coefficients as

$$\mathcal{H}(J, \psi) = \frac{C}{2}J^2 + \frac{D}{3}J^3 + (d_1 + d_2 J)\cos(\psi),$$

where $C = 4\pi b_1 m^2 + \mathcal{O}(\delta)$, $D = 8\pi b_2 m^3 + \mathcal{O}(\delta)$, $d_1 = \frac{1}{m}(2I_*)^{\frac{m}{2}}$, and $d_2 = m(2I_*)^{\frac{m}{2}-1}$. We shall take into account later the error due to the neglected terms.

Rescaling J in such a way that C becomes equal to 1, which means $\tilde{J} = CJ$, one obtains that the dynamics is described by the flow of the following Hamiltonian

$$\mathcal{H}(\tilde{J}, \psi) = \frac{1}{2}\tilde{J}^2 + \frac{\tilde{D}}{3}\tilde{J}^3 + (\tilde{d_1} + d_2\tilde{J})\cos(\psi),$$

where $\tilde{D} = D/C^2$ and $\tilde{d_1} = Cd_1$.

By means of the transformation $\tilde{J} = \gamma\hat{J}$, $t = \gamma^{-1}\tau$, and skipping again higher order terms the vector field is expressed, with respect to the new time τ, as

$$\hat{J}' = \left(\frac{\tilde{d_1}}{\gamma^2} + \frac{d_2}{\gamma}\hat{J}\right)\sin\psi, \qquad \psi' = \hat{J} + \tilde{D}\gamma\hat{J}^2 + \frac{d_2}{\gamma}\cos\psi.$$

By choosing $\gamma = \sqrt{\tilde{d_1}} = \mathcal{O}(\delta^{m/4})$ and using again simply J to denote $\hat{J}$, the vector field can be rewritten as

$$\dot{J} = (1 + dJ)\sin\psi, \qquad \dot{\psi} = J + cJ^2 + d\cos\psi,$$

where $d = \dfrac{d_2}{\gamma} = \mathcal{O}\left(\delta^{\frac{m}{4}-1}\right)$ and $c = \tilde{D}\gamma = \mathcal{O}\left(\delta^{\frac{m}{4}}\right)$. Hence, the final Hamiltonian becomes

$$\mathcal{H}(J, \psi) = \frac{1}{2}J^2 + \frac{c}{3}J^3 - (1 + dJ)\cos\psi,$$

where the change $\psi \mapsto \pi - \psi$ has been done on the ψ phase in order to have the elliptic point close to the origin. Furthermore, as the final vector field has eigenvalues $\pm 1 + o(1)$, we check that the dominant terms of γ and $\log(\lambda)$ coincide.

The dominant part of the error in the vector field, expressed in the final (J, ψ) variables, comes from terms $\gamma^2 J^3$ and $\mathcal{O}(\delta^{\frac{m}{2}-2})J\cos(\psi)$ (or $\mathcal{O}(\delta^{\frac{m}{2}-2})J^2\sin(\psi)$). They give a contribution $\mathcal{O}(\delta^{\frac{m}{2}-2})$. Furthermore, as we have the time-γ flow, the error in the map is $\mathcal{O}(\delta^{\frac{3m}{4}-2})$. On the other hand, the error due to the truncation of the BNF is $\mathcal{O}(\delta^{\frac{m+1}{2}})$, as stated in theorem 3.1. It becomes $\mathcal{O}(\delta^{\frac{m+2}{4}})$ when we express it in the variables (J, ψ). The minimum of the exponents $\frac{3m}{4} - 2$ and $\frac{m+2}{4}$ is $\frac{m+2}{4}$ for $m \geq 5$. □

Remarks.

1. The sign of c is equal to the sign of the second Birkhoff's coefficient (if $b_1 > 0$). On the other hand, d is always positive. Moreover, the modulus of c is less than the one of d for δ small enough, and both c and d are larger than the error terms for $|\delta|$ small.

2. In the scaling above it is assumed $b_1 > 0$. Otherwise, we must take $\gamma = \sqrt{-\tilde{d}_1}$ and the Hamiltonian takes the form
$$\mathcal{H}(J, \psi) = \frac{1}{2}J^2 + \frac{c}{3}J^3 + (1 - dJ)\cos\psi.$$

3. It is only necessary to consider one of the two cases above, for instance, $b_1 > 0$. In fact, changing the phase of ψ, $\psi \mapsto \psi + \pi$, in order to have the elliptic point located at the origin we reduce to the case $b_1 > 0$ where it is necessary to assume now $d < 0$.

   On the other hand, the change $J \mapsto -J$, $t \mapsto -t$, produces a change of sign of the constants. Hence, one can reduce the Hamiltonian to the case $d \geq 0$ and $|c| < d$. If $b_1 < 0$ we reduce to the same type of Hamiltonian with positive d but the sign of c is minus the sign of b_2.

In order to justify our choice of model (16) some considerations must be done. When $c = d = 0$ the model corresponds to a classical pendulum. The first Birkhoff coefficient effect (parameter d) becomes relevant when studying the behaviour of the inner and outer splittings of the island. It turns out that if $d \neq 0$ both splittings are of different order of magnitude (see section 5).

Concerning the J^3 twist term (parameter c), as observed in the proof, its effect has no dynamical relevance (for values of δ small enough) in comparison with the d parameter which is larger. But the coefficient c is necessary to check if the splittings of an island in a small neighbourhood of the elliptic point do "oscillate" or not (section 5.6).

A more dynamically important reason to consider a perturbation in the twist of the map is the following. Far from the elliptic point, that is for values of δ relatively large (see section 3.5), c could be not necessarily small (in general, both coefficients c and d are expected to be arbitrary). In particular, the outer splitting could be smaller than the inner or any splitting could be able to oscillate. Some considerations on the behaviour of the splittings far from the elliptic points are given in section 5.8.

3.5 A model away from the elliptic fixed point

Dynamics in an annulus containing a $q : m$, $0 < q < m$, $(q, m) = 1$, $m \geq 5$ resonance far away from the elliptic point can be studied by means of a perturbation of an integrable twist map. To find a Hamiltonian flow modeling a non-integrable twist map in a suitable annulus we reduce it to a normal form and compute the m-th iterate of the map to have a near-the-identity map. A straightforward computation of the Hamiltonian reduces the model to one similar to the one obtained around a fixed point.

Consider a twist map $F_\mu : (I, \varphi) \mapsto (\bar{I}, \bar{\varphi})$, μ a perturbative parameter, defined by $\bar{I} = \partial S_\mu / \partial \bar{\varphi}$, $\varphi = \partial S_\mu / \partial I$, being S_μ the generating function $S_\mu(I, \bar{\varphi}) = I\bar{\varphi} - \beta(I) - \mu \sum_{j\geq 1} \sum_{s\geq 0} \delta_{js} I^s \cos(j(\bar{\varphi} - \psi_{js}))$, with $\beta(I) = I\Delta + \sum_{k\geq 2} \beta_k I^k/k$, $\Delta = 2\pi q/m$. One can always assume $I = 0$ at resonance.

Introducing $\alpha_{jk} = j(\varphi + \Delta - \psi_{jk})$ and scaling $I = K\nu$, $\nu^2 = \pm\mu$, the corresponding map $\hat{F}_\nu : (K, \varphi) \mapsto (\bar{K}, \bar{\varphi})$ up to second order in ν is

$$\begin{aligned} \bar{\varphi} &= \varphi + \Delta + \nu\beta_2 K + \nu^2 \left(\beta_3 K^2 + \textstyle\sum_{j\geq 1} \delta_{j1} \cos(\alpha_{j1})\right) + \mathcal{O}(\nu^3), \\ \bar{K} &= K + \nu \textstyle\sum_{j\geq 1} j\delta_{j0} \sin(\alpha_{j0}) + \nu^2 K \left(\sum_{j\geq 1} \left\{ j\delta_{j1} \sin(\alpha_{j1}) + \beta_2 j^3 \delta_{j0} \cos(\alpha_{j0}) \right\}\right) + \mathcal{O}(\nu^3). \end{aligned} \tag{18}$$

Let $\mathbb{Z}_* = \mathbb{Z} \setminus \{0\}$. The near-the-identity change of variables $(\varphi, K) \to (\theta, J)$ defined by the generating function $\hat{h}_1(\theta, K) = K\theta + \nu h_1(\theta)$, where $h_1(\theta) = \sum_{j\in\mathbb{Z}_*} \eta_j e^{ij\theta}$ with $\eta_j = i\delta_{j0} \exp(ij(\Delta - \psi_{j0}))/(\exp(ij\Delta) - 1)$, if $j \neq nm$, $n \in \mathbb{Z}_*$, and $\eta_j = 0$ otherwise, allows to cancel the harmonics with $j \neq nm$.

We assume that the effect of the harmonics of order higher than m that cannot be removed is negligible (for an analytic function the amplitudes decay, so we assume they decay fast enough to be neglected). Keeping just the first relevant term, map (18) in the new coordinates up to order 3 reads

$$\begin{aligned} \bar{\theta} &= \theta + \Delta + \nu\beta_2 J + \nu^2 \left(\beta_3 J^2 + \textstyle\sum_{j\geq 1} \delta_{j1} \cos(\alpha_{j1}) - \sum_{j\in\mathbb{Z}_*} ij\eta_j \exp(ij\theta)\right) + \mathcal{O}(\nu^3), \\ \bar{J} &= J + \nu m \delta_{m0} \sin(\alpha_{m0}) + \\ &\quad + \nu^2 J \left(\textstyle\sum_{j\geq 1} \left\{ j\delta_{j1} \sin(\alpha_{j1}) + \beta_2 j^3 \delta_{j0} \cos(\alpha_{j0}) \right\} - \sum_{j\in\mathbb{Z}_*} j^2 \eta_j \exp(ij(\theta + \Delta))\right) + \mathcal{O}(\nu^3). \end{aligned} \tag{19}$$

Then, a change of variables $(J, \varphi) \to (T, \xi)$ with generating function of the form $\hat{h}_2(J, \xi) = J\xi + \nu^2 J h_2(\xi)$, where $h_2(\xi) = \sum_{j\in\mathbb{Z}_*} \tilde{\eta}_j \exp(ij(\xi))$ with $\tilde{\eta}_j = (\delta_{j1} \exp(ij(\Delta - \psi_{j1})) - ij\eta_j)/(\exp(ij\Delta) - 1)$ if $j \neq nm$, $n \in \mathbb{Z}_*$, and $\tilde{\eta}_j = 0$ otherwise, allows, as before, to cancel the harmonics with $j \neq nm$, $n \in \mathbb{Z}$. Keeping just the first non-removable harmonic the map (19) is reduced to a map $NF(F) : (T, \xi) \mapsto (\bar{T}, \bar{\xi})$ given by

$$\begin{aligned} \bar{\xi} &= \xi + \Delta + \nu\beta_2 T + \nu^2 \left(\beta_3 T^2 + \delta_1 \cos(m(\xi - \psi_1))\right) + \mathcal{O}(\nu^3), \\ \bar{T} &= T + \nu m \delta_0 \sin(m(\xi - \psi_0)) + \nu^2 T \left(m\delta_1 \sin(m(\xi - \psi_1)) + \beta_2 m^3 \delta_0 \cos(m(\xi - \psi_0))\right) + \mathcal{O}(\nu^3), \end{aligned}$$

where $\delta_j = \delta_{mj}$ and $\psi_j = \psi_{mj}$, $j = 0, 1$.

Denote by (T_m, ξ_m) the m iterate of the map $NF(F)$, that is, $(T_m, \xi_m) = NF(F)^m(T, \xi)$. A direct computation gives

$$\begin{aligned} \xi_m &= \xi + m\nu\beta_2 T + \nu^2 \left(m\beta_3 T^2 + m\delta_1 \cos(m(\xi - \psi_1)) + \gamma \cos(m(\xi - \psi_0))\right) + \mathcal{O}(\nu^3), \\ T_m &= T + \nu m^2 \delta_0 \sin(m(\xi - \psi_0)) + \nu^2 T \left(m^2 \delta_1 \sin(m(\xi - \psi_1)) + \kappa \cos(m(\xi - \psi_0))\right) + \mathcal{O}(\nu^3), \end{aligned}$$

where $\gamma = \frac{m^3(m-1)}{2}\beta_2\delta_0$, and $\kappa = \frac{m^4(m+1)}{2}\beta_2\delta_0$.

The map $NF(F)^m$ is a near-the-identity map such that can be interpolated by the time-one map of a Hamiltonian flow. If we require interpolation up to order 3, the corresponding Hamiltonian is $H(J, \varphi) = \beta_2 J^2/2 + \delta_0 \cos(\varphi) + \nu\beta_3 J^3/3 + \nu J(\delta_1 \cos(\varphi - \psi) - m/2\delta_0\beta_2 \sin(\varphi))$, which is obtained after scaling the time by νm, changing the phase to have $\psi_0 = 0$, denoting by ψ the new phase in the term in $J\cos(\varphi)$ and denoting by J and φ the corresponding action-angle variables. This Hamiltonian can be written in the form

$$H(J, \varphi) = \beta_2 J^2/2 + \nu\beta_3 J^3/3 + (d_0 + \nu d_1 J)\cos(\varphi) + \nu J k \sin(\varphi), \tag{20}$$

for suitable parameters d_0, d_1 and k.

Remark. The sinus term of the Hamiltonian above can be eliminated by choosing the change of variables generated by $\hat{h}_1(\theta, K)$ to cancel the corresponding $\mathcal{O}(\nu)$-terms such that it modifies the m-harmonic (which cannot be canceled) in a suitable way: define $\hat{h}_1(\theta, K) = K\theta + \nu\bar{h}_1(\theta)$, where $\bar{h}_1(\theta) = h_1(\theta) + 2\eta_m \sin(m(\theta - \psi_{m0}))$, $\eta_m = \delta_{m0}\beta_2/4$, and proceed as before. It is, then, a consequence of the non-uniqueness of the normal form ([15]). The model then becomes

$$H(J, \varphi) = \beta_2 J^2/2 + \nu\beta_3 J^3/3 + (\tilde{d}_0 + \nu\tilde{d}_1 J)\cos(\varphi),$$

which reduces to a Hamiltonian of the form (16) chosen as a suitable model to study dynamics in resonances close to an elliptic fixed point. When close to the elliptic fixed point the coefficients of the Hamiltonian are powers of δ but $\beta_2, \beta_3, \tilde{d}_0, \tilde{d}_1$ can be arbitrary around an invariant curve.

4 Strong resonances.

The normal form (8) derived above has the important property of having the resonant terms of order higher than the term which multiplies the first Birkhoff coefficient. This gives to the BNF a local structure of twist map around the elliptic fixed point. When considering a strong resonance, that is, $\alpha = q/m + \delta$ with $m < 5$ this property is violated. It is possible that the fixed point at the origin becomes unstable or remains stable (see [30]). In both cases the dynamics in a neighbourhood of the fixed point suffers changes due to this fact (see [21, 2]). See also [14] for a similar discussion for $m \leq 3$.

4.1 The saddle-center bifurcation and the second order resonance.

We start our brief discussion about strong resonances by considering $m = 1$. The linearised map can be the identity but generically it is a Jordan block with eigenvalues equal to 1. It corresponds then to a particular (conservative) case of the Bogdanov-Takens bifurcation [7] or, more precisely, to the saddle-center bifurcation (see [26, 8]). When crossing the critical value an elliptic fixed point and a hyperbolic one are created generically, with eigenvalues close to 1. The invariant manifolds of the hyperbolic one form a loop surrounding the elliptic point. Generically, unless the map is integrable, the invariant manifolds do not coincide and have an exponentially small splitting. The limit Hamiltonian flow generated by

$$H(x, y) = y^2/2 - \nu x - x^3/3 + \mathcal{O}(x^4, y^3)$$

(similar to the flow interpolating version (5) of the Hénon map for c small) has a loop formed by the separatrix of the saddle bounding a domain foliated by invariant curves if $\nu < 0$ (otherwise there are not fixed points). A Cantorian set of invariant curves subsists for the symplectic map, up to an exponentially small (in c or in the relevant parameter) distance of the limit separatrix. After the bifurcation one can consider BNF approach around the elliptic fixed point, as before.

When considering $m = 2$ the Jacobian of the map can be minus the identity but generically we have a Jordan block with eigenvalues equal to -1 (see [30]). We note that F^2 has a pitchfork bifurcation. A limit flow approximates F^2 in a similar way to the $m = 1$ case. In this case,

$$H(x, y) = y^2/2 + \nu x^2/2 \pm x^4/4 + \mathcal{O}(x^5, y^3).$$

The difference with the case $m = 1$ is that the fixed point exists, locally, for all values around the bifurcation point. If the sign + of the x^4 term is considered the fixed point passes from elliptic

to hyperbolic with reflexion, i.e., with negative eigenvalues when ν crosses 0 decreasing. At the bifurcation a period two elliptic orbit appears. For $\nu < 0$ we obtain a figure eight (the invariant manifolds of the hyperbolic point form two loops surrounding the elliptic points). Otherwise, for $\nu > 0$ the origin is an elliptic fixed point. In the last case expressing the truncated Hamiltonian $H(x, y) = y^2 + \nu x^2$ in Poincaré variables we found the Hamiltonian (11) for $m = 2$. On the other hand, if the sign $-$ of x^4 is considered the fixed point passes from a hyperbolic ($\nu > 0$) to an elliptic one ($\nu < 0$) and a period two hyperbolic point appears for $\nu < 0$. The invariant manifolds of the two periodic hyperbolic points form a pendulum like phase space figure surrounding the elliptic fixed point.

4.2 The third order resonance.

When considering the strong resonance $m = 3$ ($q = 1$) the normal form around the elliptic fixed point E_0 has a term of degree two which plays a relevant role in the dynamics. The BNF, being $\lambda = e^{\frac{2\pi}{3}i}$ at exact resonance, can be written as

$$z \mapsto \lambda(z + \tilde{c}\bar{z}^2 + a_1 z^2 \bar{z} + \cdots).$$

Therefore, the dominant part of the Hamiltonian approximation is given, in the generic case, by

$$H(I, \varphi) = \epsilon I + AI^2 + BI^{\frac{3}{2}} \cos(3\varphi),$$

with $A, B \in \mathbb{R}$, as it is deduced from (11) in this particular case, where ϵ plays the role of δ, that is, $\lambda = \exp(\frac{2\pi+\epsilon}{3}i)$. After scaling the I variable by $\hat{I} = A^2 I/B^2$, the time t by $\tau = tA^3/B^4$ and the change of the phase variable φ by $\hat{\varphi} = \varphi + \pi/3$ if it is necessary (in case $AB < 0$), the corresponding Hamiltonian has the form

$$H(I, \varphi) = \hat{\epsilon} I + I^2 + I^{\frac{3}{2}} \cos(3\varphi), \tag{21}$$

where $\hat{\epsilon} = \epsilon A/B^2$. The time-1 flow of (21) reproduces F^3 in a ball of radius $M\hat{\epsilon}$ (in (x, y) coordinates), with M large enough to contain the interesting local dynamics, with error $\mathcal{O}(\hat{\epsilon}^5)$. See section 6 for the use of a different scaling.

The evolution of the phase space of the vector field associated to (21) when moving $\hat{\epsilon}$ is described in figure 6. If $\hat{\epsilon} < 9/32$ there exist hyperbolic and elliptic fixed points. The hyperbolic fixed points (which become a single parabolic point when $\hat{\epsilon} = 0$) are located at a distance $\mathcal{O}(\hat{\epsilon}^2)$ from the origin, while elliptic ones are located at a finite distance of the origin for all the values of $\hat{\epsilon}$. Hence, the location of these elliptic points, if they exist at all, is strongly influenced by the missing terms in (21). Fixed points of (21) become period 3 points of the map. The separatrices of the Hamiltonian which go up to a finite distance from the origin, due to the location of the elliptic points, are also influenced by the missing terms in (21). If they exist they typically have a splitting of finite size. As a consequence, the rotational invariant curves surrounding the period 3 islands in figure 6 can be destroyed by these separatrices (see [38]).

For the model (21) a saddle-center bifurcation appears at $\epsilon = 9/32$ and the corresponding degenerated point is located at $(3/8, \pi/3)$, hence at a finite distance of the origin (there are two more $2\pi/3$-rotated degenerated points). Hence, the comments on previous paragraph about phenomena at finite distance also apply here. On the other hand, for $\hat{\epsilon} = 0$ the elliptic point is located at $(3/4, \pi/3)$ (there are two more $\pi/3$-rotated elliptic ones). None of the phenomena concerning the elliptic points (creation/destruction, rotation number, stability domain, satellites,...) neither the outer separatrices of the 3-periodic orbit can be then analysed by a perturbative approach around the origin. A similar analysis of the 1:3 resonance can be found in [6].

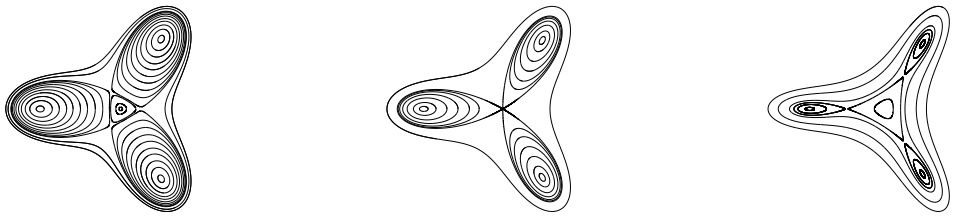

Figure 6: Sketch of the phase space of (21) for $\hat{\epsilon} < 0$ (left), $\hat{\epsilon} = 0$ (centre), and $\hat{\epsilon} > 0$ (right).

4.2.1 Application to the Hénon map

Figure 7 shows the transition through the third order resonance for the Hénon map (1). We note that coefficients A and B of Hamiltonian (21) are both finite for that map, implying a generic behaviour. The corresponding parameter $\hat{\epsilon}$ is decreasing with respect to α.

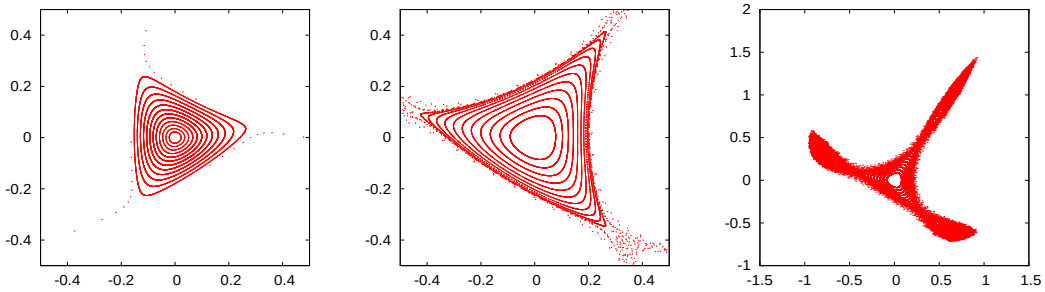

Figure 7: Dynamics of the Hénon map (1) close to the 1:3 resonance. The plots correspond to $\alpha = 1/3 + \nu$ (left) and $\alpha = 1/3 - \nu$ (center and right), with $\nu = 1/75$. Compare with figure 6. Note that the case equivalent to the central plot in figure 6 is missing. See figure 9 for that case.

The elliptic-hyperbolic 3-periodic points E_3, H_3 observed in figure 7 right are created in a saddle-node bifurcation which takes place at $\alpha = \arccos(1 - \sqrt{2})/(2\pi) \approx 0.31797$, or, in the notation of (5) at $c = \sqrt{2}$ for $x = -y = 1/\sqrt{2}$, i.e., at finite distance from the elliptic fixed point E. Increasing α the hyperbolic points H_3 go to E (as predicted by the Hamiltonian approximation (21)) and the E_3 points remain at a finite distance. For $\alpha = 1/3$ the H_3 collide with E. At the same value, the E_3 points suffer a period-doubling bifurcation and they become hyperbolic with reflexion. These facts, concerning the particular case of the Hénon map, can be directly verified by the following simple computation. The symmetries of the Hénon map (5) imply that one of the E_3 and H_3 points is on the axis $y = -x$. For these points the condition $H_c^3(x, y) = (x, y)$, taking into account that the fixed points are located at $x = \pm 1$, can be reduced to

$$c^2x^2 - 2cx - c^2 + 3 = 0 \qquad \text{and hence} \qquad x(c) = \frac{1}{c} \pm \sqrt{1 - \frac{2}{c^2}}.$$

The trace Tr of $DH_c^3(x(c), -x(c))$ can be directly computed giving

$$Tr = 2(1 + r) - 8r^2(1 - r) \qquad \text{where} \qquad r = \sqrt{c^2 - 2}.$$

Furthermore, the invariant manifolds of the hyperbolic fixed point H almost destroy the islands associated to the E_3 points and they surround the small region of invariant curves around the origin. This makes not easy to observe them for the value of α considered (see figure 9).

Another interesting feature appears when we consider the behaviour of the elliptic fixed point of the Hénon map at the exact bifurcation. The fixed point becomes parabolic under F^3. We can look for the existence of invariant manifolds of that point. To this end we use version (5) and, furthermore shift the elliptic point to the origin by $(\xi, \eta) = (x-1, y+1)$. The corresponding value of c is $3/2$. Then

$$F^3(\xi,\eta) = \left(\xi - 3(\xi\eta - \xi^2/2) + \mathcal{O}_3, \eta - 3(\xi\eta - \eta^2/2) + \mathcal{O}_3\right),$$

where $\mathcal{O}_3$ denote terms $\mathcal{O}(|(\xi,\eta)|^3)$. It is easily checked that F^3 is approximated by the time-1 flow of the Hamiltonian $H = \frac{3}{2}\xi\eta(\xi-\eta)+\mathcal{O}_4$. Using the dominant terms it is found, in particular, that $\eta = 0$ is an approximate invariant curve. Restricted to it the map reads $F^3(\xi,0) = (\xi + 3\xi^2/2 + \mathcal{O}_3, \mathcal{O}_3)$. That is, the right part is unstable and the left one is stable.

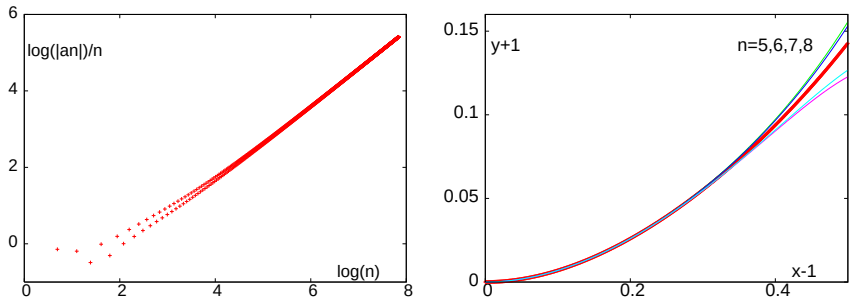

Figure 8: Left: Behaviour of the coefficients of $y+1$ as a graph on $x-1$ for the invariant manifolds at the 1:3 resonance. Right: some approximations of increasing orders.

We can search for an invariant manifold of the form $\eta = g(\xi) = (\sum_{n\geq 2} a_n \xi^n)$, computing in a recurrent way the a_k coefficients from the invariance relation. If h_1, h_2 denote the components of F^3 the condition is $h_2(\xi, g(\xi)) = g(h_1(\xi, g(\xi)))$. Figure 8 left shows the behaviour of the coefficients a_n as a function of n. The values of $\log|a_n|/n$ as a function of $\log(n)$ are plotted. A fit for large n gives a slope close to 1. In contrast to the hyperbolic fixed or periodic points for which the invariant manifolds $W^{u,s}$ are analytic (in fact, they are entire because F is entire) present manifold is only Gevrey 1. This agrees with the theoretical expectations (see [5]). It is immediate to obtain $a_2 = 3/4$, and it has been observed that $a_n > 0$ (resp. $a_n < 0$) if $n > 2$ is congruent with 0,1 (resp. 2,3) modulus 4. The right part in Figure 8 shows low order approximations by $g(\xi)$ truncated to orders between 5 and 8. See [32] for estimates of the behaviour of the error for small values of ξ for Gevrey 1 expansions. Figure 9 shows the invariant manifolds of the 1:3 resonance for the Hénon map. Note that the unstable branches intersect the stable manifold of the hyperbolic fixed point, whose unstable manifold goes to infinity. This implies the escape to ∞ for points in any neighbourhood of E. Experimentally it has been observed that all points of a neighbourhood, except E and the stable branches of the manifold, escape. Period-3 islands are also displayed in figure 9.

4.3 The fourth order resonance.

Similarly to the third order resonance the study of the fourth order one is reduced, in generic cases, to describe the dynamics of Hamiltonian

$$H(I,\varphi) = \hat{\epsilon} I + AI^2 + BI^2\cos(4\varphi),$$

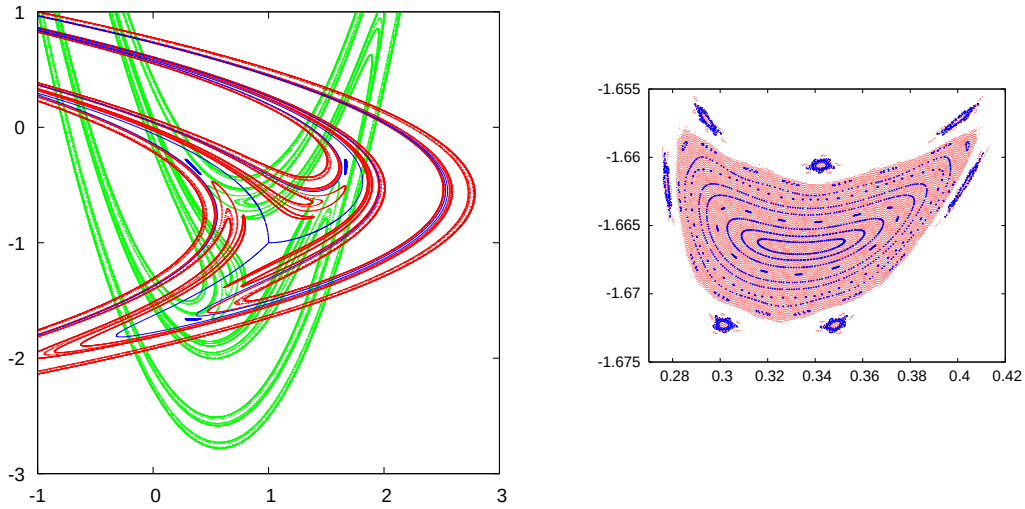

Figure 9: Invariant manifolds of the hyperbolic fixed point (red for W^u, reaching x-values close to 2.8, and green for W^s) and of the degenerated fixed point of the origin (in blue the unstable branches). The existence of intersection between them means that no rotational invariant curve exists. The plot corresponds to (5) with $c = 3/2, \alpha = 1/3$. The three small blue spots show the period-3 islands. A magnification of one of them is shown on the right. Note that inside the islands the period-3 points E_3 are at a period-doubling for this value of c.

with $A, B \in \mathbb{R}$ and where we always assume $A \neq 0$. After the change of variables $\hat{I} = \sqrt{|A|}I$, and changing the phase $\hat{\varphi} = \varphi + \pi/4$ if it is necessary, the Hamiltonian is reduced to

$$H_{\pm}(I, \varphi) = \epsilon I \pm I^2 + \xi I^2 \cos(4\varphi),$$

where $\xi = B/A$ and $\epsilon = \hat{\epsilon}/\sqrt{|A|}$, the sign + corresponding to the case $A > 0$ and we use again I instead of $\hat{I}$. Moreover, by changing the time t by $\tau = -t$ and the phase as before one can always consider the + sign in front of I^2 and $\xi < 0$, hence

$$H(I, \varphi) = \epsilon I + I^2 + \xi I^2 \cos(4\varphi). \tag{22}$$

The dynamics is then described for a fixed parameter ξ as a function of ϵ. We distinguish between $\epsilon > 0$ and $\epsilon < 0$. Figure 10 shows the different cases in the phase space when moving ϵ and ξ and assuming the generic condition $\xi \neq -1$ holds. Similar to the case of the third order resonance, the time-1 flow of (22) reproduces F^4 in a ball of radius $M\epsilon^{1/2}$ (in (x, y) coordinates), with M large enough to contain the interesting local dynamics, with error $\mathcal{O}(\epsilon^{5/2})$.

The fixed points of (22) are $p_1 = (-\epsilon/(2 + 2\xi), 0)$ and $p_2 = (-\epsilon/(2 - 2\xi), \pi/4)$ (besides the $\pi/2$-rotationally symmetric ones). Point p_1 appears if: (i) $\epsilon > 0$ and $\xi < -1$ or (ii) $\epsilon < 0$ and $-1 < \xi < 0$. In case (i) it is hyperbolic and elliptic in case (ii). Point p_2 appears if $\epsilon < 0$ for all $\xi < 0$ and it is hyperbolic. As a consequence, the families of periodic points of the map, if they exist, are located at a distance of order ϵ from the origin in the I variable. The implicit function theorem guarantees again that they subsist for the full map if ϵ is sufficiently small. As said above the case $\xi = -1$ is exceptional.

Concerning the case $\epsilon < 0$ and $-1 < \xi < 0$ (top right figure 10) note that the relative distance between the elliptic and the hyperbolic 4-periodic points, p_1 and p_2 respectively, is $\mathcal{O}(\epsilon)$. Also the separatrices of p_2 go up to a distance $\mathcal{O}(\epsilon)$.

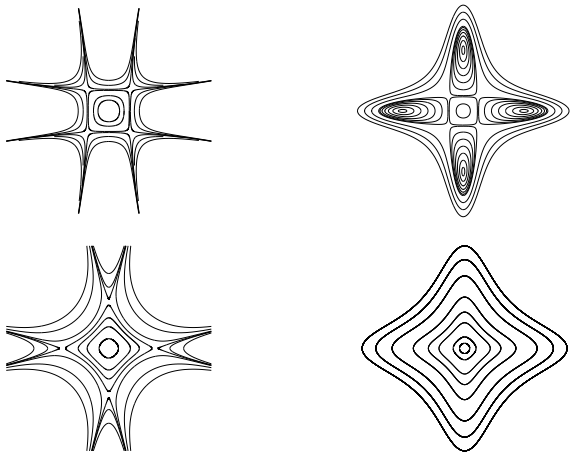

Figure 10: Sketch of the phase portrait of Hamiltonian (22) for $\epsilon < 0$ (1st row) and $\epsilon > 0$ (2nd row). Left (resp. right) plots correspond to $\xi < -1$ (resp. $-1 < \xi < 0$).

4.3.1 The exceptional case $\xi = -1$

When trying to apply the study above to the fourth order resonance of the Hénon map it is found $\xi = -1$. Hence, this bifurcation is not generic for the Hénon map. We are in the exceptional case and higher order terms in the Hamiltonian or in F^4 are needed. First we present an approach to a general discussion in the exceptional case. Later we shall turn to the case of the Hénon map. This case was already considered in [22] however we perform here a complete different analysis.

Note that from (11) we obtain a Hamiltonian flow that exactly interpolates the map up to order 3. In order to get an interpolating Hamiltonian up to order 6 (whose flow interpolates up to order 5 the map) we proceed in a more direct way. Assume first that $\hat{\epsilon} = 0$ (that is, the map is exactly at the fourth order resonance) and consider the normal form up to order 5, skipping the factor i (the rotation) and normalising the resonant term to $i\bar{z}^3$ as before, that is,

$$K(z, \bar{z}) = z + b_1 z^2 \bar{z} + i\bar{z}^3 + b_2 z^3 \bar{z}^2 + cz^5 + dz\bar{z}^4,$$

where $b_1 = b_{1r} + ib_{1i}$, $b_2 = b_{2r} + ib_{2i}$, $c = c_r + ic_i$ and $d = d_r + id_i$ are, a priori arbitrary, complex coefficients.

Consider the maps

$$K_1(z, \bar{z}) = z + b_1 z^2 \bar{z} + i\bar{z}^3 \qquad \text{and} \qquad K_2(z, \bar{z}) = z + b_2 z^3 \bar{z}^2 + cz^5 + dz\bar{z}^4.$$

Then

$$K_2 \circ K_1(z, \bar{z}) = K(z, \bar{z}) + \mathcal{O}(|z|^7).$$

On the other hand, the vector field $\dot{z} = b_1 z^2 \bar{z} + i\bar{z}^3$ interpolates the map K_1 up to order 3. In order to obtain a Hamiltonian vector field the coefficient b_1 must be purely imaginary. Hence,

$$H_4(x, y) = \left(\frac{1 + b_{1i}}{4}\right)(x^4 + y^4) - \left(\frac{3 - b_{1i}}{2}\right) y^2 x^2$$

is the corresponding Hamiltonian.

Moreover, the vector field $\dot{z} = b_2 z^3 \bar{z}^2 + cz^5 + dz\bar{z}^4$, which interpolates map K_2 up to order 5, is Hamiltonian provided $b_{2r} = 0$, $d_i = 5c_i$ and $d_r = -5c_r$ being

$$H_6(x, y) = \frac{1}{6}(b_{2i} + 6c_i)x^6 + 4c_r x^5 y + \frac{1}{2}(b_{2i} - 10c_i)x^4 y^2 + \frac{1}{2}(b_{2i} - 10c_i)x^2 y^4 - 4c_r x y^5 + \frac{1}{6}(b_{2i} + 6c_i)y^6$$

the corresponding Hamiltonian.

As the Lie bracket of both vector fields is of order higher than 5 then Hamiltonian $H(x,y) = H_4(x,y) + H_6(x,y)$ provides an interpolating flow up to order 5 (in the (x,y) variables) of the map K. Expressing Hamiltonian $H(x,y)$ in Poincaré variables it is obtained

$$H(I,\varphi) = b_{1i}I^2 + \frac{4}{3}b_{2i}I^3 + I^2\cos 4\varphi + 8c_iI^3\cos 4\varphi + 8c_rI^3\sin 4\varphi.$$

When $\hat{\epsilon} \neq 0$ the Hamiltonian $\hat{H} = \hat{\epsilon}I + H(I,\varphi)$ should be modified by adding the terms coming from the Lie bracket of both vector fields. However, we observe that this adds terms with small coefficients $\mathcal{O}(\hat{\epsilon})$ that do not affect the local dynamics. Hence, after a suitable scaling, we reduce the study of the degenerate case $b_{1i} = -1$ to the study of a Hamiltonian of the form

$$H(I,\varphi) = \epsilon I + I^2 + AI^3 - I^2\cos(4\varphi) + BI^3\cos(4\varphi) + CI^3\sin(4\varphi). \tag{23}$$

The vector field associated to $\epsilon I + H_4(I,\varphi)$ (generated by Hamiltonian (23) ignoring $\mathcal{O}(I^3)$ terms, compare with (22)) has for $\epsilon < 0$ a hyperbolic fixed point $p_1 = (-\epsilon/4, \pi/4)$. On the other hand, the vector field becomes degenerated on $\varphi = 0$. In this case, considering $\sin(4\varphi) = \mathcal{O}(\varphi)$ and $\cos(4\varphi) = 1 + \mathcal{O}(\varphi^2)$ one obtains the equation $\epsilon + 3(A+B)I^2 + \mathcal{O}(\varphi) = 0$ for the nontrivial fixed points close to $\varphi = 0$. Then, for ϵ such that $\epsilon(A+B) < 0$ this implies the existence of an elliptic fixed point at a distance $\mathcal{O}(\sqrt{-\epsilon})$, the distances being expressed in the I variable. Hence, two families of fixed points, hyperbolic points at distance $\mathcal{O}(\epsilon)$ and elliptic points at distance $\mathcal{O}(\sqrt{\epsilon})$, are born when ϵ goes from positive to negative provided $A+B > 0$. Otherwise, if $A + B < 0$, there exists a family of fixed points for $\epsilon > 0$ (elliptic points) and a family of fixed points for $\epsilon < 0$ (hyperbolic points). If $A = -B$ then other scenarios could appear when crossing $\epsilon = 0$ depending on the value of the constant C. However, according to [15] the sinus term can be removed by choosing suitable reduction changes to BNF. This modifies the values of A and B but the reasoning above holds for the new coefficients.

Furthermore, the time-1 flow of (23) reproduces F^4 in a ball of radius $M\epsilon^{1/4}$ (in (x,y) coordinates), with M large enough to contain the interesting local dynamics, with error $\mathcal{O}(\epsilon^{7/4})$.

4.3.2 The 1:4 resonance of the Hénon map

As already said, the 1:4 resonance becomes degenerate for this map. To decide about the local behaviour and the bifurcation of periodic points one has to use, at least, the order 6 discussion above. However we shall proceed in a more direct way, to illustrate the use of a different method.

First we compute the H^4_α for values $2\pi\alpha = \pi/2 + \delta$ using (1). For shortness we shall denote the Hénon map for these values as T_δ. An elementary computation gives

$$T^4_\delta(x,y) = (f,g) = (f_0 + f_1\delta + f_2\delta^2 + f_3\delta^3 + O(\delta^4), g_0 + g_1\delta + g_2\delta^2 + g_3\delta^3 + O(\delta^4)),$$

where it is enough to keep the following approximations, for $f_j, g_j, j = 0,\dots,3$ to compute periodic orbits and their stability

$$f_0 = x + 2x^2y - x^4 - 4xy^3 + 8x^3y^2 + 2y^5 - 4x^5y - 4x^2y^4 - 4x^4y^3 - 4xy^6 + 16x^6y^2 + 24x^3y^5 + y^8 + \dots,$$

$$g_0 = y - 2xy^2 + 4x^3y + y^4 - 2x^5 - 4x^2y^3 + 6x^4y^2 - 4x^6y + x^8 + \dots,$$

$$f_1 = -4y + 2x^2 + 4xy + 2x^3 - 4xy^2 - 4y^3 - 12x^2y^2 + 6y^4 + 4x^5 + 28x^4y + 22xy^4 + \dots,$$

$$g_1 = 4x - 4xy - 2y^2 + 4x^3 + 2x^2y + 4y^3 + x^4 - 12x^2y^2 + 12x^4y - 4x^3y^2 + 2y^5 + \dots,$$

$$f_2 = -8x + 8x^2 + 8xy - 4y^2 - 8x^3 - 27x^2y - 20xy^2 + \dots ,$$
$$g_2 = -8y + 2x^2 + 4y^2 + 4x^3 - 8x^2y + 11xy^2 - 4y^3 + \dots ,$$
$$f_3 = 32y/3 + \dots , \qquad g_3 = -32x/3 + \dots$$

where ... stands for higher order terms that do not affect the computations below. To look for period four points we use $T_\delta^4(x, y) = (x, y)$. We are interested in solutions which emanate from the origin for $\delta = 0$. To this end we consider the Newton polyhedra of $f - x, g - y$, the generalisation of Newton's polygon containing exponents of x, y, δ as coordinates. To decide about the possible dominant terms in the branches of solutions it is enough to use

$$2x^2y - x^4 - 4xy^3 + 2y^5 + \delta(-4y + 2x^2) + \delta^2(-8x) = 0\,,$$
$$-2xy^2 + 4x^3y + y^4 - 2x^5 + \delta(4x - 2y^2) + \delta^2(-8y) = 0\,,$$

from which we look for $x = \mathcal{O}(\delta^\alpha), y = \mathcal{O}(\delta^\beta)$. An analysis of these equations shows that only

$$\alpha = 1/2,\ \beta = 1/2, \qquad \alpha = 1/4,\ \beta = 1/2, \qquad \alpha = 1/2,\ \beta = 1/4$$

are possible. Furthermore, due to the symmetry, it is enough to consider $\alpha \le \beta$.

Using this information it is possible to solve the equations by iteration in powers of $\delta^{1/2}$ or $\delta^{1/4}$. The solutions are

$$x = \sqrt{2}\delta^{1/2} + \delta + \mathcal{O}(\delta^{3/2}), \quad y = x + \mathcal{O}(\delta^{3/2}),$$

in which case $Tr = 2 + 64\delta^2 + \mathcal{O}(\delta^3)$, a hyperbolic periodic orbit, and

$$x = \gamma\delta^{1/4} + \delta^{3/4}/\gamma + \delta + \mathcal{O}(\delta^{5/4}), \quad y = \sqrt{2}\delta^{1/2} + \delta + \mathcal{O}(\delta^{5/4}),$$

where $\gamma = 8^{1/4}$, for which one obtains $Tr = 2 - 64\sqrt{2}\delta^{3/2} + \mathcal{O}(\delta^2)$, an elliptic periodic orbit.

Figure 11 illustrates how the bifurcation of a hyperbolic and an elliptic periodic orbits occurs when crossing the 1:4 resonance. In particular this shows stability at the exact resonance, a fact already discussed in [30] using different tools. Topologically the transition occurs as in the stable $-1 < \xi < 0$ non-degenerate case. The main difference in the present case is the location of the elliptic periodic orbit and the invariant manifolds of the hyperbolic periodic orbit which go to a distance (in the (x, y) variables) $\mathcal{O}(\delta^{1/4})$ instead of $\mathcal{O}(\delta^{1/2})$ from the central elliptic point.

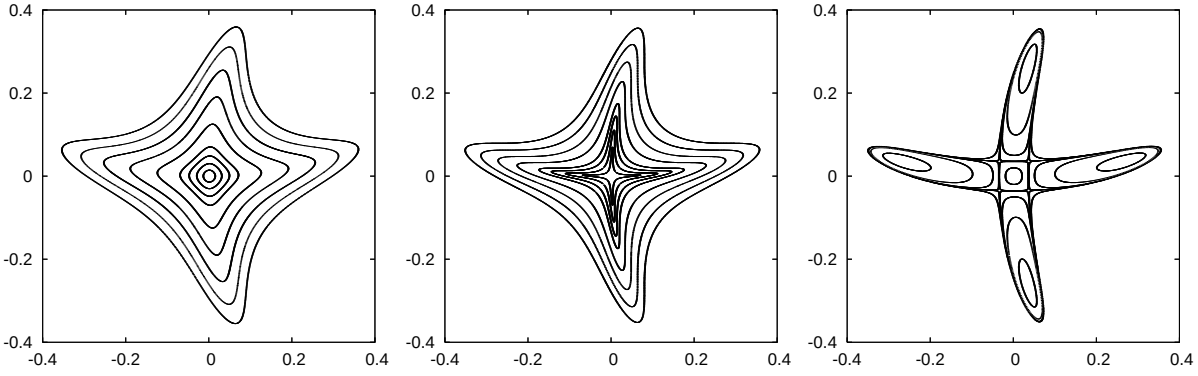

Figure 11: From left to right: some orbits of the Hénon map for $\alpha/(2\pi) = 0.2499$, 0.2500 and 0.2501, respectively.

5 Behaviour of the splittings in a generic resonance

An estimation of how far is an APM from being integrable is given by the splitting of separatrices in a resonance of the phase space. This "distance to integrable", hence, depends on the region where we are studying the map and on the resonance that we consider. In the zones where the map is close to integrable a good description of the dynamics is given by the interpolating flow. A different approach, dealing directly with the diffeomorphism for instance, has to be developed to understand dynamics where the map is not so close to integrable.

As the maps we consider (or a power of them) are ϵ-close to the identity for some small ϵ, the distance between a homoclinic point and its image is $\mathcal{O}(\epsilon)$. Hence, we consider a fixed domain in phase space and in that way we capture homoclinic points for ϵ small enough.

In this section we present first in 5.1 some facts about the splitting of separatrices in generic resonances. Some of the facts rely on rigorous proofs. Other rely on "experimental evidence" but they are presented because they suggest "reasonable assumptions" to be done for the statement of the main result in section 5.6. The result is presented after giving several definitions, several considerations on the location of the singularities and a precise statement of the assumptions. To enhance clearness we add also section 5.5 where the steps to be checked to obtain bounds on the splittings are detailed. Numerical examples on location of singularities and estimates of inner and outer splittings are shown in section 5.7, and some considerations about the behaviour of splittings at finite distance close present section.

5.1 Some preliminary facts about splitting of separatrices

Bounds of the splitting of the separatrices depend on the width of the analyticity strip of the homoclinic orbit of the interpolating Hamiltonian and on the characteristics of the map. The reader is referred to [11] to look for details on the upper bounds of such splitting. It is convenient, however, to sketch here some of the key ideas in [11].

Consider a family of analytic APM ϵ-close to the identity, for $0 < \epsilon < \epsilon_0$, and being close to the time-ϵ flow of an autonomous Hamiltonian $\mathcal{H}$ whose flow is denoted by φ_t and which has a homoclinic loop to a hyperbolic fixed point H: $F_\epsilon(x) = x + \mathcal{O}(\epsilon) = \varphi_{t=\epsilon}(x) + \mathcal{O}(\epsilon^{1+\alpha})$ for some $\alpha > 0$. Keep in mind, as an example, the Hénon map and the limit flow presented in section 2.2. One can assume also that H is the corresponding hyperbolic fixed point for all the family F_ϵ and that the dominant eigenvalue is $\lambda(\epsilon) = 1 + \mathcal{O}(\epsilon)$. To measure the distance between the stable and unstable manifolds $W^{s,u}_\epsilon$ of F_ϵ we can approximate both manifolds by the separatrix of $\mathcal{H}$. Assume this separatrix is given by some real analytic function $\sigma(t)$, which can be extended to $t \in \mathbb{C}$ until $|\mathrm{Im}\, t| < \tau$, where some singularity of σ appears. Choose a value η, perhaps small but fixed, independently of ϵ and consider the strip $\mathcal{S} = \{t \in \mathbb{C} \,|\, |\mathrm{Im}\, t| \leq \tau - \eta\}$. If the maps F_ϵ are entire, then $W^{s,u}_\epsilon$ can be extended to the image of $\mathcal{S}$ by σ. In the non-entire case one has to take a larger value of η so that $\sigma(\mathcal{S})$ do not reaches the singularities of F_ϵ. By the compactness of $\sigma(\mathcal{S})$ and the proximity of F_ϵ and $\varphi_{t=\epsilon}$ one has that both W^s_ϵ and W^u_ϵ are $\mathcal{O}(\epsilon^{1+\alpha})$-close to $\sigma(\mathcal{S})$ and, hence, they are close to each other.

On the other hand the BNF around H (which is convergent in a domain, uniformly in ϵ, see [11]) allows to define a local first integral, to be seen as an energy and transport it along W^u_ϵ. Let us denote that energy as E_u. Then one can evaluate that energy on W^s_ϵ. This function depends on the (complex) parameter used to describe W^s_ϵ and gives a measure of the distance between the manifolds. If a suitable parametrisation of W^s_ϵ is used, say with a parameter q, it turns out that

$E_u(q)$ is periodic with period $h(\epsilon) = \log(\lambda(\epsilon)) = \mathcal{O}(\epsilon)$. Then the amplitudes of the harmonics of $E_u(q)$ can be computed by shifting integrals from some real interval t_0 to $t_0 + h(\epsilon)$ to integrals from $t_0 \pm i\,(\tau - \eta)$ to $t_0 + h(\epsilon) \pm i\,(\tau - \eta)$. It follows that, for $k \neq 0$, the k-th order harmonic is bounded by $\mathcal{O}(-2\pi|k|(\tau-\eta)/h(\epsilon))$. Furthermore the zero-th order harmonic is also bounded by $\mathcal{O}(-2\pi(\tau-\eta)/h(\epsilon))$ because the maps F_ϵ must have homoclinic points (they are APM and close to a flow with a loop. The precise bounds depend on the selected value of η and can be difficult to evaluate in general. Note that as soon as $E_u(q)$ is known, one can compute the distance between W^s_ϵ and W^u_ϵ. In an equivalent way, one can consider, close to some selected homoclinic point and in local coordinates, that W^u_ϵ is the graph of a trivial function $q \to 0$ and W^s_ϵ is the graph of a function $\mathcal{G}$, as before $h(\epsilon)$-periodic in q.

Bounds obtained in such a way are very accurate and, generically, of the same order of magnitude as the splitting. To measure the splitting one can use either the angle between the manifolds on some domain away from the related hyperbolic periodic points or symplectic invariants, like the area of a lobe or the so-called homoclinic invariant (see, e.g., [18]).

To analyse the behaviour of the splittings we note that they are expected to behave not only with an exponentially small bound but more precisely according to an expression like

$$\sigma \sim A(\log\lambda)^B \ \mathrm{Re}\ (\exp(-C/\log(\lambda)))\,, \tag{24}$$

where $A > 0$, B real, C complex with $\mathrm{Re}\, C > 0$ and where λ, as before, is the eigenvalue of modulus greater than one of the hyperbolic fixed/periodic points. This fact has been observed numerically in several examples (see [11, 18]) and it has been proved for some particular cases ([12], based on ideas in [25]). Strong evidences lead to believe that for large families of analytic maps a formula like (24) holds. Later on it will be checked numerically for several resonances in the case of the Hénon map. Hence, suitable assumptions, **A2**, **A3** will be made in section 5.6.

The real part C_r of the constant C of (24) is related to the width of the analyticity strip of the homoclinic orbit of the interpolating Hamiltonian (see above) with the said exception if the maps are not entire. To be precise, let $t = \tau$ denote the closest singularity of the separatrix σ of the interpolating Hamiltonian to the real axis. Then, $C_r = 2\pi\,|\mathrm{Im}\,\tau|$. Moreover, the imaginary part C_i of C is also determined by the position of the singularity τ. In particular, $C_i = 2\pi \mathrm{Re}\,\tau$. We recall that here, and hence in expression (24), the time parametrisation of the solutions of the Hamiltonian is such that the time-$h = \log(\lambda)$ flow approximates the map.

Hence, according to (24),

$$\sigma \sim A(\log\lambda)^B \exp(-C_r/\log(\lambda))\,(\cos(C_i/\log(\lambda)) + o(1))\,, \tag{25}$$

where some phase can also appear in the cos term (eventually, and non-generically, several cos terms with the same value of C_r can appear, see [18]). The angle between the separatrices generically "oscillates", that is, changes sign, provided $C_i \neq 0$ [17, 18]. We will illustrate the agreement of the observed behaviour with formula (24) when dealing with the splitting of the separatrices of hyperbolic periodic points. Oscillatory behaviour is also found in the strong resonance of order four (section 6) and, in particular, for the Hénon map. See comments after assumption **A3** for additional information on these oscillations.

As a preliminary example where the behaviour predicted by (24) is the proper one figure 12 shows the invariant manifolds of the hyperbolic fixed point of the Hénon map (1). As it is expected [11, 13, 16] the splitting is of the form (24) with $C = C_r$ and $C_i = 0$. For $\alpha < 0.1$ the splitting is small. The corresponding values of the parameter c (see Section 2.2) are, approximately, less than 0.2. The dynamics is close to the one of the flow (6).

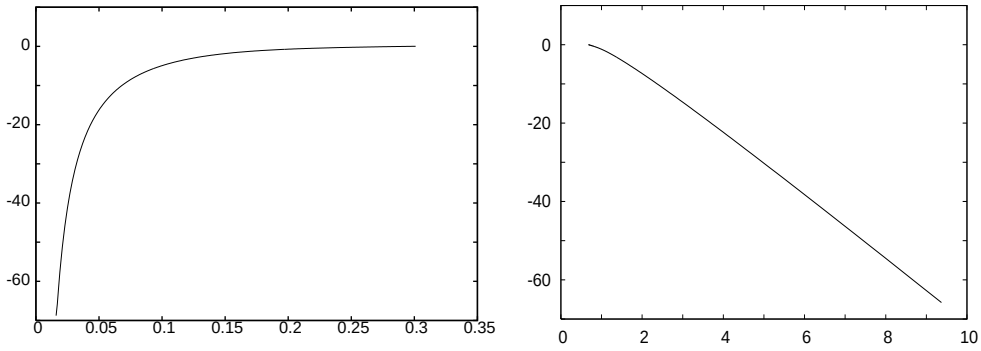

Figure 12: Splitting of the separatrices of the hyperbolic point of the Hénon map (1). Left: The decimal logarithm of the splitting (vertical axis) is represented as a function of α (horizontal axis). Right: The same logarithm is represented as a function of $1/\lambda(\delta)$. The asymptotic slope gives the constant $-C$ in (24).

The importance of the splitting of the separatrices of the fixed point of an APM F relies on the observation made in [20] about the fact that this splitting plays a role when determining the boundary of the stability region of the elliptic fixed point (see also [19, 38, 33, 37, 34]).

Along this section we will analyse the splittings of the resonant islands. Generically, an island of a m-order resonance has different splittings depending on which manifolds (inner or outer) intersect. The goal of this section is to give a proof of this fact in the non-strong resonant case for an APM satisfying suitable conditions and to illustrate it numerically. Section 6 is devoted to the case of low order resonances.

5.2 Inner and outer splittings of a generic island

We start by making precise the idea of inner and outer splittings of an island. As said, we restrict our attention along section 5 to resonances of order $m > 4$. However the inner and outer splitting idea will be used in the strong resonant case also.

Definition 5.1 *Let F be a planar map having a chain of islands $\mathcal{R}$ surrounding the origin. Let $\mathcal{I}$ be an island of the resonance strip $\mathcal{R}$. The* inner (outer) splitting σ_- (σ_+) *of $\mathcal{I}$ is the one with the property of having the closest (farthest) primary homoclinic point to the origin* (see Figure 2).

In the definition "primary" homoclinic points are such that the differences of arguments between the k-periodic hyperbolic points H and the homoclinic ones are close to π/k and, furthermore, the arcs of stable and unstable manifold used to produce the homoclinics intersect only once the ray with the argument of the homoclinic.

5.3 Previous considerations on the location of the singularities

As was stated before the exponential small part of the splitting depends on a constant $C \in \mathbb{C}$ which is itself determined by the position of the singularities of the separatrix of the limit Hamiltonian. The explicit computation of the position of the singularity will be carried out in

the next subsection. In the present one we discuss where they are expected to be in a more general framework.

Consider, in general, a Hamiltonian function of the form

$$\mathcal{H}(J,\psi) = P(J) - Q(J)\cos\psi. \tag{26}$$

Let h be the separatrix level of energy. At this level of energy we have $\cos\psi = \dfrac{P-h}{Q}$. On the other hand, $\dot{J} = Q\sin\psi$, and the relation above implies

$$\dot{J} = \pm\sqrt{Q^2 - (P-h)^2}. \tag{27}$$

Equation (27) describes the variation of J when restricted to the separatrix. We will consider the corresponding equation associated to Hamiltonian (16) and use it to determine the position of the singularities.

We recall that model Hamiltonian (16) has been obtained after suitable scalings. The error in this model is not only small, for δ small enough, but even small with respect to the relevant parameters c and d. Following the approach of [11], we are interested in the Hamiltonian because the invariant manifolds of its separatrix provide a good approximation of the invariant manifolds of the map in the complex phase space, for complex t, provided the imaginary part of t is slightly below the singularities of the separatrix. Restricting t to a compact complex strip whose boundary is close, but bounded away from the singularities, the influence of higher order terms in the map or in the Hamiltonian, can be neglected if δ is small.

Concerning the position of the singularities we note that Hamiltonian (16) can be considered as a perturbation of the classical pendulum $\mathcal{H}(J,\psi) = J^2/2 - \cos\psi$. It is easy to check that the nearest (to the real axis) singularity τ of the classical pendulum is located (both for the inner and outer separatrix) over the imaginary time axis, that is, $\mathrm{Re}\,\tau = 0$, $\mathrm{Im}\,\tau = \pi/2$. However, there is no general theory about how perturbation changes the position of the singularities. Moreover, new singularities could appear and, maybe, they are closer to the real time axis than the old ones. It is not known even how the type of singularities changes under a generic perturbation. But the location of the singularities relevant for the splitting changes mildly for small perturbations. See also assumption **A4** and how it is used in the proof of theorem 5.1.

Nevertheless, it is not hard to see that a homoclinic orbit of the complex flow generated by (16) has singularities on the imaginary time axis. The following proposition, based on results included in [4], assures that, at least, a singularity is on the imaginary axis.

Proposition 5.1 *Consider a system of the form $H(J,\psi) = P(J) - Q(J)\cos(\psi)$ where $P(J)$ is a polynomial of degree ≥ 2 and $Q(J)$ is such that $Q^2(J)$ is a polynomial. Assume*

1. $\deg(P^2) > \deg(Q^2)$, *and*
2. *there exist a point $p = (p_J, p_\psi)$, on the separatrix $H(J,\psi) = h$ such that $z \leq p_J$ for any z real fixed point of (27) and if $z = p_J$ then z is a zero of $Q^2 - (P-h)^2$ with multiplicity one.*

Then the homoclinic orbit has a singularity on the imaginary axis.

Proof. Let $S(J) = Q^2(J) - (P(J) - h)^2$. The singularities of the homoclinic orbit are given by

$$\tau = \pm\int_{p_J}^{k} \frac{dJ}{\sqrt{S(J)}},$$

where $|k| = \infty$, following a suitable complex path, and p_J is the first coordinate of a point p that satisfies assumption 2. We choose the real path of integration $(p_J, +\infty)$. Then,

$$I := \pm i\tau = \int_{p_J}^{+\infty} \frac{dJ}{\sqrt{-S(J)}}.$$

By assumption 1, $\lim_{J\to+\infty} S(J) = -\infty$, hence for $J > p_J$ one has $-S(J) > 0$ by assumption 2. In particular, $I \in \mathbb{R} \cup \{+\infty\}$. Clearly, the convergence of I would imply the result. For any $q > p_J$ assumption 2 provides the convergence in the interval $[p_J, q]$. By hypothesis $S(J)$ is a polynomial. Put $S(J) = a_0 + a_1 + \cdots + a_m J^m$ being $m = \deg(S) = \deg(P^2) \geq 4$, $a_m < 0$. Then, using the change of variables $J = w^{-1}$, it follows

$$\int_q^{+\infty} \frac{dJ}{\sqrt{-S(J)}} = \int_q^{+\infty} \frac{dJ}{\sqrt{-a_0 - a_1 - \cdots - a_m J^m}} = \int_0^{\eta} \frac{dw}{w^2\sqrt{-a_0 - \cdots - \frac{a_m}{w^m}}},$$

with $\eta = q^{-1}$ a finite value. This integral converges since $m \geq 4$. □

Remark. When computing the position of the singularities as an integral on a path going to ∞ one has to take into account that the only singularities of interest for our purpose are the so-called "singularities visible from the real axis". See [18] for definition and details.

5.4 Analytic estimate of the position of the singularities

To analytically compute the singularities τ_+ and τ_- related to the outer and inner separatrices, respectively, of the limit Hamiltonian (16) we note that the equation on the separatrix (27) becomes

$$\dot{J} = \sqrt{\tilde{p}(J)}, \qquad \text{so that} \qquad dt = \frac{dJ}{\sqrt{\tilde{p}(J)}},$$

being $\tilde{p}(J) = Q^2 - (P - h)^2$, $P(J) = J^2/2 + cJ^3/3$, $Q(J) = 1 + dJ$ and $h = 1 + (1 - 6cd - (1 - 4cd)^{3/2})/12c^2$. The value $J = J_h$ corresponding to the position of the hyperbolic points should be a root of $\tilde{p}(J)$ with multiplicity 2 (since $\dot{J}(J_h) = 0$ and because the symmetries of the BNF). Let $p(J)$ be the polynomial of degree four such that $\tilde{p}(J) = (J - J_h)^2 p(J)$.

As we want to estimate the time to reach the singularity for the external and the internal part of the separatrix we have to consider the following integrals

- Singularity of the outer separatrix: $\tau_+ = \displaystyle\int_{z_1}^{k_1} \frac{dJ}{(J - J_h)\sqrt{p(J)}}$,
- Singularity of the inner separatrix: $\tau_- = \displaystyle\int_{z_2}^{k_2} \frac{dJ}{(J - J_h)\sqrt{p(J)}}$,

where z_1 and z_2 are the maximum of the external branch of the separatrix and the minimum of the internal branch, respectively. In particular, z_1 and z_2 are zeros of the polynomial $p(J)$ since they are fixed points of equation (27). On the other hand we expect the singularities to be found when integrating on a real path of the J variable (hence, when the limits of integration are such that $|k_j| = \infty$, $j = 1, 2$).

We look for the closest singularity $\tau_\pm$ to the real axis. In a singularity either $|J| = \infty$ and/or $|\psi| = \infty$. Consider the restriction of a Hamiltonian system of the form (26) to the separatrix

level h of energy. The corresponding vector field has $|\psi| = \infty$ with $|J|$ finite if, and only if, $Q(J) = 0$. For instance, if $Q(J) = 1 + dJ$ then $J = -1/d$ is a particular value where a singularity is found. Nevertheless, in our study of the behaviour of the splittings this singularity, say τ_* defined by $Q(J(\tau_*)) = 0$, plays no role. In fact, τ_* is not a singularity of the separatrix $\sigma(\tau) = \{(J(\tau), \psi(\tau)) \,|H(J(\tau), \psi(\tau)) = h\}$, last assertion meaning that $\sigma(\tau)$ can be extended analytically over it. The reason is that it is not a singularity of the vector field itself but of the change from Cartesian coordinates to a Poincaré variables. Note that the factor $Q(J)$ comes (after some scalings) from the factor $(2I)^{m/2}$ of the resonant part of Hamiltonian (11). Hence, $Q(J) = 0$ if, and only if, $I = 0$. The original vector field in Cartesian coordinates is well-defined but Poincaré variables are not defined at the origin.

Remark. In particular, the elliptic point E_0 around which the BNF is considered is generically (and with infinity codimension) in the closure of the separatrix of any resonance when considering the separatrix as a one-dimensional complex submanifold of $\mathbb{C}^2$.

For simplicity, in the computation of the singularities we distinguish different cases according to the c and d parameters of the limit interpolating Hamiltonian (16).

Case $c = d = 0$. Hamiltonian (16) becomes $H(J, \psi) = J^2/2 - \cos(\psi)$. As said before it corresponds to the non-perturbed pendulum Hamiltonian. The closest outer τ_+ and inner τ_- singularities to the real axis are such that $\operatorname{Re}\tau_+ = \operatorname{Re}\tau_- = 0$ and $\operatorname{Im}\tau_+ = \operatorname{Im}\tau_- = \pi/2$.

Case $d > 0$, $c = 0$. Hamiltonian (16) reads $H(J, \psi) = J^2/2 - (1 + dJ)\cos(\psi)$. The equation on the separatrix is $\dot{J} = (J + d)\sqrt{p_2(J)}$, being $p_2(J) = -(J + 2 - d)(J - 2 - d)/4$. The outer (resp. inner) splitting has closest singularity τ_+ (resp. τ_-) such that

$$\operatorname{Re}\tau_\pm = 0, \quad \operatorname{Im}\tau_\pm = \int_{\pm 2+d}^{\pm\infty} \frac{dJ}{(J+d)\sqrt{-p_2(J)}} = \frac{1}{\sqrt{1-d^2}}\left(\frac{\pi}{2} \mp \arcsin d\right).$$

Hence the difference between the distances to the closest singularities of the outer splitting and the inner one is given by $\tau_+ - \tau_- \approx -2d + \mathcal{O}(d^3)$ and, as a consequence, it is of the order $\mathcal{O}(\delta^{\frac{m}{4}-1})$.

When $J = -1/d$ we have $|\psi| = \infty$ and the corresponding time value τ_* verifies $\tau_* = \tau_+$. As said before, this point τ_* plays no role at all when studying the splitting behaviour.

Case $d > 0$, $c \neq 0$. The role of c on the position of the singularities is to introduce a real part on them. As a consequence the splitting is able to oscillate depending on the ratio of the real part of the singularity and the logarithm of the dominant eigenvalue of the hyperbolic point. The following analysis shows that oscillation is not possible, at least close to the creation of the resonance, in the case under consideration. We recall that $c << d$ (see remarks in section 3.4).

The differential equation over the separatrix is given by $\dot{J} = -\sqrt{p_6(J)}$ (we use $p_i(J)$ to denote a degree i polynomial). Note that the value $J = J_h$ is a double zero of the vector field. So that

$$\dot{J} = (J - J_h)\sqrt{p_4(J)}.$$

A simple calculation gives

$$J_h = \frac{-1 + \sqrt{1 - 4dc}}{2c},$$

and

$$\begin{aligned} p_4(J) &= \frac{1}{3} - \frac{1}{72c^2} + \frac{5d}{36c} - \frac{4d^2}{9} + \frac{2}{3}\sqrt{1-4cd} + \frac{\sqrt{1-4cd}}{72c^2} - \frac{d\sqrt{1-4cd}}{9c} \\ &+ \left(\frac{1}{36c} + \frac{2c}{3} - \frac{\sqrt{1-4cd}}{36c} + \frac{4}{9}d\sqrt{1-4cd}\right) J + \left(\frac{-1}{12} + \frac{cd}{3} - \frac{1}{6}\sqrt{1-4cd}\right) J^2 \\ &+ \left(\frac{-2c}{9} - \frac{1}{9}c\sqrt{1-4cd}\right) J^3 - \frac{c^2}{9}J^4. \end{aligned}$$

The computation of zeros of $p_4(J)$ gives

$$\begin{array}{ll} z_1 = (2+d) + \frac{1}{3}\left(-4-6d-3d^2-d^3\right)c + \mathcal{O}(c^2), & z_3 = -\frac{3}{2c} + 2d + 2d^2c + \mathcal{O}(c^2), \\ z_2 = (-2+d) + \frac{1}{3}\left(-4+6d-3d^2+d^3\right)c + \mathcal{O}(c^2), & z_4 = -\frac{3}{2c} - 2d + \left(\frac{8}{3} + 2d^2\right)c + \mathcal{O}(c^2). \end{array}$$

Assume $c > 0$. The outer splitting singularity τ_+ is purely imaginary and is given by

$$\operatorname{Im}\tau_+ = \int_{z_1}^{+\infty} \frac{dJ}{(J-J_h)\sqrt{-p_4(J)}}.$$

On the other hand the inner splitting singularity τ_- is given by

$$\begin{aligned} \operatorname{Re}\tau_- &= \int_{z_3}^{z_4} \frac{dJ}{(J-J_h)\sqrt{p_4(J)}}\ , \\ \operatorname{Im}\tau_- &= \int_{z_2}^{z_3} \frac{dJ}{(J-J_h)\sqrt{-p_4(J)}} + \int_{z_4}^{-\infty} \frac{dJ}{(J-J_h)\sqrt{-p_4(J)}}. \end{aligned}$$

In the case $c < 0$ it is the outer splitting singularity the one that has a real part different from zero while the inner splitting singularity is purely imaginary.

By means of the reduction of the elliptic integrals to standard Legendre kinds (see Appendix A) it can be deduced that the outer singularity admits the expansion

$$\operatorname{Im}\tau_+ = \frac{1}{\sqrt{1-d^2}}\left(\frac{\pi}{2} - \arcsin(d)\right) + \frac{4}{3}\ c\ \log|c| + \mathcal{O}(c), \tag{28}$$

with $\operatorname{Re}\tau_+ = 0$ if $c > 0$ and $\operatorname{Re}\tau_+ = -4c + \mathcal{O}(c^2)$ otherwise.

In a similar way it is found that the inner one is given by

$$\operatorname{Im}\tau_- = \frac{1}{\sqrt{1-d^2}}\left(\frac{\pi}{2} + \arcsin(d)\right) - \frac{4}{3}\ c\log|c| + \mathcal{O}(c), \tag{29}$$

with $\operatorname{Re}\tau_- = 4c + \mathcal{O}(c^2)$ if $c > 0$ and $\operatorname{Re}\tau_- = 0$ otherwise.

Remark. As in the case $c = 0$, the value $\tau_* = \frac{1}{\sqrt{1-d^2}}\left(\frac{\pi}{2} - \arcsin(d)\right) + \frac{2}{3}\ c + \mathcal{O}(c)$, corresponding to the time for which $J = -1/d$ and $|\psi| = \infty$ plays no role and, hence, has been ignored in the computation of the position of the closest singularities.

5.5 Sketch of the steps to follow

To study both outer and inner splittings in our problem we need several ingredients. The main goal is to be able to "separate" the exponential rates of decrease of inner and outer splittings.

According to section 5.4 the respective singularities are located at points whose distance to the real time axis differs by $2d(1+\mathcal{O}(\delta^\beta))$ for some $\beta > 0$. This is based of the simple model (16) which, in principle, is only suitable for the resonance strip. On the other hand, as described in 5.1, the approximation of $W_\epsilon^{u,s}$ by the separatrix holds only, in general, on a strip of the form $\mathcal{S}$ with η finite and one would like to have η small compared to d. Consider the following items:

- A first important question is how one has to formulate the problem. We assume that the initial family of maps is given in Cartesian coordinates, say (x, y), having the elliptic fixed point at the origin. After the normal form step, to a suitable order, we change to action-angle coordinates (I, φ) and one has to take into account that a small neighbourhood of the fixed point must be excluded because of the choice of coordinates.

  We are interested in a real phenomenon, the splitting of real separatrices at a resonant zone. This can be measured, in an equivalent way, either in (x, y) or in (I, φ) coordinates. But, according to 5.1, this requires a complex extension. The extension is done in (I, φ) variables. Note that this is different to what it is obtained by just considering (x, y) as complex variables. But the estimates on the real phase space will be the correct ones.

- It turns out that the approximating Hamiltonian $\mathcal{H}(J, \psi)$ given in (16) is, in principle, not enough for our purposes. To be concrete, for the derivation of (16) one has used $\tilde{I} = I - I_*$ assuming $\tilde{I}/I_* < 1$ (in fact $<< 1$) to be able to expand $\mathcal{H}(\tilde{I}, \varphi)$ on the resonant zone. Now we need an approximation in a very large domain in the complex phase space in the (J, ψ) variables.

  Indeed, we would like to reduce the width of the analyticity strip of the separatrix of the Hamiltonian not by a finite amount η independent of δ as stated in section 5.1 but by a quantity which is small compared to $d = \mathcal{O}(\delta^{m/4-1})$ in (16), as mentioned above. Hence, the values of J have to be large and tend to ∞ when δ tends to zero.

  Essentially what we plan to do is to use the Hamiltonian (11) using the changes introduced in 3.4, without any further simplification. See the proof of theorem 5.1.

- Changing the approximating Hamiltonian implies changes in the location of the singularities of the separatrix. Hence, one has to check that the difference of these locations is still small compared to d.

- The bound of the difference between the APM and the time-γ map of the Hamiltonian derived in Proposition 3.1 has to be modified because of two reasons: the approximating Hamiltonian has changed and the domain in the (J, ψ) variables will be now larger. As we shall see, a key role is played by suitable scalings. The domain in the J variable will be large, but going back to the I variable, as in Theorem 3.1, we will see that it is still small.

- Finally one has to pay attention to the fact that the APM needs not to be an entire function. It can have singularities at some finite distance of the elliptic fixed point in the (x, y) or (I, φ) variables. Again the scaling used will show that the singularities move far away in the (J, ψ) variables, so that they become irrelevant.

5.6 Main result: difference between inner and outer splitting

The information on the position of the singularities given in subsection 5.4 and the minor corrections to be done below allows to rigorously prove the difference between the upper bounds of inner and the outer splitting for non-strong generic resonances of a one-parameter family F_δ

of APM. We will skip, as usual, the δ dependence of F_δ and write F when no confusion can be produced. Let us make precise the assumptions before writing the statement of the theorem.

First assumption. This assumption concerns the genericity of the family of APM. We have seen that F can be reduced to a BNF around E_0 (section 3.1). We assume that

A1 The first Birkhoff coefficient $b_1(\delta)$ is non zero for $\delta = 0$. This condition is generic.

Second assumption. This assumption concerns the behaviour of the exponential small part of the inner and outer splittings. We comment on the outer one, the inner one being similar, replacing the subscript $+$ by $-$.

Let p_{0+} be a transversal homoclinic point associated to the outer separatrix of a hyperbolic m-periodic point P_H of the m-resonance strip of F. Let $p_{1+} = F(p_{0+})$. It is well known (see, e.g., [11] and subsection 5.1) that between p_{0+} and p_{1+} the invariant stable manifold $W^s_+(P_H)$ can be represented as the graph of a periodic function $\mathcal{G}^s_+ = \mathcal{G}^s_+(q)$, while $W^u_+(P_H)$ is the graph of the zero-function. The period is equal to $h = \log(\lambda)$ and can be scaled to 2π for convenience. Let us denote as $G_+(s)$ this scaled function. We can write $G_*(s) = \sum_{k=-\infty}^{\infty} c_k \exp(ik\, 2\pi s)$ which depends on δ. Furthermore the splitting is real for real values of s. Hence c_{-k} is the complex conjugate of c_k for all $k \geq 0$. We refer to the contribution coming from the terms having coefficients c_k and c_{-k} as the "k-th harmonic". Observe that if in the original q variable, that is, before the scaling, the manifolds can be extended up to $|\mathrm{Im}\, s| \leq M_+$ then the amplitude of this harmonic is $\mathcal{O}(\exp(-2\pi k M_+/\log(\lambda)))$. If the family of maps is approximated by the time-$\log(\lambda)$ of a limit Hamiltonian having a separatrix $\gamma_+(t)$ then M_+ can be taken slightly smaller than the half-width of the strip of analyticity of γ_+.

Definition 5.2 *We say that a splitting is generic if in the scaled s variable the coefficients of the first harmonic c_1, c_{-1} are bounded away from zero when the small parameter in the family of maps tends to zero.*

We explicitly assume that

A2 The splittings are generic in the sense of the above definition.

Third assumption. It deals with the exact behaviour of the splitting. According to [11] given $\hat\eta > 0$, then an upper bound of the splitting is of the form $\sigma \leq N \exp\left(-\frac{2\pi\, \mathrm{Re}\, \tau - \hat\eta}{\log(\lambda(\epsilon))}\right)$ for ϵ small enough, $N = \mathcal{O}(1)$ and τ is the closest singularity to the real axis of the separatrix γ of the limit Hamiltonian. For concreteness we assume here that ϵ is the small parameter in the family. It is obvious that the effect of N can be included in $\hat\eta$ with a minor modification of $\hat\eta$. Comparing with (24) it is clear that the role of $\hat\eta$ is to take care of the factors of the form $A\log(\lambda)^B$ which are due to the behaviour of the manifolds (of the families of maps and of the limit flow) in $\gamma(t)$ for t close to τ. To this end it is enough that $\hat\eta = \mathcal{O}(\log(\lambda)\log(\log(\lambda)))$. A more flexible assumption is

A3 There exists a fixed $\alpha > 0$, sufficiently small, such the splittings (inner and outer) satisfy the condition

$$\sigma_\pm = \exp\left(-\frac{2\pi\, \mathrm{Re}\, \tau_\pm - \eta_\pm}{\log(\lambda(\epsilon))}\right)\left(\cos\left(\frac{2\pi\, \mathrm{Im}\, \tau_\pm}{\log(\lambda(\epsilon))} - \phi_\pm\right) + o(1)\right),$$

where $|\eta_\pm| < \log(\lambda(\epsilon))^{1-\alpha}$ for ϵ sufficiently small. Here $\tau_\pm$ denote the position of the relevant singularities of the separatrices $\gamma_\pm$ associated to inner and outer splittings and $\phi_\pm$ are suitable phases.

Note that in the case of oscillation assumption **A2** does not hold on a vicinity of the values of ϵ for which $\cos(C_i/\log(\lambda)) = 0$ in (25). Then the second harmonic is the one which dominates, generically. This occurs in exponentially small intervals in ϵ. At these places new homoclinic points can appear or disappear. Several kinds of "pathological" phenomena can occur, like a dependence of the splitting as a function of ϵ which tends to a quasiperiodic function in the parameter $1/\epsilon$, see [18].

Fourth assumption. This assumption concerns the possible singularities of F. First we comment on the entire case. Under the assumptions **A2** and **A3** the splittings of the m-order resonance for a family of *entire* maps behaves as $\exp(-C/\log(\lambda))$, with C close to $2\pi\tau_{\pm}$.

The entire condition of the paragraph above is due to the fact that it is necessary to extend F_ϵ analytically to a domain which contains the image under the separatrix $\gamma_\pm$ of the temporal complex strip $|\mathrm{Im}\, t| < \tau_\pm - \hat{\eta}$. The existence of singularities of F can make this extension impossible. However a key point is played by the fact that to derive an approximating Hamiltonian to describe a resonance a scaling has been introduced. The scaling is, essentially, of the order of magnitude of the width of the resonance.

We are interested in a domain $\mathcal{D}$, complex extension of a domain of finite size, in the (I, φ) variables, for all ϵ sufficiently small, containing the elliptic fixed point E_0 and the resonance zone that we are analysing. Assume that $F = F_\epsilon$ is a meromorphic family of maps (when expressed in (I, φ) variables and complexified) such that they have the closest singularity to $\mathcal{D}$ at a distance $D(\epsilon)$ from $\mathcal{D}$. We assume

A4 The value $D(\epsilon)$ is bounded from below by $\hat{D} > 0$ when ϵ goes to 0.

Note that, assumption **A4** is also generic for m-resonances of an area preserving family of maps. We remark that in theorem 5.1 below it is not assumed the map to be an entire map, being our results on the inner and outer splittings valid for the meromorphic case under the hypothesis that the singularity remains at a finite distance when the current small parameter (which will be a power of δ depending on the order of the resonance) goes to zero.

We can now make precise the statement of the theorem concerning the inner and outer splittings.

Theorem 5.1 *Let F be an APM. Assume that it has an m-order resonance strip, $m > 4$, located at an average distance $I = I_* = \mathcal{O}(\delta)$ from the elliptic fixed point and δ is sufficiently small. Under the assumptions* **A1**, **A2**, **A3** *and* **A4**, *the following conclusions hold.*

a) The outer splitting is larger than the inner one being the difference between the position of the corresponding nearest singularities $\mathcal{O}(\delta^{m/4-1})$.

b) Neither the inner nor the outer splittings oscillate.

Proof. Assume first that F is entire. We start working in the (I, φ) variables and then, after locating the resonance zone, we pass to (J, ψ) variables with the changes introduced in section 3.4. But after writing (17) we do not expand in powers of $\tilde{I}$ because now we are interested in values of $\tilde{I}$ which are large compared to I_*. Instead $(I_* + \tilde{I})^m$ is written as $I_*^m(1 + \tilde{I}/I_*)^m$. Then we return to the Hamiltonian (11). Written in the (J, ψ) variables of 3.4, the Hamiltonian becomes

$$\mathcal{H}_{new}(J, \psi) = \frac{1}{2}J^2 + \frac{\tilde{c}_3}{3}J^3 + \frac{\tilde{c}_4}{4}J^4 + \ldots - (1 + \tilde{d}J)^m \cos\psi, \tag{30}$$

where $\tilde{c}_j = \mathcal{O}(\delta^{(m/4)(j-2)})$ and $\tilde{d} = \mathcal{O}(\delta^{(m/4)-1})$.

Let us now consider a domain of size $\mathcal{O}(\delta^{1-\mu})$ in I where $1 > \mu > 0$ will be chosen later. The domain should be simply connected and should avoide a neighbourhood of $I = 0$ to prevent from problems with the angle. In this domain the difference between the m-th power of the map and the time-1 flow of (17) was estimated in theorem 3.1. The error has two contributions:

- The error due to the normal form, which turns out to be $\mathcal{O}(\delta^{\frac{m+1}{2}(1-\mu)})$.
- The error due to the lack of commutativity of vector fields (12) and (13). In section 3.3 this was estimated on an annulus of size $\mathcal{O}(\delta^{1+\nu})$, with $\nu > 0$, in the r variable. Now should be studied in a domain of I of size $\mathcal{O}(\delta^{1-\mu})$. This produces a final error $\mathcal{O}(\delta^{\frac{m+1-\mu}{2}(1-\mu)})$, which is the dominant one.

Passing to the (J, ψ) variables the domain has size $\mathcal{O}(\delta^{-\frac{m}{4}+1-\mu})$ and the difference between the m-th power of the map and the time-γ flow of (30) is $\mathcal{O}(\delta^{\frac{m+1-\mu}{2}(1-\mu)-\frac{m}{4}})$. The error is still of an order in δ which is greater than $m/4$, the order which appears in γ, provided $\mu < 1/(m+2)$, for instance. Hence the flow of (30) is sufficiently good for our purposes.

Next step is to see how big has to be the domain in J, that is, how big must be $\delta^{-\frac{m}{4}+1-\mu}$ so that the difference in the integrals in subsection 5.4 when the improper integrals are replaced by integrals in a large but finite domain, up to some big J_b, is small compared to d. Taking, for instance, the case $d > 0, c = 0$ we have

$$\int_{J_b}^{\infty} \frac{dJ}{(J+d)\sqrt{-p_2(J)}} \approx \int_{J_b}^{\infty} \frac{dJ}{J^2} = J_b^{-1},$$

which is small compared to d if $J_b >> \delta^{-\frac{m}{4}+1}$. Hence, any positive value of μ is enough. The same results are obtained in the other cases for the Hamiltonian (16) or with Hamiltonian (30).

Finally we must check that the difference of the integrals of the type considered in proposition 5.1 using either the simplified Hamiltonian (16) or the Hamiltonian (30), both of them along the corresponding separatrix, can also be neglected. That is, it is small compared to d. One has to estimate differences of integrals like

$$\int_{J_{0,new}}^{J_b} \frac{dJ}{\sqrt{(1+\tilde{d}J)^m - (\frac{1}{2}J^2 + \frac{\tilde{c}_3}{3}J^3 + \frac{\tilde{c}_4}{4}J^4 + \ldots - h_{new})^2}} - \int_{J_0}^{J_b} \frac{dJ}{\sqrt{(1+m\tilde{d}J) - (\frac{1}{2}J^2 + \frac{\tilde{c}_3}{3}J^3 - h)^2}},$$

where $J_{0,new}, J_0$ are the lower limits, zeros of the corresponding polynomial, which are only slightly different. The values of h and h_{new} correspond to the energies on the separatrix, both of them close to 1. It is convenient to write the integrals as

$$\int_{J_0}^{\delta^{-\frac{m}{4}+1+\nu}} + \int_{\delta^{-\frac{m}{4}+1+\nu}}^{\delta^{-\frac{m}{4}+1-\nu}} + \int_{\delta^{-\frac{m}{4}+1-\nu}}^{\delta^{-\frac{m}{4}+1-\mu}},$$

where $0 < \nu < \mu$, to check the dominant contributions in each piece. In all cases the differences are small compared to d. Therefore, the changes in the location of the singularities are irrelevant compared to the computations done in 5.4. This includes, in particular, the changes in the real part, which are checked to be small compared to c.

By assumptions **A2** and **A3** the statement a) of the theorem is now a direct consequence of the computations of the section 5.4 and the estimates just done. Note that the role of the allowed changes in the exponents, $\eta_{\pm} = |\delta^{m/4}|^{1-\alpha}$ (see **A3**), is dominated by the fact that the difference of the location of the singularities of the inner and outer separatrices is $\mathcal{O}(|\delta|^{m/4-1})$.

Concerning the statement b) it is enough to observe that the effect of the parameter c in the position of the singularity adds a real part of the same order than $\log\lambda$, both are $\mathcal{O}(|\delta|^{\frac{m}{4}})$ provided $b_1 \neq 0$ (assumption **A1**) and hence, the splittings do not oscillate. In other words, the corresponding cosine factor of the splitting behaviour has a dominant part which remains constant when changing δ.

It remains to clarify the role of the singularities of F. The important fact is that, due to the scaling in I to produce the final Hamiltonian (16), which essentially consists in dividing the action by $|\delta|^{m/4}$, the singularities of F are sent to a distance bounded from below by $\hat{D}|\delta|^{-m/4}$ by assumption **A4**. When using a path in J to estimate the location of the singularities, as done in section 5.4 we loose control of what happens beyond $\hat{D}|\delta|^{-m/4}$. But the contribution to the integral from $\hat{D}|\delta|^{-m/4}$ to ∞ in all cases considered in section 5.4 with dominant parts of the integrands of the form $\frac{1}{J^2}$ or $\frac{1}{cJ^3}$ is $\mathcal{O}(|\delta|^{m/4})$. Hence, it is dominated by the difference of the location of the singularities, $2d = \mathcal{O}(|\delta|^{m/4-1})$. $\square$

Remarks.

1. Assumptions **A1** and **A4** are very easy to check on a given family. Assumptions **A2** and **A3** can require more work, as they are related to global properties. Despite this is true for general splitting phenomena, in present case, the m-order resonance, the simplicity of the Hamiltonian (16) can make checks easier.

2. If $b_2 = 0$ the role of c is played by the J^4 skipped term of Hamiltonian (16) (or, in general, by the first coefficient non zero of a J^k, $k \geq 4$ term). As noticed in the proof of proposition 3.1 it is expected to be of order $\delta^{m/2}$ (or, in general, of higher order). In particular, in this degenerate case the splitting never oscillates (for δ small enough).

3. For δ small enough the outer splitting is greater than the inner one (just because $d > 0$). However, for δ large enough it is possible that the inner splitting becomes larger than the outer (see comments in subsection 5.8).

4. If we assume that the angle between the invariant manifolds at both homoclinic points $\sigma_\pm$ to behave as (24), then from expressions (28) and (29) we estimate the ratio of the splittings σ_+/σ_- to behave as $\tilde{A}(\log\lambda)^{\tilde{B}}\exp\left(-2\pi(\tau_+ - \tau_-)/(\log\lambda)\right)$, where $\tilde{B}$ is the difference between the constants B of the outer and inner splittings, $\tilde{A}$ is the ratio between the constants A of the outer and inner splittings and $\tau_+ - \tau_- = -2d + \frac{8}{3}c\log(|c|) + \mathcal{O}(c, d^2)$.

5. Note that the angle between the separatrices decreases as the distance of the singularity from the real axis increases. Hence, $\sigma_+ > \sigma_-$, at least for λ close enough to 1, that is, close to the creation of the resonance, if, and only if, $\operatorname{Im}\tau_+ < \operatorname{Im}\tau_-$. As d is positive last inequality is verified for δ small enough. As a conclusion, the outer splitting is larger than the inner one. Of course, as said in the second remark, high order terms affect the conclusions above for λ not too close to 1, that is, for larger values of δ.

5.7 Numerical computations of the singularities and the inner-outer splittings

The position of the singularities can be computed by direct integration of the vector field generated by the Hamiltonian (16) along a suitable complex path of time. Figure 13 shows the results obtained. The behaviour is the one expected according to the approximations on the location of the singularities given above.

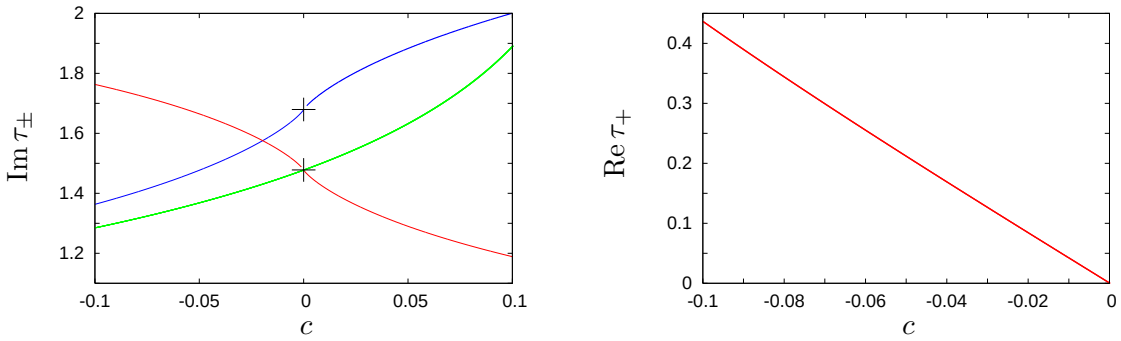

Figure 13: Position of the singularities with respect c ($d = 0.1$). Left: Imaginary part of the singularities (τ_- blue, upper increasing curve, τ_+ red, decreasing curve). As an extra information the time $\tau = \tau_*$ when the origin is reached and $|\psi| = \infty$ is shown (green, lower increasing curve). The crosses show the value when $c = 0$, being the distance between them $\approx -2d$. Right: Real part of the singularity of the outer separatrix ($c < 0$).

Concerning the behaviour of the splittings we want to give a numerical evidence that they behave as predicted. Consider the 1:7 resonance for the Hénon map (1). Figure 14 shows the splitting of separatrices of this resonance as a function of the parameter α of the map. Multi-precision has been used to compute small splittings. We refer to [18] for additional information on this type of computations.

We recall that Hamiltonian (16) generates a flow $\varphi^{\mathcal{H}}$ such that $\varphi^{\mathcal{H}}_{t=\gamma}(I,\varphi) = F(I,\varphi) + \mathcal{O}(\delta)$, where $\gamma = \log(\lambda)(1+\mathcal{O}(\delta))$ being λ the dominant eigenvalue of the m-periodic hyperbolic point associated to the m-order resonant island. According to this and the theory in [11], assume that the behaviour of the inner and outer splitting is, as predicted before, of the form

$$\sigma_\pm \sim A_\pm (\log\lambda)^{B_\pm} \exp(-2\pi(\operatorname{Im}\tau_\pm)/\log\lambda), \tag{31}$$

where

$$\operatorname{Im}\tau_+ = \frac{1}{\sqrt{1-d^2}}\left(\frac{\pi}{2} - \arcsin d\right) + \frac{4}{3}c\log|c| + \mathcal{O}(c) = \frac{\pi}{2} - d + \frac{4}{3}c\log|c| + \mathcal{O}(c,d^2),$$

$$\operatorname{Im}\tau_- = \frac{1}{\sqrt{1-d^2}}\left(\frac{\pi}{2} + \arcsin d\right) - \frac{4}{3}c\log|d| + \mathcal{O}(c) = \frac{\pi}{2} + d - \frac{4}{3}c\log|c| + \mathcal{O}(c,d^2).$$

Hence,

$$h\log\sigma_\pm = \tilde{A}_\pm h + B_\pm h\log h - 2\pi(\operatorname{Im}\tau_\pm),$$

being $h = \log\lambda$ and $\tilde{A}_\pm = \log(A_\pm)$. Taking into account that $d = \mathcal{O}(\delta^{\frac{m}{4}-1}) = \mathcal{O}(h^{\frac{m-4}{m}})$ and $c = \mathcal{O}(\delta^{\frac{m}{4}})$ we obtain

$$h\log\sigma_\pm = -\pi^2 - k_\pm h^{\frac{m-4}{m}} + \tilde{A}_\pm h + B_\pm h\log h,$$

where, according to the theory we have developed, it is expected

$$k_+ = -k_-.$$

If we fit the splitting data (Figure 14) by a function of the form

$$f(x) = C + k(x^{\frac{3}{7}}) + Ax + Bx\log(x),$$

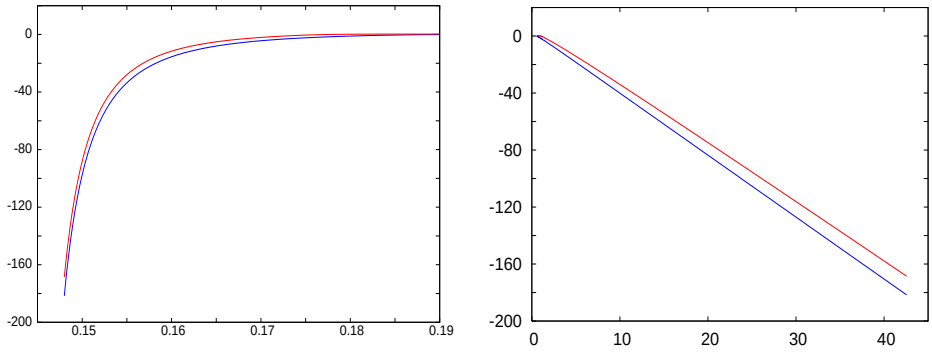

Figure 14: Left: Decimal logarithm of the inner and outer splitting of the 1:7 resonance for the Hénon map (1) as α varies. The step size in α is 10^{-4}. The bifurcation of the period 7 orbits is produced for $\alpha = 0.\widehat{142857}$. The inner splitting is the smaller one. Right: The same $\log_{10}$ of the splittings as a function of $1/\lambda(\delta)$.

in the interval $[0, 0.2]$ we obtain the values

$$C = -9.87632,\ k = 1.65482,\ A = 8.35777,\ B = -2.60782,$$

for the outer splitting, while for the inner one

$$C = -9.87895,\ k = -1.42068,\ A = 7.69933,\ B = -1.75694.$$

According to the theoretical results $\tau_{\pm} \to \pi/2$ as $\delta \to 0$, hence $C \to -\pi^2 \approx -9.869604$ in good agreement with the values obtained.

Figure 15 shows splitting results for several resonances and ranges of α for the Hénon map (1). As expected, in all the cases, at least for the relatively small values of δ considered for each resonance, the outer splitting is larger than the inner one.

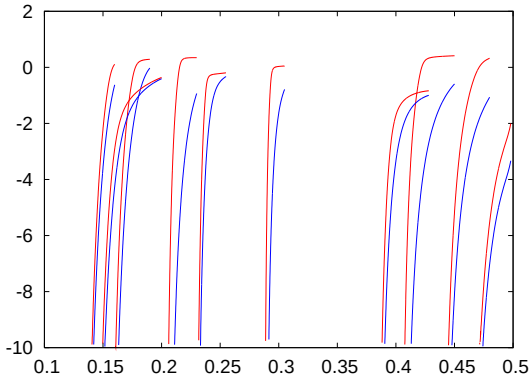

Figure 15: From left to right, it is represented the decimal logarithm of the splitting of the resonances 1:9, 1:8, 1:7, 1:5, 2:9, 2:7, 3:8, 2:5, 3:7 and 4:9, respectively. Each pair of red and blue lines corresponds to the outer and inner splitting, respectively, of a different resonance. Note that in all the cases shown the outer splitting (red) is greater than the inner one (blue). In the x-axis it is represented the value of α.

5.8 On the behaviour of the splittings at finite distance

In general we can consider not only what happens in a neighbourhood of the elliptic fixed point but far away, in a given annulus. The limit Hamiltonian can be reduced to a Hamiltonian like (20) as was stated in section 3.5. We recall that the map considered in that section is assumed to be a perturbation of a twist map F_0 when $\mu = 0$. Let $\rho(I)$ be the rotation number of F_0.

Then, a result similar to Theorem 5.1 follows by replacing b_1 and b_2 (which appear in the constants c and d of the Hamiltonian) by derivatives of the rotation number $\frac{d\rho}{dI}\Big|_{I=I_*}$ and $\frac{d^{(2)}\rho}{dI^2}\Big|_{I=I_*}$, respectively. The main difference concerns the order of magnitude of the corresponding constants c and d, since in particular, it can be $|c| > d$. Also higher order resonant terms, not considered in the reduced Hamiltonian model we are dealing with, can play a relevant role.

When c and d are arbitrary numbers the position of the inner and outer closest singularities can change and it can happen that the inner one has imaginary part smaller than the imaginary part of the outer singularity. It is possible, then, to have the inner splitting greater than the outer. From the computation of the position of the singularities it is expected in this case to have $c < 0$ (see expressions (28) and (29), and figure 13), but higher order terms can change this behaviour.

An evidence that for finite distance the largest splitting can be the inner one is the shape of the pairs of splittings in figure 15. For large values of δ some of them become closer. In fact, in figure 16 it is represented the behaviour of the inner and outer splittings of the 2:11 resonance. Clearly, at some distance the inner one becomes larger.

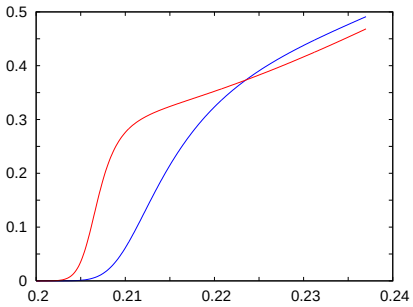

Figure 16: Outer splitting (red), the larger one for $\alpha < 0.223$, and inner splitting (blue) of the 2:11 resonance for the Hénon map in the form (1). The x-axis shows the value of α.

Moreover, the following example, contained in [36], shows that the inner splitting can be expected to be larger than the outer for δ big enough. Consider an integrable twist map expressed in Poincaré coordinates

$$T : \begin{pmatrix} I \\ \theta \end{pmatrix} \longmapsto \begin{pmatrix} I \\ \theta + \alpha(I) \end{pmatrix},$$

where $(I, \theta) \in (0, 1) \times (0, 2\pi)$. Assume $\alpha(I) = b_0 + b_1 I + b_2 I^2$, that is, only the first and the second Birkhoff coefficients are different from zero. Let G denote the generating function associated to T, that is $G(\hat{\theta}, I) = \hat{\theta} I - S(I)$, where $S(I) = -b_0 I - (b_1/2) I^2 - (b_2/3) I^3$. By perturbing the generating function

$$\tilde{G}(\hat{\theta}, I) = \hat{\theta} I - S(I) + \epsilon \sin \hat{\theta},$$

we construct a non-integrable map T_ϵ close to the map T,

$$T_\epsilon : \begin{pmatrix} I \\ \theta \end{pmatrix} \longmapsto \begin{pmatrix} I + \epsilon \cos(\theta + \alpha(I)) \\ \theta + \alpha(I) \end{pmatrix}. \tag{32}$$

Figure 17 displays the invariant manifolds for the 1:2 resonance for different sets of parameters of the model (32). One checks that for some values the inner splitting is greater than the outer one and how changing torsion coefficients the inner becomes smaller than the outer one.

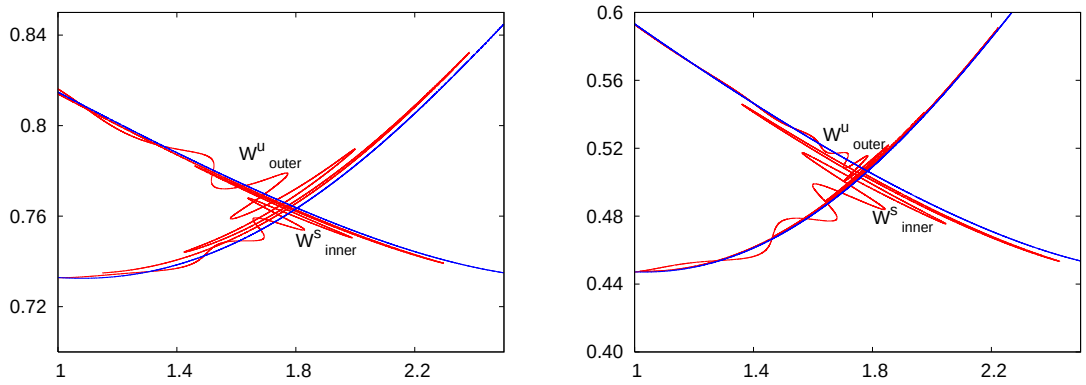

Figure 17: Different splittings observed for the model (32) with $b_0 = 0$. For the left (right) plot the values $b_1 = 0.2$, $b_2 = 4$ and $\epsilon = 0.14$ ($b_1 = 6$, $b_2 = -2$ and $\epsilon = 0.14$) have been used.

6 Inner and outer splitting for low order resonances

The analysis of the behaviour of the splittings of the strong resonances differs from the one obtained for generic ones (see also [14]).

6.1 Behaviour of the splittings in the 1:3 resonance

Inner splitting. Hamiltonian (21) allows to study the splitting of the inner separatrix for $\hat{\epsilon} < 0$ as well as the corresponding one for $\hat{\epsilon} > 0$. The change of coordinates $J = I + \hat{\epsilon}/2$, $\psi = 3\varphi$, gives (after removing a constant from the Hamiltonian)

$$H(J, \psi) = P(J) - Q(J)\cos(\psi), \tag{33}$$

where $P(J) = J^2$, and $Q(J) = -(J - \hat{\epsilon}/2)^{3/2}$. The equation on the separatrix (at energy level h) is given by $\dot{J} = \sqrt{p_4(J)}$ being $p_4(J) = (J - \hat{\epsilon}/2)^3 - (J^2 - h)^2$.

Let $p_h = (J_h, \psi_h)$ be the hyperbolic point. Then $p_4(J) = 0$ has $J = J_h$ as a double solution. On the other hand the maximum $J = J_M$ on the separatrix (at finite distance) is also a solution because $\dot{J} = 0$. Last zero of $p_4(J)$ is located at $\mathcal{O}(\hat{\epsilon})$ of $J = 0$ which is the value obtained for the unperturbed case $\hat{\epsilon} = 0$.

The singularities of the homoclinic orbit are given by $\tau = \int_{J_M}^{+\infty} dJ/\sqrt{p_4(J)}$ and, as Hamiltonian (33) satisfies the hypothesis of proposition 5.1, τ is imaginary. As a consequence, the splitting

of separatrices does not oscillate. The behaviour of this splitting is expected to be similar to the case of generic resonances $m > 4$.

We can proceed in a more direct way to estimate the constant of the exponential decay of the splitting. Note, see equation (14), that the radius I_* in this case is of order $\mathcal{O}(\delta^2)$ and, hence, $\log(\lambda) = \mathcal{O}(\delta)$. This suggests to introduce $I_{new} = I/\mu^2$, $t_{new} = \mu\, t$, where $\mu = |\hat{\epsilon}|$. Keeping the names I, t for the new action and time, Hamiltonian (21) becomes

$$H = \sigma I + I^{\frac{3}{2}} \cos(3\varphi) + \mathcal{O}(\mu),\ \sigma = \text{sign}(\epsilon).$$

When expressed in Cartesian coordinates ($x = \sqrt{2I}\cos\varphi$, $y = \sqrt{2I}\sin\varphi$) the above Hamiltonian becomes

$$H(x,y) = \frac{\sigma}{2}(x^2+y^2) + \frac{1}{2\sqrt{2}}(x^3 - 3xy^2) + \mathcal{O}(\mu)$$

For $\sigma = 1$ the hyperbolic 3-periodic orbit is located at $I = 4/9 + \mathcal{O}(\mu)$ and $\varphi = \pi/3, \pi, 5\pi/3$. On the other hand, for $\sigma = -1$ the hyperbolic 3-periodic orbit is located at $I = 4/9 + \mathcal{O}(\mu)$ and $\varphi = 0, 2\pi/3, 4\pi/3$. In both cases the separatrices approximately form an equilateral triangle and the line $x = \sigma\sqrt{2}/3$ approximates one of the separatrices. The restriction of the Hamiltonian vector field to this separatrix can be reduced to

$$\dot{y} = \frac{\sqrt{2}}{2} - \frac{3}{2\sqrt{2}}\, y^2 + \mathcal{O}(\mu).$$

Ignoring the $\mathcal{O}(\mu)$ terms it is easy to check that the singularity is located at $\tau = \pm i\pi/\sqrt{3}$. Hence, the splitting does not oscillate and $\sigma \sim A(\log(\lambda))^B \exp(-C/(\log(\lambda))$ with $C = \mathcal{O}(1)$, is the expected behaviour of the splitting.

Outer splitting. Concerning the outer splitting of the 1:3 resonance we note that it cannot be studied by normal form analysis around the elliptic fixed point. It remains finite when crossing the 1:3 resonance as is shown in figure 18 for the Hénon map (5). In this formulation of the Hénon map the elliptic-hyperbolic bifurcation (saddle-center) takes place at $c = c_3 = \sqrt{2}$ and the 3-periodic parabolic orbit on the symmetry axis $y = -x$ has $x = 1/\sqrt{2}$.

Considering H_c^3 the distance between the elliptic and the hyperbolic points behaves as $\sqrt{c - c_3}$ (similar to the saddle-center bifurcation of the origin for the map H_c). The splitting seems to be exponentially small with respect the natural parameter $c - c_3$. This explains the behaviour close to $c = c_3$ observed in the figure.

Increasing c the splitting becomes finite. It has a maximum at $c \approx 1.44794$ and for greater values seems to monotonically decay. The 1:3 resonant bifurcation takes place at $c = 1.5$.

6.2 Behaviour of the splittings in the 1:4 resonance

We recall that the Hénon map has a not generic behaviour at the fourth order resonance. Hence, we first describe the non-degenerate case and later we analyse the changes due to the non-genericity.

6.2.1 Order four resonance: the non-degenerate case

Let be $\psi = 4\varphi$. According to (22) the Hamiltonian is

$$H = H(I,\psi) = \epsilon I + I^2(1 + \xi\cos(\psi)).$$

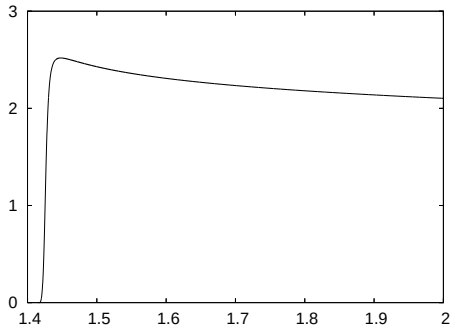

Figure 18: Outer splitting for the 1:3 resonance of the Hénon map (5). Note that the splitting is finite when crossing the value $c = 1.5$ where the bifurcation takes place.

We can always take $\xi < 0, \xi \neq -1$. No fixed points appear, beyond the origin, if $\epsilon > 0, \xi > -1$ (see figure 10). Assume first $\epsilon > 0, \xi < -1$ and scale I, t by ϵ ($I_{new} = I/\epsilon$, $t_{new} = \epsilon t$). We keep the name I for the action. Then

$$H = I + I^2(1 + \xi\cos(\psi)).$$

From

$$\psi' = 1 + 2I(1 + \xi\cos(\psi)), \quad I' = \xi I^2\sin(\psi),$$

we have the fixed point $\psi = 0, I = -1/(2(1+\xi))$, which is hyperbolic on the level $H = -1/(4(1+\xi))$. From this it follows

$$I' = \sqrt{P_4(I)}, \quad P_4(I) = (\xi I^2)^2 - \left(I + I^2 + \frac{1}{4(1+\xi)}\right)^2.$$

The coefficient of I^4 is $\xi^2 - 1$ and the zeros are located at

$$I_1 = \frac{-1 - \sqrt{2\xi/(1+\xi)}}{2(1-\xi)}, \quad I_2 = \frac{-1 + \sqrt{2\xi/(1+\xi)}}{2(1-\xi)}, \quad I_3 = I_4 = -\frac{1}{2(1+\xi)}$$

satisfying $I_1 < 0 < I_2 < I_3 = I_4$. The singularity of the inner separatrix has

$$\mathrm{Re} = \int_{-\infty}^{I_1} dI/\sqrt{P_4(I)}, \quad \mathrm{Im} = \int_{I_1}^{I_2} dI/\sqrt{-P_4(I)}.$$

Now consider $\epsilon < 0$. The scaling by $\mu = |\epsilon|$ leads to

$$H = -I + I^2(1 + \xi\cos(\psi)).$$

If $\xi < -1$ only the hyperbolic fixed point $\psi = \pi, I = 1/(2(1-\xi))$ appears, while for $\xi > -1$ there is an elliptic fixed point on $\psi = 0, I = 1/(2(1+\xi))$ and a hyperbolic one on $\psi = \pi, I = 1/(2(1-\xi))$. In both cases the level of energy of the hyperbolic point is $-1/(4(1-\xi))$. As before, one has

$$I' = \sqrt{P_4(I)}, \quad P_4(I) = (\xi I^2)^2 - \left(I - I^2 - \frac{1}{4(1-\xi)}\right)^2$$

and the polynomial has $\xi^2 - 1$ as coefficient of degree 4 and zeros

$$I_1 = \frac{1 + \sqrt{-2\xi/(1-\xi)}}{2(1+\xi)}, \quad I_2 = \frac{1 - \sqrt{-2\xi/(1-\xi)}}{2(1+\xi)}, \quad I_3 = I_4 = \frac{1}{2(1-\xi)}$$

both in the case $\xi < -1$ and $\xi > -1$. But now

$$0 < I_2 < I_3 = I_4 < I_1 \quad \text{if} \quad \xi > -1, \qquad I_1 < 0 < I_2 < I_3 = I_4 \quad \text{if} \quad \xi < -1.$$

Hence, if $\xi > -1$ the inner and outer separatrices have purely imaginary singularities given, respectively, by

$$\mathrm{Im}_{in} = \int_{-\infty}^{I_2} dI/\sqrt{-P_4(I)}, \quad \mathrm{Im}_{out} = \int_{I_1}^{\infty} dI/\sqrt{-P_4(I)},$$

while for $\xi < -1$ the singularity of the (inner) separatrix has

$$\mathrm{Re} = \int_{-\infty}^{I_1} dI/\sqrt{P_4(I)}, \quad \mathrm{Im} = \int_{I_1}^{I_2} dI/\sqrt{-P_4(I)}.$$

We note that as all these integrals reduce to the form $\int \frac{dI}{(I-A)\sqrt{(I-B)(I-C)}}$ for ξ-depending values of A, B, C, the singularities can be computed as functions of ξ, obtaining the following result

$\epsilon > 0,\ \xi < -1$:

$$\mathrm{Re} = \sqrt{\tfrac{(1+\xi)}{2\xi}} \log\left(\tfrac{(3\xi-1)+2\sqrt{2\xi(\xi-1)}}{1+\xi}\right), \quad \mathrm{Im} = \sqrt{\tfrac{2(\xi+1)}{\xi}}\pi$$

$\epsilon < 0,\ \xi > -1$:

$$\mathrm{Im}_{in} = \sqrt{\tfrac{\xi-1}{2\xi}}\left(\pi + 2\arctan\left(\sqrt{\tfrac{-2\xi}{1+\xi}}\right)\right), \quad \mathrm{Im}_{out} = \sqrt{\tfrac{\xi-1}{2\xi}}\left(\pi - 2\arctan\left(\sqrt{\tfrac{-2\xi}{1+\xi}}\right)\right)$$

$\epsilon < 0,\ \xi < -1$:

$$\mathrm{Re} = \sqrt{\tfrac{2(\xi-1)}{\xi}} \log\left(\tfrac{\sqrt{-2\xi}-\sqrt{-(1+\xi)}}{\sqrt{1-\xi}}\right), \quad \mathrm{Im} = \sqrt{\tfrac{2(\xi-1)}{\xi}}\pi$$

6.2.2 Order four resonance: the degenerate case

In the degenerate case $\xi = -1$ the relevant Hamiltonian, according to (23), is of the form

$$\epsilon I + I^2(1 - \cos(\psi)) + I^3(a + b\cos(\psi) + c\sin(\psi)).$$

We shall assume $\nu := a + b \neq 0$, that is, we study a problem of codimension exactly 1. Topologically the phase portrait is similar to the non-degenerate case. The parameter ϵ plays the same role as before and the conditions $1 + \xi > 0, 1 + \xi < 0$ are replaced by $\nu > 0, \nu < 0$, respectively. The parameter c plays a minor role.

Let be $\mu = |\epsilon|$ as before. Scaling I, t by μ leads to

$$H = \pm I + I^2(1 - \cos(\psi)) + \mu I^3(a + b\cos(\psi) + c\sin(\psi)),$$

where the $\pm$ sign is the sign of ϵ. The corresponding equations are

$$\psi' = \pm 1 + 2I(1 - \cos(\psi)) + 3\mu I^2(a + b\cos(\psi) + c\sin(\psi)),\ I' = -I^2\sin(\psi) + \mu I^3(b\sin(\psi) - c\cos(\psi)).$$

We discuss the behaviour for the different ϵ, ν cases. If $\epsilon > 0, \nu > 0$ there are no fixed points beyond the origin.

- Case $\epsilon > 0, \nu < 0$. Only a hyperbolic point located at

$$\psi = \mathcal{O}(\mu^{1/2}), \quad I = (3\mu|\nu|)^{-1/2}(1 + \mathcal{O}(\mu^{1/2})),$$

appears, on the level of energy $\frac{2}{3}(3\mu|\nu|)^{-1/2}(1+\mathcal{O}(\mu^{1/2}))$. The hyperbolic point has an inner separatrix. Let

$$P_3 = I + I^2 + a\mu I^3, \quad P_1 = 1 - b\mu I, \quad Q_3 = c\mu I^3.$$

The values of $\cos(\psi), \sin(\psi)$ can be obtained from the energy level and then

$$I' = -\sqrt{P_6}, \quad P_6 = P_1^2 I^4 + Q_3^2 - P_3^2.$$

The coefficient of I^6 in P_6 is $\mu^2(b^2+c^2-a^2)$ and the zeros are

$$I_1 = \frac{2\nu}{\mu(b^2+c^2-a^2)},\ I_2 = \frac{-2}{(3\mu|\nu|)^{1/2}},\ I_3 = \frac{-1}{(27\mu|\nu|)^{1/4}},\ I_4 = \frac{1}{(27\mu|\nu|)^{1/4}},\ I_5 = I_6 = \frac{1}{(3\mu|\nu|)^{1/2}},$$

where only the dominant terms are displayed. All the corrections are of the form $1+o(1)$ for $\epsilon \to 0$. If we assume $b^2+c^2-a^2 > 0$ the zeros are ordered: $I_1 < I_2 < I_3 < I_4 < I_5$. Anyway I_1 plays no role. This is natural: undoing the scaling it is located at a finite distance and, hence, influenced by higher order terms. Furthermore, it is immediately checked that integrals like $\int_{-\infty}^{I_1} dI/\sqrt{P_6(I)}$ are $\mathcal{O}(\mu)$. The value I_5 corresponds to the hyperbolic fixed point and I_4 to the approximate intersection of the (inner) separatrix of that point with $\psi = \pi$.

The singularities of the separatrix have dominant terms with

$$\mathrm{Re} = \int_{I_2}^{I_3} dI/\sqrt{P_6(I)}, \quad \mathrm{Im} = \left(\int_{I_1}^{I_2} + \int_{I_3}^{I_4}\right) dI/\sqrt{-P_6(I)}.$$

To compute the last integral we introduce $K = (27\mu|\nu|)^{1/4} I$. Expressions like $I - I_j, j \neq 3, j \neq 4$, can be replaced by $-I_j(1+o(1))$. The integral is then equal to

$$\int_{I_3}^{I_4} dI/\sqrt{-P_6(I)} = \frac{\pi}{2}(27\mu|\nu|)^{1/4}.$$

We introduce now $J = (3\mu|\nu|)^{1/2} I$ to compute the first part of Im. The dominant terms give

$$(27\mu|\nu|)^{1/4} \int_{-\infty}^{-2} \frac{dJ}{J(J-1)\sqrt{-4-2J}} = \frac{1}{6}(3-\sqrt{6})(27\mu|\nu|)^{1/4}\pi.$$

The integral from I_2 to I_3 is a little bit more delicate. Let $0 < m << 1$, $\tilde{I} = \frac{-m}{(3\mu|\nu|)^{1/2}}$ and $\tilde{m} = m(\mu|\nu|/3)^{-1/4}$. We write $\int_{I_2}^{I_3} = \int_{I_2}^{\tilde{I}} + \int_{\tilde{I}}^{I_3}$. For the second part we use K as before and the integral becomes

$$\int_{\tilde{I}}^{I_3} \frac{dI}{\sqrt{P_6(I)}} = \frac{1}{2}(27\mu|\nu|)^{1/4} \int_{-\tilde{m}}^{1} \frac{dK}{\sqrt{K^2-1}} = \frac{1}{2}(27\mu|\nu|)^{1/4} \left(\log(2m) + \frac{1}{4}\log(3/(\mu|\nu|))\right).$$

To obtain the value of $\int_{I_2}^{\tilde{I}}$ we use J as above and have the contribution

$$\int_{I_2}^{\tilde{I}} \frac{dI}{\sqrt{P_6(I)}} = (27\mu|\nu|)^{1/4} \int_{-2}^{-m} \frac{dJ}{J(J-1)\sqrt{4+2J}} = -\frac{1}{2}(27\mu|\nu|)^{1/4}\log(m) + \mathcal{O}(1).$$

This cancels, as it should be, the term in $\log(m)$. Hence the real part of the singularity is of the order $\mu^{1/4}\log(1/\mu)$.

- Case $\epsilon < 0, \nu < 0$. An hyperbolic point is found close to $\psi = \pi, I = 1/4$. It has only an inner separatrix. Proceeding as in the previous case we obtain

$$I' = \sqrt{P_6(I)}, \quad P_6(I) = \mu^2(b^2 + c^2 - a^2)\Pi_{j=1}^6(I - I_j),$$

where, keeping only dominant terms, the zeros are located at

$$I_1 = \frac{2\nu}{\mu(b^2+c^2-a^2)}, \quad I_2 = -(\mu\nu)^{-1/2}, \quad I_3 = \frac{1}{8}, \quad I_4 = I_5 = \frac{1}{4}, \quad I_6 = (\mu\nu)^{-1/2}.$$

It is clear that $I_2 = -I_6$ are imaginary. Only imaginary part appears in the singularity, and its dominant contribution is given by

$$\int_{-\infty}^{1/8} \frac{dI}{(\frac{1}{4} - I)\sqrt{\frac{1}{4} - 2I}} = 2\pi.$$

- Case $\epsilon < 0, \nu > 0$. This is the most interesting case. It has an hyperbolic fixed point located near $\psi = \pi, I = 1/4$, which has inner and outer separatrices, and an elliptic fixed point near $\psi = 0, I = (3\mu\nu)^{-1/2}$. The expression of P_6 and I_j is as in the previous case, but now $I_2 = -I_6$ are real. Note that I_3 and I_6 give, approximately, the minimum distance from the inner separatrix to the origin and the maximum distance from the outer separatrix to the origin, respectively.

The dominant part of the location of the singularities for the inner splitting is

$$\mathrm{Re}_{in} = \int_{-\infty}^{I_2} \frac{dI}{\sqrt{P_6(I)}}, \quad \mathrm{Im}_{in} = \int_{I_2}^{I_3} \frac{dI}{\sqrt{-P_6(I)}}, \quad \text{and} \quad \mathrm{Im}_{out} = \int_{I_6}^{I_1} \frac{dI}{\sqrt{-P_6(I)}}$$

for the outer splitting. In particular $\mathrm{Re}_{in} = \mathrm{Im}_{out}$. The value Im_{in} equals 2π, according to a computation done in the previous case. Let us compute Im_{out}. Similar to the first case we introduce $K = (\mu\nu)^{-1/2}I$, obtaining

$$\int_{I_6}^{I_1} \frac{dI}{\sqrt{-P_6(I)}} \approx \frac{(\mu\nu)^{1/4}}{\sqrt{2}} \int_1^{\infty} \frac{dk}{K^{3/2}\sqrt{K^2 - 1}} = \frac{(\Gamma(3/4))^2}{\sqrt{\pi}}(\mu\nu)^{1/4}.$$

For readers' convenience we summarize the results obtained for the strong resonances in table 6.2.2. From inspection of the table and the bounds of the error given after (21), (22) and (23), the proof of theorem 5.1 can be adapted to prove

Theorem 6.1 *Let F be an APM. Assume that it has an m-order resonance $m = 3$ or $m = 4$, either non-degenerate ($\xi \neq -1$) or degenerate ($\xi = -1, \nu \neq 0$), as described in section 4. Then, close to the bifurcation parameter, and under conditions* **A1**, **A2**, **A3** *and* **A4** *the outer splitting is larger than the inner one when both of them exist.*

7 An example of dynamical consequences: the 1:4 and higher order resonances for the Hénon map

The different size of both splittings has some dynamical consequences to be analysed in future works. Let us consider first the 1:4 resonance to sketch some ideas. As was established in section

	Limit Hamiltonian ($\sigma = \text{sign}(\epsilon)$, $\mu = \lvert\epsilon\rvert$)	Param.	Inner splitting singularity (Re$+i$ Im)	Outer splitting singularity (Re$+i$ Im)
1:3 res.	$\sigma I + I^{\frac{3}{2}} \cos(3\varphi)$		$\text{Re} = 0,\ \text{Im} = \frac{\pi}{\sqrt{3}}$	$\mathcal{O}(1)$
1:4 res. generic case	$\sigma I + I^2(1 + \xi \cos(4\varphi))$	$\epsilon > 0$ $\xi < -1$	$\text{Re} = \sqrt{\frac{(1+\xi)}{2\xi}}\ \log \Omega$ $\Omega = \frac{(3\xi-1)+2\sqrt{2\xi(\xi-1)}}{1+\xi}$ $\text{Im} = \sqrt{\frac{2(\xi+1)}{\xi}}\ \pi$	$\nexists$
		$\epsilon > 0$ $\xi > -1$	$\nexists$	$\nexists$
		$\epsilon < 0$ $\xi < -1$	$\text{Re} = \sqrt{\frac{2(\xi-1)}{\xi}} \log \Omega$ $\Omega = \frac{\sqrt{-2\xi}-\sqrt{-(1+\xi)}}{\sqrt{1-\xi}}$ $\text{Im} = \sqrt{\frac{2(\xi-1)}{\xi}}\pi$	$\nexists$
		$\epsilon < 0$ $\xi > -1$	$\text{Re} = 0$ $\text{Im} = \sqrt{\frac{\xi-1}{2\xi}}\,(\pi + \Omega)$ $\Omega = 2 \arctan\left(\sqrt{\frac{-2\xi}{1+\xi}}\right)$	$\text{Re} = 0$ $\text{Im} = \sqrt{\frac{\xi-1}{2\xi}}\,(\pi - \Omega)$ $\Omega = 2 \arctan\left(\sqrt{\frac{-2\xi}{1+\xi}}\right)$
1:4 res. non-generic case	$\sigma I + I^2(1 - \cos\,\psi) +$ $\mu I^3(a + b\cos\,\psi + c \sin\,\psi)$ $(\psi = 4\varphi)$	$\epsilon > 0$ $\nu > 0$	$\nexists$	$\nexists$
		$\epsilon > 0$ $\nu < 0$	$\text{Re} \approx \frac{\Omega}{8}\mu^{\frac{1}{4}}\ \log \frac{1}{\mu}$ $\text{Im} \approx \pi(1 - \frac{1}{\sqrt{6}})\,\Omega\,\mu^{\frac{1}{4}}$ $\Omega = (27\lvert\nu\rvert)^{\frac{1}{4}}$	$\nexists$
		$\epsilon < 0$ $\nu < 0$	$\text{Re} \approx 0$ $\text{Im} \approx 2\pi$	$\nexists$
	Notation: $\nu = a + b$	$\epsilon < 0$ $\nu > 0$	$\text{Re} \approx \frac{(\Gamma(3/4))^2}{\sqrt{\pi}}\nu^{\frac{1}{4}}\mu^{\frac{1}{4}}$ $\text{Im} \approx 2\pi$	$\text{Re} \approx 0$ $\text{Im} \approx \frac{(\Gamma(3/4))^2}{\sqrt{\pi}}\nu^{\frac{1}{4}}\mu^{\frac{1}{4}}$

Table 1: Strong resonances. Position of the singularities in the studied cases.

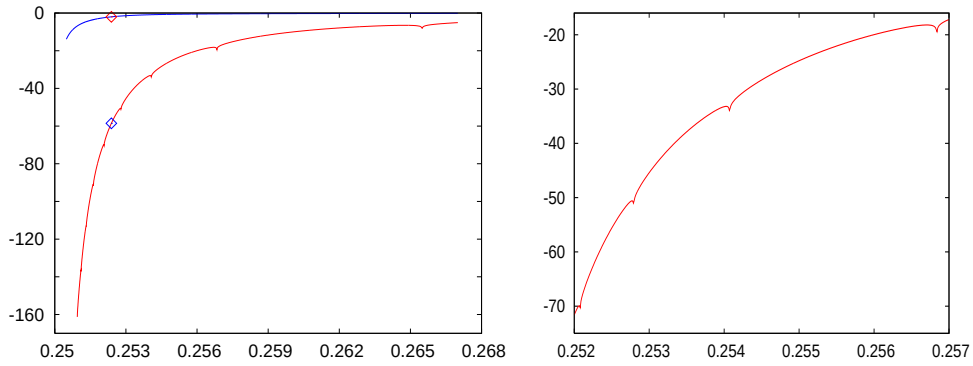

Figure 19: Left: logarithm ($\log_{10}|\sigma|$) of the inner (red) and outer (blue) splittings as a function of α. Right: magnification where different places where the inner splitting becomes zero can be guessed (see text). The marked points correspond to $\alpha \approx 0.2524$.

4 this resonance has a non-generic behaviour for the Hénon map. In particular, the invariant manifolds related to the outer splitting go to a distance $\mathcal{O}(\delta^{1/4})$ instead of $\mathcal{O}(\delta^{1/2})$. This is reflected in the behaviour of the splittings. Figure 19 shows the behaviour of the splittings of this resonance as a function of α.

Two considerations concerning the figure have to be done:

- There is a big difference in the order of the size of the splittings. For instance, for $c = 1.015$ ($\alpha \approx 0.25238741368$) corresponding to the value marked in figure 19 left, the outer splitting is $\sigma_+ \approx 2.5238741368 \times 10^{-1}$ while the inner one is $\sigma_- - 2.986620731 \times 10^{-59}$.

- The inner splitting oscillates (see case $\epsilon < 0$, $\nu > 0$ of 6.2.2). This is the reason why we observe the "peaks" in figure 19 right, which correspond to zeros of the splitting (in the log scale used in the figure we would observe vertical asymptotes if an extremely small step in α would be used). According to the theory it is expected $\sigma_- \sim A\delta^B \exp(-C_r/\delta)\cos(-C_i/\delta)$, with $C_i = \mathcal{O}(\delta^{1/4})$. Figure 20 shows the corresponding behaviour.

  Moreover, the ten first observed zeros of the splitting decreasing α from $\alpha = 0.267$ on are, approximately: 0.265492, 0.256837, 0.254073, 0.252793, 0.252078, 0.251631, 0.251327, 0.251111, 0.250949, 0.250824. According to the theory, the real part of the position of the singularity is at a distance $\mathcal{O}(\delta^{1/4})$. This means that the zeros of the splitting should be equidistributed with respect to $x = \delta^{-3/4}$ or, equivalently, that the fitting of the zeros by a function of the form $ax^c + b$ should have $c = 1$. Ignoring the three first zeros and fitting the others it is obtained $c \approx 1.00286$ which is quite in agreement with the expectations.

The splitting of the resonances plays a key role in destroying the rotational invariant curves. This holds both for low order and high order resonances. It is also well-known that the effects it produces can be analysed in terms of the separatrix map. In particular, it can be shown that, if the splitting is exponentially small with respect to δ, so is the distance from the separatrix at which invariant curves exist. Moreover, the qualitative dynamics in Birkhoff zones (for instance, between two invariant rotational curves) can be understood in terms of the biseparatrix map. An explanation of these ideas and a derivation of the proper models can be found in [38].

The interaction of different resonances and the homoclinic tangle help to understand the behaviour of the stability domain. In the case of the Hénon map "stability domain" refers, simply,

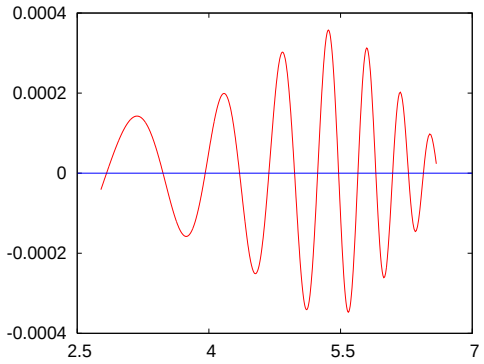

Figure 20: It is represented $\delta^B \exp(Cx)\sigma_-$, with $B = 5$, $C = 0.374$, as a function of $1/\delta^{1/4}$. The values of B and C have been obtained experimentally.

to the set of points which do not escape to ∞ (letting aside sets of zero measure, like the stable manifold of the fixed hyperbolic point). For other maps a suitable definition should be given. The stability domain contains points in invariant curves and also points in confined chaotic zones. Sudden changes in the size of the stability domain are due to the destruction of "outer" rotational invariant curves surrounding islands and this destruction is due to the splitting of separatrices of different resonances. As an example consider the Hénon map in the form (5) close to the 1:4 resonance (that is close to $c = 1$). See also [34] for several additional examples. We show in figure 21 how the stability domain drastically changes close to the value $c = 1.015$ where it has been observed such a big difference in the order of the size of the splitting. Figure 22 shows the evolution of the size of the stability domain. Clearly there are big jumps in the size of the stability domain when invariant curves surrounding large islands and the chaotic orbits associated to the tangle of the corresponding hyperbolic periodic points, are destroyed. The most relevant jumps in size correspond to the 1:3 and 1:4 resonances, but many other can be identified, including secondary resonances, i.e., the resonances inside the islands. Similar patterns occur for other resonances when the invariant rotational curves are destroyed and the corresponding islands are "thrown away" from the central component of the stable domain which contains the elliptic fixed point.

Indeed, one could suspect that the behaviour of the 1:4 resonance is exceptional for the Hénon map because of the non-generic character of this resonance. To illustrate that this is not the case figure 23 shows the domain of stability shortly after the destruction of the invariant curves surrounding islands of periods 6 and 5, respectively. Despite the parameter δ is far from being small, the different size of inner and outer splittings has the following effect: The outer splitting is large enough to destroy all outer rotational invariant curves, while the inner one is so small that invariant curves rather close to the hyperbolic periodic points still subsist. These curves have "quite sharp" behaviour close to these points and the instability channels which separate the curves from the large islands are narrow. Compare, e.g., with the inner and outer splittings for the 1:5 resonance shown in figure 15.

8 Conclusions and final remarks

The use of Birkhoff normal form and the interpolating Hamiltonian have allowed to study the dynamics in chains of resonant islands that emanate from the elliptic point when changing the

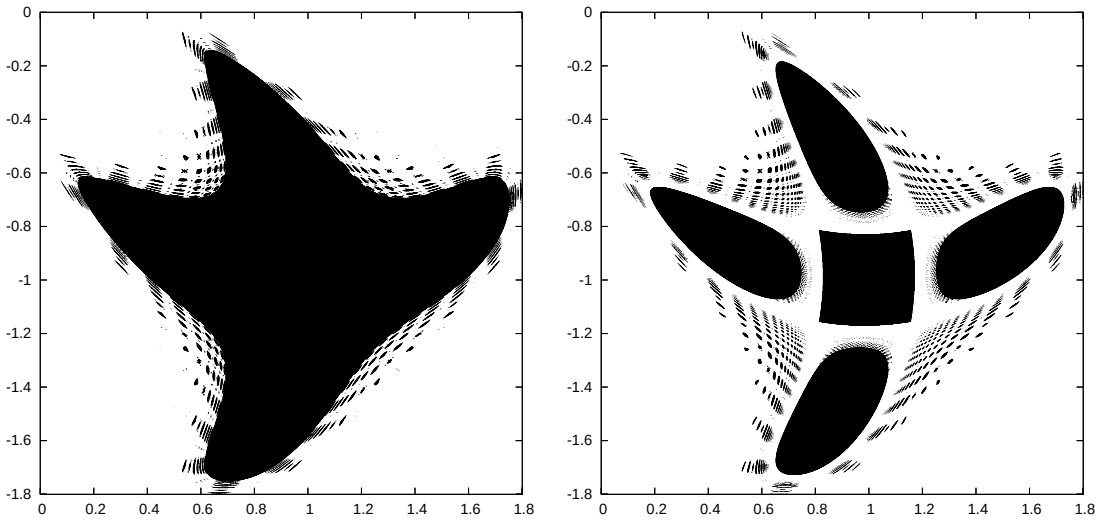

Figure 21: Stability domain of the Hénon map (5) for $c = 1.014$ (left) and for $c = 1.015$ (right). See text for additional information. In the electronic version one can magnify the plots to check details of the domain. This applies also to figure 23.

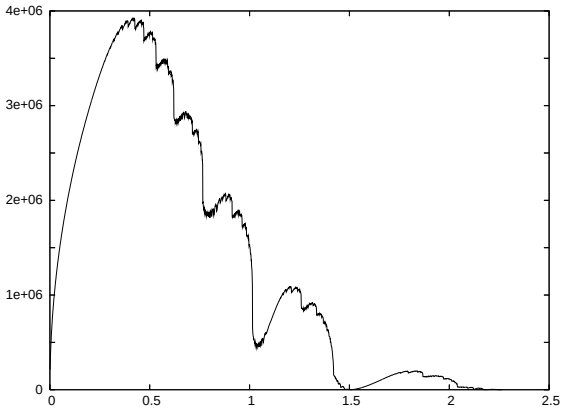

Figure 22: Number of points in the stability region of map (5) as a function of the parameter c. We have chosen a mesh of $N \times N$ points, with $N = 3100$, in the region $[-1, 2.1] \times [-2.1, 1]$. We use the "orbits method" which, roughly speaking, consists in iterating enough times, say $m > 10^7$ times, using a value m which depends on the point in such a way that the number of points that remain stable when doing $\tilde{m} = 10^4$ additional iterates to each point in the domain is not changing (see [38] for details).

rotation number at that point. The accuracy of the interpolating Hamiltonian (11) becomes relevant when studying the splitting of separatrices (section 5).

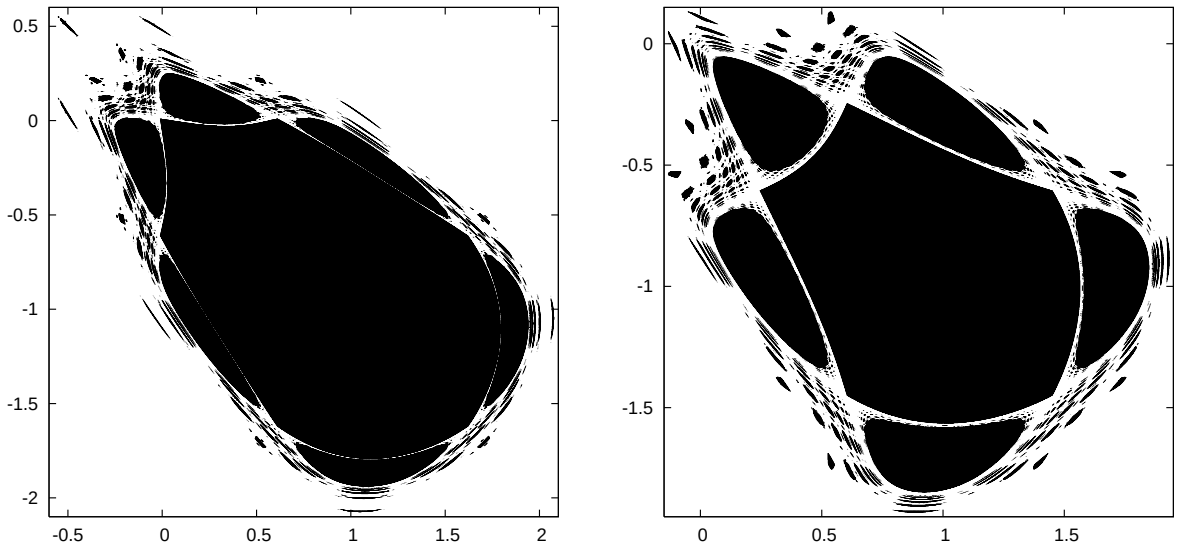

Figure 23: Stability domain of the Hénon map (5) for $c = 0.621$ (left) and for $c = 0.721$ (right). These values are close to the values of c for which all the invariant curves surrounding islands of periods 6 and 5, respectively, are destroyed.

As mentioned in the introduction there are several examples of APM where the difference between the inner and outer splitting has been observed. In this work a precise description in terms of the twist properties was given.

As both splittings, according to the theory developed, are generically different the distance at which the 'last' invariant curve is expected to be is generically different in the upper and lower part of an island. These invariant curves determine the chaotic domain containing the manifolds. As a consequence the chaotic region surrounding the pendulum-like separatrices that determine a generic resonance is not of the same size in the top and bottom part of the island. Note that this also affects the transport properties of the map.

On the other hand, there is a big interest in the study of weakly dissipative maps. An important point is to describe how the phase space evolves as we approach the conservative case. In this conservative limit the different size of both splitting plays a relevant role in determining the probability of capture in a resonance (see [36]).

These topics will be considered in future works.

Acknowledgments

This work has been supported by grants MTM2006-05849/Consolider (Spain) and CIRIT 2006 SGR-1028 (Catalonia). The second author is pleased also to acknowledge support during the first steps of this work by Ph.D. grant 2003FI00318 (Catalonia).

The authors are indebted to Ernest Fontich, Anatoly Neishtadt, Arturo Olvera and Dmitri Treschev for helpful discussions and suggestions. The comments of the referees are warmly

acknowledged. They helped to give more details in some key points.

The second author wants also to thank Groningen and Warwick Dynamical System groups for hospitality. Specially, several discussions with Henk Broer and Vassili Gelfreich on these and related topics helped to clarify some difficulties.

A The behaviour of the splitting: elliptic integrals

The study of the inner and outer splitting in the case $c, d \neq 0$ has been reduced to study the width of analyticity of the separatrix of the flow by means of elliptic integrals. For the outer splitting one has

$$\tau_+ = \int_{z_1}^{+\infty} \frac{dJ}{(J - J_h)\sqrt{p_4(J)}}, \tag{34}$$

and for the inner one

$$\tau_- = \int_{z_2}^{-\infty} \frac{dJ}{(J - J_h)\sqrt{p_4(J)}}, \tag{35}$$

as was explained in Section 5.2.

We use Legendre's reduction of elliptic integrals to estimate them. The reader is referred to [1] to get an overview of the methods. We just recall that the fundamental functions of Legendre theory are defined by

$$F(\phi,k)=\int_0^\phi \frac{du}{\sqrt{1-k\sin^2 u}},\ E(\phi,k)=\int_0^\phi \sqrt{1-k\sin^2 u}du,\ \Pi(N,\phi,k)=\int_0^\phi \frac{du}{(1-N\sin^2 u)\sqrt{1-k\sin^2 u}}$$

and are known as a elliptic integrals of first, second and third type, respectively.

Lemma. *Assume $0 < c < d$. Then*

$$\operatorname{Re}\tau_+ = 0, \qquad \operatorname{Im}\tau_+ = \frac{1}{\sqrt{1-d^2}}\left(\frac{\pi}{2} - \arcsin d\right) + \frac{4}{3}c\log c + \mathcal{O}(c),$$

$$\operatorname{Re}\tau_- = 4c, \qquad \operatorname{Im}\tau_- = \frac{1}{\sqrt{1-d^2}}\left(\frac{\pi}{2} + \arcsin d\right) - \frac{4}{3}c\log c + \mathcal{O}(c).$$

Proof. Any quartic polynomial q_4 can be written as

$$q_4(J) = (a_1J^2 + 2b_1J + c_1)\ (a_2J^2 + 2b_2J + c_2) = s_1(J)s_2(J).$$

We compute $\operatorname{Im}\tau_+$. For $q_4(J) = -p_4(J)$, we choose $s_1(J) = (J - z_1)(J - z_2)$ and $s_2(J) = \frac{c^2}{9}(J - z_3)(J - z_4)$. Then, we obtain a decomposition of the polynomials $s_i(J)$ in the form

$$s_i(J) = A_i(J - \alpha)^2 + B_i(J - \beta)^2,$$

where α and β are defined by

$$\alpha = \sqrt{\frac{c_1 - \lambda_1 c_2}{a_1 - \lambda_1 a_2}} = d + \mathcal{O}(c), \qquad \beta = -\sqrt{\frac{c_1 - \lambda_2 c_2}{a_1 - \lambda_2 a_2}} = \frac{-3}{2c} + \mathcal{O}(c),$$

being λ_i roots of the equation $p(\lambda) = (a_1 - \lambda a_2)(c_1 - \lambda c_2) - (b_1 - \lambda b_2)^2 = 0$.

Constants A_i and B_i are defined by

$$\begin{aligned} A_1 &= \frac{\lambda_2(a_1-\lambda_1 a_2)}{\lambda_2-\lambda_1} = \frac{-16d^2c^2}{9}+\mathcal{O}(c^3), & B_1 &= \frac{-\lambda_1(a_1-\lambda_2 a_2)}{\lambda_2-\lambda_1} = 1+\mathcal{O}(c^2), \\ A_2 &= \frac{a_1-\lambda_1 a_2}{\lambda_2-\lambda_1} = \frac{c^2}{9}+\mathcal{O}(c^3), & B_2 &= \frac{-(a_1-\lambda_2 a_2)}{\lambda_2-\lambda_1} = \frac{-16c^4}{81}+\mathcal{O}(c^5). \end{aligned}$$

We focus our attention on the outer splitting, that is, on the integral (34). We observe that in $(z_1,+\infty)$ there is no root of the polynomial $p_4(J)$.

The change of variables $t=(J-\beta)/(J-\alpha)$ reduces the integral (34) to a sum of integrals

$$I_1+I_2=\int_{\frac{z_1-\beta}{z_1-\alpha}}^1 \frac{R_{even}(t)}{\sqrt{(B_1t^2+A_1)(B_2t^2+A_2)}}dt+\int_{\frac{z_1-\beta}{z_1-\alpha}}^1 \frac{tR_{odd}(t)}{\sqrt{(B_1t^2+A_1)(B_2t^2+A_2)}}dt,$$

where

$$R_{even}(t)=\frac{\beta-J_h+(J_h-\alpha)t^2}{(\beta-\alpha)\left((\beta-J_h)^2-(\alpha-J_h)^2t^2\right)} \quad \text{and} \quad R_{odd}(t)=\frac{-1}{\left((\beta-J_h)^2-(\alpha-J_h)^2t^2\right)}.$$

The right term I_2 can be computed in terms of elementary functions. A simple calculation gives

$$I_2=\frac{1}{\sqrt{1-d^2}}\frac{\pi}{2}+\left(\frac{4}{3}+\frac{\pi}{4}\left(\frac{2d-d^2-2d^3}{(1-d^2)^{\frac{3}{2}}}\right)\right)c+\mathcal{O}(c^2).$$

We split integral I_1 as a sum of two integrals

$$\begin{aligned} I_1=I_{11}+I_{12} &= \frac{1}{(\beta-\alpha)(\alpha-J_h)}\int_{\frac{z_1-\beta}{z_1-\alpha}}^1 \frac{dt}{\sqrt{(B_1t^2+A_1)(B_2t^2+A_2)}} \\ &+ \frac{J_h-\beta}{\alpha-J_h}\int_{\frac{z_1-\beta}{z_1-\alpha}}^1 \frac{dt}{\left((\beta-J_h)^2-(\alpha-J_h)^2t^2\right)\sqrt{(B_1t^2+A_1)(B_2t^2+A_2)}} \end{aligned}$$

The integral I_{11} can be reduced to a first kind of Legendre. In fact, I_{11} can be expressed as

$$I_{11}=C_1\frac{1}{\sqrt{1-k}}\left(F\left(\arctan\sqrt{m_1-1},1-\frac{k}{k-1}\right)-F\left(\arctan\sqrt{m_1\frac{z_1-\beta}{z_1-\alpha}-1},1-\frac{k}{k-1}\right)\right),$$

where $m_1=-\dfrac{B_1}{A_1}$, $m_2=-\dfrac{B_2}{A_2}$, $k=\dfrac{m_2}{m_1}$, and $C_1=\dfrac{1}{(\beta-\alpha)(\alpha-J_h)\sqrt{-A_1A_2m_1}}$.

We approximate the above integral using

$$1-\left(1-\frac{k}{k-1}\right)\sin^2(u)\approx\frac{k}{k-1}+\cos^2(u), \tag{36}$$

and the consequent integral can be calculated directly

$$I_{11}=\left(\frac{1}{d}-\left(\frac{2}{3}-\frac{2}{d^2}\right)c+\mathcal{O}(c^2)\right)\left(-\log c+\mathcal{O}(1)\right).$$

The integral I_{12} can be reduced to Legendre third kind

$$I_{12}=C_2\left(\Pi\left(\frac{N}{N-1},i\,\mathrm{arccosh}\,\sqrt{m_1},\frac{k}{k-1}\right)-\Pi\left(\frac{N}{N-1},i\,\mathrm{arccosh}\,\frac{\sqrt{m_1}(z_1-\beta)}{z_1-\alpha},\frac{k}{k-1}\right)\right),$$

where

$$C_2 = \frac{-i(J_h - \beta)}{(1-N)(\beta - J_h)^2(\alpha - J_h)\sqrt{-A_1 A_2 m_1(1-k)}},$$

$$m_1 = -\frac{B_1}{A_1},\ m_2 = -\frac{B_2}{A_2},\ k = \frac{m_2}{m_1},\ N = \left(\frac{\alpha - J_h}{\beta - J_h}\right)^2.$$

By using the approximation (36) the integral above can be reduced to a sum of two integrals, I_{121} and I_{122}. The first one is similar to the one obtained for the integral I_{11} and can be calculated directly to obtain

$$I_{121} = \left(\frac{-1}{d} - \left(\frac{2}{3} + \frac{2}{d^2}\right)c + \mathcal{O}(c^2)\right)(-\log c + \mathcal{O}(1)).$$

The second one can be evaluated by using the change of variables $t = \cosh(x)$ and it is obtained

$$I_{122} = \frac{-1}{\sqrt{1-d^2}} + \mathcal{O}(c).$$

To sum up, the singularity of the outer splitting behaves according to

$$\operatorname{Re}\tau_+ = 0, \quad \operatorname{Im}\tau_+ = \frac{1}{\sqrt{1-d^2}}\left(\frac{\pi}{2} - \arcsin d\right) + \frac{4}{3}c\log c + \mathcal{O}(c).$$

In a similar way, it is obtained the behaviour of the singularity for the inner splitting both for the imaginary part and the real part. □

References

[1] M. Abramowitz and I.A. Stegun. *Handbook of Mathematical Functions.* National Bureau of Standards. Applied Mathematics Series - 55, 1972.

[2] V.I. Arnold. *Chapitres supplémentaires de la théorie des équations différentielles ordinaires.* Ed. Mir, 1978.

[3] V.I. Arnold, V.V. Kozlov, and A.I. Neishtadt. *Mathematical aspects of classical and celestial mechanics. Dynamical Systems III.* Third edition. Encyclopaedia of Mathematical Sciences, 3. Springer-Verlag, 2006.

[4] I. Baldomà. *Contribution to the Study of Invariant Manifolds and the Splitting of Separatrices of Parabolic Points.* PhD thesis, Universitat de Barcelona, 2001.

[5] I. Baldomà and A. Haro. One dimensional invariant manifolds of Gevrey type in real-analytic maps. *Discrete Contin. Dyn. Syst. Ser. B*, 10(2-3):295–322, 2008.

[6] H. Broer, H. Hanßmann, A. Jorba, J. Villanueva, and F. Wagener. Normal-internal resonances in quasi-periodically forced oscillators: a conservative approach. *Nonlinearity*, 16(5):1751–1791, 2003.

[7] H. Broer, R. Roussarie, and C. Simó. Invariant circles in the Bogdanov-Takens diffeomorphisms. *Ergodic Theory Dynam. Systems*, 16:1147 – 1172, 1996.

[8] H.W. Broer, S.N. Chow, Y. Kim, and G. Vegter. A normally elliptic Hamiltonian bifurcation. *Z. Angew. Math. Phys.*, 44(3):389–432, 1993.

[9] B.V. Chirikov. A Universal Instability of Many-Dimensional Oscillator System. *Phys. Rep.*, 52:264 – 379, 1979.

[10] H.R. Dullin, J.D. Meiss, and D. Sterling. Generic twistless bifurcations. *Nonlinearity*, 13:203–224, 1999.

[11] E. Fontich and C. Simó. The Splitting of Separatrices for Analytic Diffeomorphism. *Ergodic Theory Dynam. Systems*, 10:295 – 318, 1990.

[12] V.G. Gelfreich. A proof of the exponentially small transversality of the separatrices for the standard map. *Comm. Math. Phys.*, 201(1):155–216, 1999.

[13] V.G. Gelfreich. Exponentially small splitting of separatrices for area preserving maps. *Chaos Solitons Fractals*, 11(1-3):241–243, 2000.

[14] V.G. Gelfreich. Near strongly resonant periodic orbits in a Hamiltonian system. *Proc. Natl. Acad. Sci. USA*, 99(22):13975 – 13979, 2002.

[15] V.G. Gelfreich. Unique resonant normal forms for area preserving maps at an elliptic fixed point. Preprint, 2008.

[16] V.G. Gelfreich and V.F. Lazutkin. Splitting of separatrices: perturbation theory and exponential smallness. *Russian Math. Surveys*, 56(3):499–558, 2001.

[17] V.G. Gelfreich, V.F. Lazutkin, and M.B. Tabanov. Exponentially small splittings in Hamiltonian Systems. *Chaos*, 1(2):137–142, 1991.

[18] V.G. Gelfreich and C. Simó. High-precision computations of divergent asymptotic series and homoclinic phenomena. *Discrete Contin. Dyn. Syst. Ser. B*, 10(2-3):511–536, 2008.

[19] M. Giovannozzi. Stability domain and invariant manifolds of 2d area-preserving diffeomorphisms. *Celestial Mech. Dynam. Astronom.*, 68(2):177–192, 1997.

[20] G. Gomez, A. Jorba, J. Masdemont, and C. Simó. *Study of Poincaré maps for orbits near lagrangian points*. ESOC Contract 9711/91/D/ID(SC), Final Report, 1993.

[21] J. Guckenheimer and P. Holmes. *Nonlinear Oscillations, Dynamical Systems, and Bifurcations of Vector Fields*. Ed. Springer. Applied natural sciences, 42, 1997.

[22] H. Hanßmann. *Local and semi-local bifurcations in Hamiltonian dynamical systems*, volume 1893 of *Lecture Notes in Mathematics*. Springer-Verlag, 2007. Results and examples.

[23] M. Hénon. Numerical study of quadratic area-preserving mappings. *Quart. Appl. Math.*, 27:291 – 312, 1969.

[24] A. Jorba. A methodology for the numerical computation of normal forms, centre manifolds and first integrals of Hamiltonian systems. *Experiment. Math.*, 8(2):155 – 195, 1999.

[25] V.F. Lazutkin. Splitting of separatrices for the Chirikov's standard map. Preprint http://www.ma.utexas.edu/mp_arc/index-98.html, 1998.

[26] K.R. Meyer. Generic bifurcation of periodic points. *Trans. AMS*, 149:95–107, 1970.

[27] A.I. Neishtadt. The separation of motions in systems with rapidly rotating phase. *J.Appl. Math. Mech.*, 48:133 – 139, 1984.

[28] A. Olvera. Estimation of the amplitude of resonance in the general standard map. *Experiment. Math.*, 10(3):401–418, 2001.

[29] C.L. Siegel and J.K. Moser. *Lectures on Celestial Mechanics*. Ed. Springer Verlag, 1971.

[30] C. Simó. Stability of degenerate fixed points of analytic area preserving maps. *Astérisque*, 98 – 99:185 – 194, 1982.

[31] C. Simó. Invariant curves of analytic perturbed nontwist area preserving maps. *Regul. Chaotic Dyn.*, 3(3):180 – 195, 1998. J. Moser at 70.

[32] C. Simó. Analytic and numeric computations of exponentially small phenomena. In *International Conference on Differential Equations, Vol. 1, 2 (Berlin, 1999)*, pages 967 – 976. World Sci. Publ., River Edge, NJ, 2000.

[33] C. Simó. Studies in dynamics: From local to global aspects. Lecture given at the opening of the 2007-2008 course in the Societat Catalana de Matematiques, Barcelona, http://www.maia.ub.es/dsg/2007/index.shtml, 2007.

[34] C. Simó. Some properties of the global behaviour of conservative low dimensional systems. In *Foundations of Computational Mathematics: Hong Kong 2008*, volume 363 of *London Math. Soc. Lecture Notes Series*, pages 163–189. Cambridge Univ. Press, 2009, in press.

[35] C. Simó and C. Valls. A formal approximation of the splitting of separatrices in the classical arnold's example of diffusion with two equal parameters. *Nonlinearity*, 14:1707 – 1760, 2001.

[36] C. Simó and A. Vieiro. A Numerical Exploration of Weakly Dissipative Two-Dimensional Maps. In *Proceedings of ENOC'05*, 2005.

[37] C. Simó and A. Vieiro. Towards a global study of Area Preserving Maps. Examples, Models and Applications. Slides of talks given at the workshops Chaos and Ergodicity of Realistic Hamiltonian Systems Centre de recherches mathematiques, Montreal and Workshop on Mathematical Aspects of Celestial Mechanics IHP and Observatoire de Paris, Paris, http://www.maia.ub.es/dsg/2007/index.shtml, 2007.

[38] C. Simó and A. Vieiro. Dynamics close to separatrix and Birkhoff zones. -, In progress 2008.

[39] S. Smale. Diffeomorphisms with many periodic points. In *Differential and Combinatorial Topology (A Symposium in Honor of Marston Morse)*, pages 63–80. Princeton Univ. Press, 1965.

[40] F. Takens. Forced oscillations and bifurcations. In *Applications of global analysis, I (Sympos., Utrecht State Univ., Utrecht, 1973)*, pages 1–59. Comm. Math. Inst. Rijksuniv. Utrecht, No. 3–1974. Math. Inst. Rijksuniv. Utrecht, Utrecht, 1974.

[41] S. Ushiki. Sur le liaisons-cols des systèmes dynamiques analytiques. *C.R. Acad. Sci. Paris Ser. A*, 291:447–449, 1980.